

PONTIFICIA UNIVERSIDAD  
CATÓLICA DEL PERÚ

Escuela de Posgrado



IMPACT OF ONE LOOP CORRECTIONS ON LIGHT  
NEUTRINO MASSES IN THE LOW SCALE SUSY SEESAW

Tesis para optar el grado académico de Doctor en  
Física que presenta:

*Omar Giancarlo Suarez Navarro*

Asesor:

*Dr. Joel Jones Pérez*

Lima, 2023


## Informe de Similitud

Yo, Joel Jones Pérez, docente de la Escuela de Posgrado de la Pontificia Universidad Católica del Perú, asesor de la tesis de investigación titulada "Impact of One Loop Corrections on Light Neutrino Masses in the Low Scale Susy Seesaw", del autor Omar Giancarlo Suarez Navarro, dejo constancia de lo siguiente:

- El mencionado documento tiene un índice de puntuación de similitud de 16%. Así lo consigna el reporte de similitud emitido por el software *Turnitin* el 08/11/2023.
- He revisado con detalle dicho reporte y la Tesis, y no se advierte indicios de plagio. Se debe añadir que varias de las similitudes corresponden a una publicación realizada por el mismo autor en una revista indizada. Dicho trabajo se encuentra citado en la tesis.
- Las citas a otros autores y sus respectivas referencias cumplen con las pautas académicas.

Lugar y fecha:

Lima, 08/11/2023

Apellidos y nombres del asesor / de la asesora: Jones Pérez, Joel	
DNI: 40711425	Firma 
ORCID: 0000-0002-2037-6369	

# Acknowledgements

First of all, I want to thank my family: *Pedro, Eymi, Sol, Ivan, and Dylan*. I do not need to write much to express what I feel.

I would like to thank my supervisor, Dr. Joel Jones Pérez, for his constant support throughout this process. I will always be grateful for everything, and I personally owe him a lot. Additionally, I want to thank Dr. Alberto Gago and Dr. José Bazo for their work in the High Energy group at PUCP (HEP-PUCP). I also want to thank Dr. Werner Porod for his advice on this work.

I want to thank my friends, colleagues, and the people who helped me in some way: Solange P., Nhell C., Javier M., Felix D., Anthony C., Dante, Jairo, Sandro, Álvaro, Juan M., Simon M., Oscar L., and others.

Finally, I would like to thank CienciActiva/CONCYTEC for financing this project under Grant N° 236-2015-FONDECYT and research internship DAAD Germany-2017, project N° 131-2017-FONDECYT. I also acknowledge funding from project DGI-2021-C-0020 during the last stage of the work

# Abstract

This thesis covers the study of one-loop quantum corrections to the light neutrino masses. In the first part, we examine the extension of the standard model with right-handed neutrinos, where the Seesaw type I is present, allowing accessible masses for experimental searches. However, considering the corrections to the light neutrinos masses requires the pairs of heavy neutrinos to appear as pseudo Dirac particles, implying a suppression of the LNV parameters. In the second part, the supersymmetric contributions are analyzed in order to relax the lepton number violation (LNV) restrictions and achieve a greater difference between the heavy neutrino masses, as well as large mixings. When analyzing the destructive interference between the supersymmetric (which we describe as reducible and irreducible) and non-supersymmetric contributions, we found parameter regions where cancellations occur, however they are very small. So, the addition of SUSY does not guarantee the effect called screening, and the cases that are favorable need some degree of fine-tuning. In all cases, the numerical results of the analytical one-loop expressions calculated in the  $\nu_R$ SM and  $\nu_R$ MSSM models are checked with SPheno.

# Resumen

Esta tesis cubre el estudio de las correcciones cuánticas a un loop a las masas de neutrinos ligeros. En la primera parte, examinamos la extensión del modelo estándar con neutrinos de mano derecha, donde está presente el Seesaw tipo I, que permite masas accesibles para su búsqueda experimental. Sin embargo, el considerar correcciones a las masas de los neutrinos ligeros requiere que los pares de neutrinos pesados sean considerados como pseudo-Dirac, implicando una supresión de los parámetros LNV. En la segunda parte, se analizan las contribuciones supersimétricas para relajar las restricciones sobre los parámetros de violación de número leptónico (LNV) y lograr una mayor diferencia entre las masas de neutrinos pesados, así como mezclas grandes. Al analizar la interferencia destructiva entre las contribuciones supersimétricas (que describimos como reducibles e irreducibles) y no supersimétricas, encontramos regiones de parámetros donde ocurren cancelaciones, pero que son muy pequeñas. Por lo tanto, agregar solo SUSY no garantiza el efecto llamado screening, y los casos que son favorables necesitan cierto grado de ajuste. En todos los casos, los resultados numéricos de las expresiones analíticas a un loop calculadas en los modelos  $\nu_R$ SM y  $\nu_R$ MSSM se verifican con SPheno.

# Table of Contents

Acknowledgements	ii
Abstract	iii
List of Tables	viii
List of Figures	ix
Introduction	xiii
<b>1 GENERAL ASPECTS: NEUTRINO PHYSICS</b>	<b>1</b>
1.1 Neutrino mass matrix . . . . .	1
1.2 Seesaw Mechanism . . . . .	5
1.3 Casas-Ibarra parametrization . . . . .	6
<b>2 ONE LOOP CORRECTIONS TO NEUTRINO MASS IN THE <math>\nu_R</math> STANDARD MODEL EXTENSION</b>	<b>8</b>
2.1 $Z^0$ Boson Contribution . . . . .	9
2.2 Neutral Scalar Contribution . . . . .	12
2.3 Charged Scalar Contribution . . . . .	15
2.4 Numerical Evaluation . . . . .	17

<b>3</b>	<b>ONE LOOP CORRECTIONS IN THE <math>\nu_R</math>MSSM</b>	<b>26</b>
3.1	Lagrangian in the $\nu_R$ MSSM extension . . . . .	27
	Neutral Higgs masses . . . . .	28
	Charged Higgs . . . . .	29
	Sneutrino mass . . . . .	30
	Neutralinos . . . . .	31
	Charginos . . . . .	32
3.2	One loop corrections to neutrinos mass of non-SUSY contributions . . . . .	33
	3.2.1 Neutral and charged scalar contributions . . . . .	34
3.3	One loop corrections to neutrino mass in SUSY . . . . .	37
	3.3.1 The Mass Insertion Approximation (MIA) . . . . .	38
	3.3.2 Conventions for lepton number violation and conserving mass insertions	41
	3.3.3 Reducible and Irreducible contributions to one loop to the neutrino masses in SUSY . . . . .	45
	3.3.4 Irreducible contributions . . . . .	46
	Pure gaugino case . . . . .	47
	Gaugino-Higgsino case . . . . .	48
	3.3.5 Reducible contributions . . . . .	48
	Pure Higgsino case . . . . .	49
	Pure gaugino case . . . . .	49
	Gaugino-Higgsino case . . . . .	50
<b>4</b>	<b>SEARCHING FOR CANCELLATIONS</b>	<b>52</b>
4.1	Non-SUSY contributions in benchmark scenario . . . . .	53
4.2	Irreducible SUSY contributions in benchmark scenario . . . . .	54
	4.2.1 Degenerate R sneutrino exploration . . . . .	57
	4.2.2 Non-degenerate R sneutrinos exploration . . . . .	62

4.3	Reducible SUSY contributions in Benchmark Scenario . . . . .	64
4.3.1	Degenerate R sneutrinos exploration . . . . .	66
<b>5</b>	<b>CONCLUSIONS</b>	<b>71</b>
<b>A</b>	<b>Casas-Ibarra Parametrization</b>	<b>73</b>
<b>B</b>	<b>Generalities</b>	<b>77</b>
B.1	Propagators . . . . .	77
B.2	Loop Integral Approximation . . . . .	77
	<b>Bibliography</b>	<b>81</b>





# List of Tables

2.1	Maximum values of $\gamma_{56}$ and $U_{a5}$ allowed without exceeding corrections to the neutrino masses by 50%. . . . .	24
3.1	Fields and superpartners in the model. To clarify, $\hat{\nu}_R^c$ appears only in the MSSM extension, hence the name $\nu_R$ MSSM . . . . .	27
3.2	Gauge supermultiplets in the MSSM. . . . .	27
4.1	The signs for SUSY and Non-SUSY contributions when $a_\nu = 0$ and $a_\nu \neq 0$ . . . . .	57
4.2	Hierarchies for $\mu, M_1, M_2$ and $m_{\tilde{L}}$ which will be used to describe and identify the degree of interference with the irreducible and reducible contributions. . . . .	60
4.3	Numerical values of the parameters used in [9]. . . . .	62
4.4	We show the signs for $G_{\text{red}}$ fixing $\tan \beta = 8$ and $M_A = 1100$ GeV. . . . .	66

# List of Figures

1.1	The small mass of the standard model neutrinos is due to that there are very heavy states $\nu_R$ . . . . .	6
2.1	One Loop Diagrams in the $\nu_R$ SM. Top panel: contributions from the neutral Higgs, Goldstone, and $Z^0$ boson. Lower panel: Contributions from charged Goldstone boson (where $\ell_a$ is the charged lepton). . . . .	10
2.2	Dependence of loop function, conveniently normalized, with respect to $v_{\text{SM}}^2/M$ . . . . .	18
2.3	Flavour-independent behaviour of $\delta M_L$ on $M_5$ , fixing $M_6$ for different values. . . . .	20
2.4	Real (left) and imaginary (right) part of the matrix elements of $\delta M_L$ , setting $\gamma_{56} = 5$ . The upper(lower) panels have $M_6 = 10^{-1}(10^3)$ GeV. . . . .	21
2.5	The light mass behaviour respect to variation of $\gamma_{56}$ , for fixed heavy masses. The dashed gray horizontal lines denote the neutrino masses at tree level. Largest, intermediate and smallest eigenvalues are shown in black, red and blue, respectively. . . . .	22
2.6	The blue, red and black lines represent the eigenvalues $m_1$ , $m_2$ and $m_3$ respectively for $\gamma_{56} = 2$ (Left column) and $\gamma_{56} = 8$ (Right column). The dashed horizontal lines represent the masses of light neutrinos at tree level. . . . .	23
2.7	Upper panel: Maximum value of $ U_{a5} ^2$ as a function of $M_5$ , for $M_6 = \{10^{-1}, 10^2\}$ GeV. Lower panel: values of $\gamma_{56}$ that maximize $ U_{a5} ^2$ . Specific values for $M_5$ and $M_6$ are shown in Table 2.1. . . . .	25

3.1	The one-loop contributions involving neutral (Left) and charged scalar (Right) fields in the context of non-supersymmetric model. . . . .	35
3.2	General one loop Feynman diagram including the mass insertions $\Delta_N$ . . . . .	38
3.3	One loop diagram with two propagators that allows to form the $I_2(m_0^2, m^2)$ expression. . . . .	39
3.4	One loop diagram with one (Left) and two (Right) mass insertions. . . . .	40
3.5	Upper panel: $(v_{SM}/m_0)f_3(m_0^2, m_1^2, m_2^2)$ is shown for fixed $m_2 = 10(600)$ GeV in blue (red) lines (left). For $m_0 = 100$ GeV, the symmetry of $f_3$ with respect to $m_1$ and $m_2$ appears (right). Lower panel: we have $(v_{SM}^3/m_0^3)f_4(m_0^2, m_1^2, m_2^2, m_3^2)$ for fixed $m_2 = m_3 = 10(600)$ GeV in blue (red) lines (left). The symmetry of this function by setting $m_0 = m_2 = 100$ GeV is shown on the right . . . . .	42
3.6	Lepton number convention for the scalar fields $\tilde{\nu}_L$ and $\tilde{\nu}_R^c$ . . . . .	43
3.7	Three types of Feynman diagrams in which MI will be included, where $O_{rb}$ are the neutralino mixing matrix elements. . . . .	45
3.8	Pure gaugino one loop diagrams. In all diagrams the shaded(black) blobs indicate LNV(LNC) insertions. . . . .	47
3.9	Mixed diagrams with one LNV mass insertion. . . . .	48
3.10	Pure-higgsino diagram with one LNV mass insertion. . . . .	49
3.11	One loop diagrams with three mass insertion. a) Three LNV insertions. b) Two LNC and one LNV insertion. . . . .	50
3.12	Mixed one loop diagram with two mass insertion. Shaded(black) blobs indicate LNV(LNC) insertions . . . . .	51
4.1	Ratio between loop functions, $g(M_h, M_A, \tan \beta)/f(M_h)$ . Gray (dark green) region is excluded by $H/A \rightarrow \tau^+\tau^-$ [59] ( $H^\pm \rightarrow tb$ [60]) searches. The region to the left of the purple curve is excluded, as here the light Higgs boson couplings do not match with measurements [61]. We show results for $M_h = 40(200)$ GeV on the left (right). . . . .	54

4.2	The left panel corresponds to the case where $M_5 = 40$ GeV, while the right panel represents the scenario with $M_5 = 200$ GeV. In both panels with $\mu < 0$ , we have fixed values for $\tan \beta = 8$ , $\gamma_{56} = 8$ , and $M_A = 1100$ GeV. . . . .	58
4.3	We show the scatter plot with the same parameters as in Fig. 4.2 but with $\mu > 0$ . . . . .	59
4.4	We show the behavior of $G_{\text{irr}}^{gg+gh}$ for the order of the parameters shown in the table. There are four scenarios, see Table 4.2, that are identified as: upper left panel (a) and right (b), lower left panel (c) and right (d) . . . . .	61
4.5	The maximum $\Delta M_{65}$ allowed as a function of $\mu$ (Left panel) and $a_\nu$ (Right panel). Here we consider the spectrum of parameters in Table 4.3, with $\gamma_{56}=8$ and $ U_{\mu 5}  = 1.3 \times 10^{-7}$ . . . . .	63
4.6	Left: Dependence of $R_{gh+gg}^{\text{irr}}$ with $m_{\tilde{\nu}_{R6}}$ , for several values of $\Delta M_{65}$ . Heavy neutrino mass is set to $M_5 = 40$ GeV. Right: Maximum allowed value of $ U_{\mu 5} ^2$ , as a function of $\Delta M_{65}/M_5$ , for two values of $M_5$ . Limits on the Standard Seesaw are shown in red. Blue and gray lines show limits for the spectrum described in the text. For gray lines, the SUSY contribution is larger than the one from 2HDM. . . . .	64
4.7	The $R$ parameter is depicted considering the contributions from pure Gaugino and mixed terms for $b_\nu > 0$ and $\mu < 0$ . The parameters are being randomly varied for $M_A = 1100$ GeV and $\tan \beta = 8$ . . . . .	67
4.8	We show the higgsino-higgsino contribution for $b_\nu > 0$ and $\mu < 0$ with $\tan \beta = 8$ and $M_A = 1100$ GeV. . . . .	68
4.9	We have the same hierarchy in the parameters described in Fig. 4.4 for $b_\nu < 0$ and $\mu < 0$ . . . . .	69
4.10	Values of $R_{gg+gh+hh}^{\text{red}}$ parameter for different values of $m_{\tilde{L}}$ and $ \mu $ , with $M_5 = 200$ GeV (right) and $M_5 = 40$ GeV (left). . . . .	70
4.11	Maximum allowed $\Delta M_{65}$ as a function of $b_\nu$ , for the SUSY spectrum considered in Table 4.3, with $\tan \beta = 2$ . We set $\gamma_{56} = 8$ , such that $ U_{\mu 5} ^2 = 1.3 \times 10^{-7}$ . . . . .	70

A.1 Behavior of  $\sinh \gamma$  and  $\cosh \gamma$  for small values of gamma. For values greater than 3, both hyperbolic functions are equal. . . . . 76



# Introduction

There are many open questions in particle physics, and one of them relates to a very special particle called neutrino. Why is it a special particle? In principle, a neutral particle has two possible descriptions. One is in the Dirac framework, where particles and antiparticles are different and Lepton number-conserving processes are involved. The second comes from the Majorana description, where particles and antiparticles are the same and new Lepton number violation (LNV) signals could appear [1]–[3]. This is known as the neutrino nature problem. Another fact that makes neutrinos important is that the Standard Model (SM) can not explain why they are massive, or how their mass originates.

Within the framework of the SM of particle physics, after spontaneous symmetry breaking (SSB), neutrinos remain without acquiring mass, unlike charged quarks and leptons, which do. This is because, in the SM, mass terms are not considered for neutrinos since there are only left chirality fields for them. However, observations derived from neutrino oscillation experiments have provided conclusive evidence that light neutrinos do indeed have mass [4], raising the imminent need for an extension of the SM to explain this phenomenon.

The Seesaw Model [5]–[8] is proposed as a solution to the problem of how the masses of light neutrinos are generated. To address this point, new fields with the right chirality are introduced. These particles interact with left-handed neutrinos through their mixing. In principle, the masses of these new particles could be adjusted so that they are not excessively heavy, which would facilitate their detection in experiments carried out in colliders. However, the naive Seesaw predicts very small mixings and is therefore not very useful in practice. Nevertheless, the number of right handed neutrinos is not restricted and could be considered free parameters within the model. An interesting observation occurs when you have two heavy neutrinos. It is possible to achieve new textures in the mass matrix that can reproduce the observed light neutrino masses and that allow for large mixing.

In order to calculate one-loop corrections to light neutrino masses, we will consider the  $\nu_R$ SM, which is nothing more than the extension of the SM with Right Handed (RH)

neutrinos. The problem observed is that when including the contributions to one loop, the corrections are very large, which forces a fine-tuning to be considered between the tree-level and one loop masses in order to reproduce the observed neutrino masses. The option to avoid this is to reduce the mixing; however, this would lead to heavy neutrinos not being observed in collider searches. Despite what was mentioned above, a special case can be found where a cancellation occurs between the contributions, which corresponds to the case when the masses of the RH neutrinos are degenerate. This can be attributed to the slight breaking of lepton number symmetry, suggesting that LNV effects might not be observable at colliders.

In the context of the supersymmetric extension of the type I seesaw, interesting results were presented in [9] where the masses of the neutrinos are generated radiatively, with contributions from heavy neutrinos and sneutrinos. Here they show that large LNV parameters are allowed and that the sneutrino loops help keep the corrections under control. If considerable LNV is allowed, it would be possible to relax the constraints on the differences in the masses of heavy neutrinos, allowing a direct interpretation of the experimental results. In this context, we seek to corroborate and carry out a more in-depth analysis of this so-called SUSY-screening effect, trying to understand when and in what parameter region this can occur.

The work presented in this thesis considers the supersymmetric extension of Seesaw type I, where we collect the supersymmetric contributions classified as reducible and irreducible according to their dependence or not on the LNV parameter  $B_\nu$ . We use the mass insertion method to clearly and concisely show the parameters involved in the loop diagrams mediated by neutralinos and sneutrinos. Depending on the number of mass insertions, it will be possible to know what type of LNV terms will affect light neutrino masses, as well as which of them will be more significant or not. In this context, we also address the diagrams involving the non-supersymmetric contributions in order to quantify the destructive interference between the SUSY and non-SUSY contributions. This was done with the intention of obtaining large mixings and differences between the  $N_h$  masses.

To achieve our objectives, we divide this work as follows: In Chapter 1, there is a brief introduction to neutrino masses and the parametrization applied to the mass matrix and mixings. In Chapter 2, we provide the analytical expression of the one-loop corrections to the light neutrino masses in the SM extension with right-handed neutrinos and their

numerical analysis. Chapter 3 shows a brief introduction to SUSY, the one-loop expression corrections in the mass insertion framework, and also the non-supersymmetric contributions. The mass insertion method is present in detail, which helps to better show the parameters involved in SUSY. In Chapter 4, we have the results corresponding to the analysis made with SUSY and non-SUSY contributions, showing the regions where destructive interference occurs. Finally, in Chapter 5, we present the conclusions of the work.





# GENERAL ASPECTS: NEUTRINO PHYSICS

## 1.1 Neutrino mass matrix

Fermionic fields ( $\Psi_f$ ) can be expressed as having two components with different chiralities, known as right- and left-handed,  $\Psi_f = \Psi_L + \Psi_R$ . In particular, the mass terms in the Lagrangian can be written using these two components as:

$$m_f \bar{\Psi}_L \Psi_R + h.c \quad (1.1)$$

In the SM, the mass generation mechanism arises from the interaction with the Higgs field, where the mass is described as:

$$m_f = \frac{v_{\text{SM}}}{\sqrt{2}} Y_f, \quad (1.2)$$

where  $m_f$ ,  $v_{\text{SM}}$  and  $Y_f$  are the Dirac fermion mass, SM Vacuum Expectation Value (VEV) and Yukawa coupling respectively. However, this does not occur with all particles. Neutrinos manifest themselves in different way. In the SM, these particles only have one type of chirality (Left) therefore it is not possible to have a mass term like the other fermions.

Neutrino oscillation experiments showed that these particles have small masses [10]–[13]. So, to understand a little more, we will do a brief review of this topic.

As we know, vectors can be written as a linear combination of others. For neutrinos, the most relevant bases are known as the interaction ( $\mathcal{B}_I$ ) and mass ( $\mathcal{B}_M$ ) bases. The states

in the interaction basis,  $\nu_{e,\mu,\tau}$ , do not have definite masses but interact with a specific charged lepton flavour. These can be written as the superposition of states  $\nu_{1,2,3}$ , in the mass basis with defined eigenvalues  $m_{1,2,3}$ . The  $|\nu_k\rangle$  and  $|\nu_\alpha\rangle$  objects  $\in \mathcal{B}_{I,M}$  are related as:

$$|\nu_\alpha\rangle = \sum_{k=1,2,3} U'_{\alpha k}{}^* |\nu_k\rangle, \quad (\alpha = e, \mu, \tau) \quad (1.3)$$

where  $U'$  is a unitary matrix that indicates the "weight" in the linear combination of each state. The mixing matrix in the case of three neutrinos is known as the PMNS matrix (Pontecorvo-Maki-Nakagawa-Sakata). This matrix, inspired by the mixing matrix for quarks, can be parameterized as [14]:

$$U_{\text{PMNS}} = \begin{pmatrix} 1 & 0 & 0 \\ 0 & c_{23} & s_{23} \\ 0 & -s_{23} & c_{23} \end{pmatrix} \begin{pmatrix} c_{13} & 0 & s_{13} e^{-i\delta_{\text{CP}}} \\ 0 & 1 & 0 \\ -s_{13} e^{i\delta_{\text{CP}}} & 0 & c_{13} \end{pmatrix} \begin{pmatrix} c_{12} & s_{12} & 0 \\ -s_{12} & c_{12} & 0 \\ 0 & 0 & 1 \end{pmatrix} \begin{pmatrix} e^{i\beta_1} & 0 & 0 \\ 0 & e^{i\beta_2} & 0 \\ 0 & 0 & 1 \end{pmatrix}, \quad (1.4)$$

where  $s_{ij}(c_{ij}) = \sin\theta_{ij}(\cos\theta_{ij})$ , with the mixing angles  $\theta_{ij}$  ( $i, j = 1, 2, 3$ ). The parameters  $\delta_{\text{CP}}$ ,  $\beta_{1,2}$  are known as the Dirac and Majorana phases respectively [15]–[17]. With this in hand, it is possible to deduce the neutrino oscillation probability to generate  $\nu_\alpha$  and detect  $\nu_\beta$ . The expression that is obtained after the neutrinos of energy  $E$  have traveled a distance  $L$  is [15]:

$$P_{\nu_\alpha \rightarrow \nu_\beta} = \sum_{k,j} U'_{\alpha k}{}^* U'_{\beta k} U'_{\alpha j} U'_{\beta j} \exp\left(-i \frac{\Delta m_{kj}^2 L}{2E}\right), \quad (1.5)$$

where

$$\Delta m_{kj}^2 = m_k^2 - m_j^2. \quad (1.6)$$

The function in Eq. (1.5) depends on the neutrino mass splitting. Oscillation experiments [18], [19] confirm that this probability is not zero and that therefore  $\Delta m_{kj}^2 \neq 0$ . This confirmation implies that there must be another type of physics to explain the origin of these masses and what their exact values would be. In order to solve this discrepancy, new SM extensions should be considered.

One of them we can find in the literature includes new RH fields for neutrinos [7], [20]–[22]. These particles are commonly called Sterile because it does not participate in weak interactions (The interaction with matter will occur only gravitationally or some other interaction beyond the SM). They are invariant under the group symmetry of the

SM ( $SU(3)_C \otimes SU(2)_L \otimes U(1)_Y$ ). Additionally, there is not an exact limit on the number of these RH fields. We will call the  $\nu_R$ SM extension to the SM with right-handed neutrinos in order to explain the masses of active neutrinos.

Including the right chirality it is possible to use the Higgs mechanism to write mass terms:

$$M_D \bar{\nu}_L \nu_R \quad (1.7)$$

where  $M_D$  represent the Dirac neutrino mass. This term is equivalent to the one found for the other fermions as in Eq. (1.2). Neutrinos of this nature lead to processes where the total lepton number is conserved even though the lepton flavor can be violated[15], [23].

Then another description for the neutrino masses is possible, considering that they are neutral particles, which is forbidden for quarks or charged leptons. The new concept when RH neutrinos are included is known as the Majorana description. It is important to define how particles and antiparticles are related. To do this, we must understand how the charge conjugation operator ( $C$ ) [24], [25] behaves. For fermions this is as follows:

$$\Psi^C = C\bar{\Psi}^T \quad (1.8)$$

Then  $C$  changes the chirality of the particle from left-handed neutrino to right-handed and vice versa. If we consider the neutrinos as Majorana particles, the neutrino field can be written as:

$$\nu = \nu_L + \nu_L^C, \quad (1.9)$$

which satisfies the Majorana condition :

$$\nu = \nu^C. \quad (1.10)$$

With this observation, we can conclude that distinguishing between a particle and its antiparticle is not possible.

In contrast to the Dirac case, here only one chiral field is necessary to generate the neutrino mass term. The singlet  $\nu_R$  can satisfy the condition in Eq. (1.10), which allows us to write a mass term:

$$\mathcal{L}_{mass}^\nu \supset \frac{1}{2} M_R \bar{\nu}_R \nu_R^c + h.c. \quad (1.11)$$

When we have these kinds of particles new processes could appear. One of the signals that usually describe this new window is the lepton number symmetry violation (For example in neutrinoless double beta decay  $\Delta L = 2$ ), in contrast with the Dirac case.

Considering the general case with Dirac and Majorana masses, we can extend the SM Lagrangian as [1], [26], [27]:

$$\mathcal{L}_\nu = i\bar{\nu}_{R_s}\not{\partial}\nu_{R_s} - \left( (Y_\nu)_{as}\bar{L}_a\tilde{\Phi}\nu_{R_s} + \frac{1}{2}(M_R)_{ss'}\bar{\nu}_{R_s}\nu_{R_{s'}}^c + \text{H.c.} \right) \quad (1.12)$$

where we have Yukawa couplings ( $Y_\nu$ ) and Majorana masses ( $M_R$ ) for the RH neutrinos. After SSB, we can obtain the tree level neutrino mass matrix

$$M_\nu^{\text{tree}} = \begin{pmatrix} 0 & M_D \\ M_D^T & M_R \end{pmatrix}. \quad (1.13)$$

In this case the Left-Left (LL) part of the neutrino mass matrix is zero [15]. In our definition, the Dirac mass is written as follows:

$$M_D = \frac{v_{\text{SM}}}{\sqrt{2}}Y_\nu^*, \quad (1.14)$$

The dimensions of the  $M_R$  and  $M_D$  matrices depend on the number of RH neutrinos that are added to the model. The matrix  $M_\nu^{\text{tree}}$  is diagonalized by a unitary matrix  $U$  as:

$$U^T M_\nu^{\text{tree}} U = \hat{M}_\nu, \quad (1.15)$$

where  $\hat{M}_\nu$  is a diagonal matrix with the neutrino masses. In the case with three RH neutrinos the eigenvalues are labeled as  $m_n$  ( $n = 1, 2, \dots, 6$ ) and the mass states like  $\nu_i, N_j$  with  $i = 1, 2, 3$  and  $j = 4, 5, 6$  respectively. Focusing on the LL part of the neutrino mass matrix, we obtain an important relation that will help us to simplify some calculations in the next sections. We can rewrite Eq. (1.15) as  $M_\nu^{\text{tree}} = U^* \hat{M}_\nu U^\dagger$  to get:

$$\sum_n U_{an}^* (\hat{M}_\nu)_n U_{a'n}^* = 0. \quad (1.16)$$

The indices  $a$  and  $a'$  represent the different active neutrinos flavors  $\nu_e, \nu_\mu$  and  $\nu_\tau$ . Here we have that  $M_\nu^{\text{tree}}$  and  $U$  matrices are  $6 \times 6$ . Therefore, the matrices  $U_{ai}$  and  $U_{si}$  that compose  $U$  are  $3 \times 6$ . In addition, from the unitarity of the mixing matrix,

$$U^\dagger U = U U^\dagger = \mathbb{1}, \quad (1.17)$$

we have:

$$\begin{aligned} \sum_i U_{ai} U_{a'i}^* &= \delta_{aa'}, & \sum_i U_{si} U_{s'i}^* &= \delta_{ss'} \\ \sum_i U_{ai} U_{si}^* &= 0, & \sum_i U_{si} U_{ai}^* &= 0. \end{aligned} \quad (1.18)$$

The indices  $s$  and  $s'$  that have been shown in the previous equations indicate the sterile neutrinos  $s_1$ ,  $s_2$  and  $s_3$ . If we rewrite Eq. (1.15) with one mixing matrix multiplying the diagonal matrix  $\hat{M}_\nu$ , that equality leads us to finally obtain this expression:

$$\sum_n U_{an}^* m_n = \sum_s (M_D)_{as} U_{sn}. \quad (1.19)$$

## 1.2 Seesaw Mechanism

In order to better understand this solution to the neutrino mass problem, we will take as an example the analytical diagonalization of  $M_\nu^{\text{tree}}$  in the  $1 + 1$  scenario, where we have one active and a sterile state. These eigenvalues are:

$$m_{2,1} = \frac{1}{2} \left( M_R \pm \sqrt{M_R^2 + 4M_D^2} \right). \quad (1.20)$$

If  $M_D \ll M_R$  (very large masses for heavy neutrinos),

$$m_1 = -\frac{M_D^2}{M_R}, \quad m_2 = M_R, \quad (1.21)$$

where  $m_2$  is the same order and heavy as  $M_R$ , also  $\nu_1$  is very light because it is suppressed by  $M_R$ . This is the essence of the so-called Seesaw: one mass is suppressed because another is too heavy (Fig.1.1)[21]. Here we have the typical seesaw that helps to explain the neutrino mass problem. However it is difficult to prove because it implies very large masses for  $M_R$  [1], [28], [29], even for  $M_D$  around the electroweak scale ( $Y_\nu \approx 1$ ).

In general for the Seesaw, one can obtain the light neutrino masses to an excellent approximation by diagonalizing the matrix [15], [30]:

$$M_{\text{light}}^{\text{tree}} = -M_D M_R^{-1} M_D^T. \quad (1.22)$$

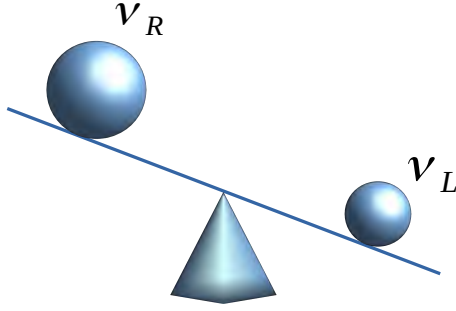


Figure 1.1: The small mass of the standard model neutrinos is due to that there are very heavy states  $\nu_R$ .

### 1.3 Casas-Ibarra parametrization

On the standard seesaw model, the heavy neutrinos couple to SM particles via the mixing matrix  $U$ , which diagonalizes the full mass matrix shown in Eq. (1.13). When including  $N = 3$  sterile neutrinos, this matrix can be decomposed into four  $3 \times 3$  blocks:

$$U = \begin{pmatrix} U_{al} & U_{ah} \\ U_{sl} & U_{sh} \end{pmatrix}. \quad (1.23)$$

Here,  $\ell = 1, 2, 3$  labels the three light (mostly active) neutrinos  $\nu_\ell$ , with masses  $m_1, m_2, m_3$ , while  $h = 4, 5, 6$  labels the three heavier (mostly sterile) neutrinos  $N_h$ , with masses  $M_4, M_5, M_6$ . Assuming that the lepton mass matrix is diagonal at tree level, each block can be parametrised in the following way [27], [31]:

$$\begin{aligned} U_{al} &= U_{\text{PMNS}} H, & U_{ah} &= i U_{\text{PMNS}} H \hat{m}_\ell^{1/2} R^\dagger \hat{M}_h^{-1/2}, \\ U_{sl} &= i \bar{W} \bar{H} \hat{M}_h^{-1/2} R \hat{m}_\ell^{1/2}, & U_{sh} &= \bar{W} \bar{H}, \end{aligned} \quad (1.24)$$

Here,  $\hat{m}_\ell$  and  $\hat{M}_h$  are diagonal matrices containing the light and heavy neutrino masses, respectively. Following [22], we assume that the measured masses and mixing of light neutrinos do not change considerably by the running from the neutrino mass scale to the seesaw scale.  $U_{\text{PMNS}}$  is a unitary matrix (See Eq. (1.4)), which would correspond to the PMNS neutrino mixing matrix when  $H \rightarrow I$ . The hermitian  $H$  and  $\bar{H}$  matrices are defined

by:

$$H = \left( I + \hat{m}_\ell^{1/2} R^\dagger \hat{M}_h^{-1} R \hat{m}_\ell^{1/2} \right)^{-1/2} \quad (1.25)$$

$$\bar{H} = \left( I + \hat{M}_h^{-1/2} R \hat{m}_\ell R^\dagger \hat{M}_h^{-1/2} \right)^{-1/2} . \quad (1.26)$$

These can be understood as describing departures from unitarity in  $U_{a\ell}$  and  $U_{sh}$ , respectively. Finally, the complex orthogonal matrix  $R$  is parametrized as:

$$R = \begin{pmatrix} \tilde{c}_{45} & \tilde{s}_{45} & 0 \\ -\tilde{s}_{45} & \tilde{c}_{45} & 0 \\ 0 & 0 & 1 \end{pmatrix} \begin{pmatrix} \tilde{c}_{46} & 0 & -\tilde{s}_{46} \\ 0 & 1 & 0 \\ \tilde{s}_{46} & 0 & \tilde{c}_{46} \end{pmatrix} \begin{pmatrix} 1 & 0 & 0 \\ 0 & \tilde{c}_{56} & \tilde{s}_{56} \\ 0 & -\tilde{s}_{56} & \tilde{c}_{56} \end{pmatrix} . \quad (1.27)$$

where  $\tilde{s}_{ij}$  and  $\tilde{c}_{ij}$  are the sines and cosines of a complex angle,  $\rho_{ij} + i\gamma_{ij}$ . From this parametrization, one can rebuild the Dirac and Majorana masses appearing in Eq. (1.13):

$$M_D = -i U_{\text{PMNS}}^* H^* \hat{m}_\ell^{1/2} \left( \hat{m}_\ell R^\dagger + R^T \hat{M}_h \right) \hat{M}_h^{-1/2} \bar{H} \quad (1.28)$$

$$\approx -i U_{\text{PMNS}}^* H^* \hat{m}_\ell^{1/2} R^T \hat{M}_h^{1/2} \bar{H} , \quad (1.29)$$

$$M_R = \bar{H}^* \left( \hat{M}_h - \hat{M}_h^{-1/2} R^* \hat{m}_\ell^2 R^\dagger \hat{M}_h^{-1/2} \right) \bar{H} . \quad (1.30)$$

The unitary  $\bar{W}$  matrix allows for redefinitions of the sterile basis, and in this work will be set to  $\bar{W} = I$ . For more details about the parameterization see the Appendix A.

# ONE LOOP CORRECTIONS TO NEUTRINO MASS IN THE $\nu_R$ STANDARD MODEL EXTENSION

In the work we are considering three RH neutrinos, with light neutrinos getting masses from the Seesaw mechanism. We will see that, loop corrections to masses can affect their values significantly. What is of importance in this particular case is that non-zero elements are produced in the LL sector of  $M_\nu^{\text{tree}}$ , which was previously prohibited by the Standard Model. The loop-corrected neutrino mass matrix is  $M_\nu^{\text{full}} = M_\nu^{\text{tree}} + \delta M_\nu$ , where:

$$\delta M_\nu = \begin{pmatrix} \delta M_L & \delta M_D \\ \delta M_D^T & \delta M_R \end{pmatrix} \quad (2.1)$$

The light neutrino masses including loop corrections can be obtained by:

$$M_{\text{light}}^{\text{full}} = M_{\text{light}}^{\text{tree}} + \delta M_L - \delta M_D M_R^{-1} M_D^T - M_D M_R^{-1} \delta M_D^T + M_D M_R^{-1} \delta M_R M_R^{-1} M_D^T \quad (2.2)$$

Although we have written  $\delta M_D$ ,  $\delta M_R$  and  $\delta M_L$  on the “active-sterile” basis, in the following these will be calculated on the neutrino mass basis. For this we need to the general expression for Self-Energy [30], [32]:

$$\Sigma(p) = A_L(p^2) \not{p} P_L + A_R(p^2) \not{p} P_R + B_L(p^2) P_L + B_R(p^2) P_R, \quad (2.3)$$

where  $p$  is the neutrino momentum. We will take  $p^2$  to be negligible. The coefficients  $A_{L,R}$  and  $B_{L,R}$  follow:

$$A_L = A_L^\dagger \quad A_R = A_R^\dagger \quad B_R = B_L^\dagger \quad (2.4)$$



If the Majorana condition in Eq. (1.10) is considered [33], [34], we must require:

$$\Sigma(p) = C (\Sigma(p))^T C^{-1} \quad (2.5)$$

where  $C$  is the Charge Conjugation Operator. This implies:

$$A_L = A_R^T \quad B_L = B_L^T \quad B_R = B_R^T \quad (2.6)$$

In the calculation of the corrections, as seen in [30], [35], [36], we will only consider the contributions to the term  $B_L$ . Given the conditions imposed in Eq. (2.5) the contributions to  $B_R$  lead to the same result. The terms  $B_{L,R}$  are related to contributions to mass [32], [37] and therefore are the part that interests us. On the other hand,  $A_{L,R}$  is related to corrections to the kinetic terms [33], in other words, to wave-function renormalization. These will be taken into account primarily when higher-order loops are included.

The one loop calculations in the active-sterile basis can be obtained from the following expression[38]:

$$\delta M_\nu = U^* B_L U^\dagger. \quad (2.7)$$

Each part of the tree-level neutrino mass matrix receives some correction, so we can express these as follows:

$$(\delta M_L)_{aa'} = \sum_{(i,j)} U_{ai}^* (B_L)_{ij} U_{a'j}^* \quad (2.8)$$

$$(\delta M_D)_{as} = \sum_{(i,j)} U_{ai}^* (B_L)_{ij} U_{sj}^* \quad (2.9)$$

$$(\delta M_R)_{ss'} = \sum_{(i,j)} U_{si}^* (B_L)_{ij} U_{s'j}^*. \quad (2.10)$$

Our objective in the next sections is calculate  $B_L$ . The contributions come mainly from the neutral scalar ( $H$ ),  $Z^0$  and Goldstone bosons ( $G^0, G^\pm$ ). The diagrams with the  $W^\pm$  boson will not be taken into account because they only contribute to  $A_L$  or  $A_R$  [37]. In the next sections we will describe the contributions to each part of the neutrino mass matrix.

## 2.1 $Z^0$ Boson Contribution

We illustrate the interaction Lagrangian of the  $Z$  boson with the neutrinos on the mass basis to derive the equations for a loop in this case. In addition, as a notation that will

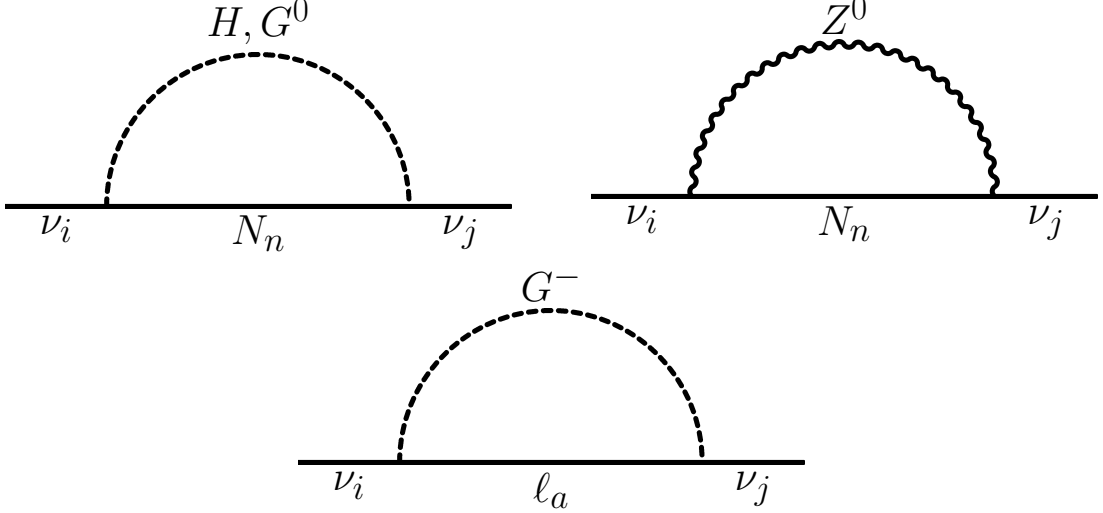


Figure 2.1: One Loop Diagrams in the  $\nu_R$ SM. Top panel: contributions from the neutral Higgs, Goldstone, and  $Z^0$  boson. Lower panel: Contributions from charged Goldstone boson (where  $\ell_a$  is the charged lepton).

be used throughout the rest of the work,  $g_2$  is the gauge coupling constant of the  $SU(2)_L$  group, and  $c_W$  as is the cosine of the Weinberg angle:

$$-\mathcal{L}_\nu^Y \supset \frac{g_2}{2c_W} \bar{\nu}_i \gamma^\mu \left[ P_L U_{ai}^* U_{aj} - P_R U_{ai} U_{aj}^* \right] N_j Z_\mu \quad (2.11)$$

In the upper right panel of Fig. 2.1, we find the diagram mediated by the  $Z^0$  boson. In the following, we will work on the Feynman gauge,  $\xi = 1$ . The full self-energy can be written:

$$-i\Sigma_{ij}^{Z^0} = \sum_{n,a,a'} \int \frac{d^d k}{(2\pi)^d} \left( \frac{ig_2}{2c_W} \right) \gamma^\mu (P_L U_{ai}^* U_{an} - P_R U_{ai} U_{an}^*) (S_F)_n \times \left( \frac{ig_2}{2c_W} \right) \gamma^\nu (P_L U_{a'n}^* U_{a'j} - P_R U_{a'n} U_{a'j}^*) S_{\mu\nu} \quad (2.12)$$

where  $P_L$  and  $P_R$  are the chirality projectors and  $S_F$ ,  $S_{\mu\nu}$  are the fermion and  $Z^0$  boson propagators respectively.

To start, let us define the loop integral in  $d$  dimensions using the function  $I$  as follows:

$$I(M^2, m^2) = \int \frac{d^d k}{(2\pi)^d} \frac{Q^\varepsilon}{(q^2 - M^2 + i\epsilon)(k^2 - m^2 + i\epsilon)} \quad (2.13)$$

We use  $d = 4 - \varepsilon$  in this scheme, where  $Q$  is the renormalization scale and  $q = p - k$  is the momentum of the particles in the boson line.

If we substitute the expressions for the propagators, we can write the loop function  $I(M_{Z^0}^2, m_n^2)$ , where  $M_{Z^0}$  and  $m_n$  are the boson  $Z^0$  and neutrino mass respectively. The

self-energy that is proportional to  $\not{p}$  is not of our interest because it gives contributions to the  $A_{L,R}$  terms in Eq. (2.3). With that, we can write:

$$-i\Sigma_{ij}^{Z^0} \supset i \left( \frac{g_2}{2c_W} \right)^2 \sum_{n,a,a'} \gamma^\mu (P_L U_{ai}^* U_{an} - P_R U_{ai} U_{an}^*) m_n \times \gamma^\nu (P_L U_{a'n}^* U_{a'j} - P_R U_{a'n} U_{a'j}^*) g_{\mu\nu} I(M_{Z^0}^2, m_n^2). \quad (2.14)$$

This can be simplified applying  $\gamma^\mu \gamma_\mu = d$ , where  $d$  is the number of space-time dimensions. As we mentioned before, to calculate  $\Sigma$  we only need  $B_L$ , according to Eq. (2.3), so:

$$(B_L^{Z^0})_{ij} = \frac{ig_2^2}{4c_W^2} \sum_{n,a,a'} U_{ai} U_{an}^* m_n dI(M_{Z^0}^2, m_n^2) U_{a'n}^* U_{a'j}, \quad (2.15)$$

The solution of this integral  $I$  is evaluated by the dimensional regularization ( See Appendix B), leading to:

$$(B_L^{Z^0})_{ij} = \frac{g_2^2}{16\pi^2 c_W^2} \sum_n C_{in}^* m_n \left( \tilde{k} - \frac{1}{2} + \ln \frac{m_n^2}{Q^2} + \left( \frac{m_n^2}{M_{Z^0}^2} - 1 \right)^{-1} \ln \frac{m_n^2}{M_{Z^0}^2} \right) C_{nj} \quad (2.16)$$

where  $\tilde{k} = \frac{2}{\epsilon} - \ln 4\pi + \gamma_E$ . In order to simplify our expressions we define the mixings product as  $C_{ij} = \sum_a U_{ai}^* U_{aj}$ . We can calculate  $\delta M_L$  using the Eq. (2.8)

$$(\delta M_L^{Z^0})_{aa'} = \sum_{ij} U_{ai}^* (B_L^{Z^0})_{ij} U_{a'j} \quad (2.17)$$

$$= \frac{g_2^2}{16\pi^2 c_W^2} \sum_n U_{an}^* m_n \left( \tilde{k} - \frac{1}{2} + \ln \frac{m_n^2}{Q^2} + \left( \frac{m_n^2}{M_{Z^0}^2} - 1 \right)^{-1} \ln \frac{m_n^2}{M_{Z^0}^2} \right) U_{a'n} \quad (2.18)$$

In Eq. (2.18), we cancel the divergence  $\tilde{k}$  and the factor  $-1/2$  using the properties of the mixing matrices, see Eq. (1.16). We can simplify this expression even further by eliminating the term  $\ln(m_n^2/Q^2)$  through the addition/subtraction of  $\ln(m_n^2/M_{Z^0}^2)$ . If we do this, we can express Eq. (2.18) as:

$$(\delta M_L^{Z^0})_{aa'} = \frac{g_2^2}{16\pi^2 c_W^2} \sum_n U_{an}^* \frac{m_n^3}{M_{Z^0}^2} \left( \frac{m_n^2}{M_{Z^0}^2} - 1 \right)^{-1} \ln \frac{m_n^2}{M_{Z^0}^2} U_{a'n}, \quad (2.19)$$

which can be written in terms of  $Y_\nu$  using Eq. (1.19) with  $c_W^2 = g_2/\sqrt{g_2^2 + g_1^2}$  and  $M_{Z^0} = (v_{\text{SM}}/2)\sqrt{g_2^2 + g_1^2}$ :

$$(\delta M_L^{Z^0})_{aa'} = \frac{1}{8\pi^2} \sum_{n,s,s'} (Y_\nu^*)_{as} U_{sn} m_n \left( \frac{m_n^2}{M_{Z^0}^2} - 1 \right)^{-1} \ln \frac{m_n^2}{M_{Z^0}^2} (Y_\nu^*)_{a's'} U_{s'n} \quad (2.20)$$

We can see the suppression with two Yukawa couplings ( $Y_\nu^2$ ), meaning this is comparable to  $M_{\text{light}}^{\text{tree}}$ .

As we have commented before, the neutrino mass matrix does not only receive corrections to the LL sector. It is possible to also calculate the contributions to the Left-Right and Right-Right part of  $M_\nu^{\text{tree}}$ . For  $\delta M_D$ ,

$$(\delta M_D^{Z^0})_{as} = \sum_{i,j} U_{ai}^* (B_L^{Z^0})_{ij} U_{sj}^* \quad (2.21)$$

$$= \frac{ig^2}{2c_W^2} \sum_{n,i,j} U_{ai}^* C_{in}^* m_n d I(M_{Z^0}^2, m_n^2) C_{nj} U_{sj}^* \quad (2.22)$$

$$= 0 \quad (2.23)$$

Finally, we complement these results with the expression for  $\delta M_R^{Z^0}$ ,

$$(\delta M_R^{Z^0})_{ss'} = \sum_{i,j} U_{si}^* (B_L^{Z^0})_{ij} U_{s'j}^* \quad (2.24)$$

$$= \frac{ig^2}{2c_W^2} \sum_{n,i,j} U_{si}^* C_{in}^* m_n d I(M_{Z^0}^2, m_n^2) C_{nj} U_{s'j}^* \quad (2.25)$$

$$= 0 \quad (2.26)$$

Happily we will not work too much because in both cases zero is obtained as a final result due to the condition of the product of the mixing matrices  $U_{aj}$  and  $U_{sj}$  in Eq. (1.18).

## 2.2 Neutral Scalar Contribution

The  $Z^0$  propagator can be written in the  $R_\xi$  gauge as seen in Eq. (B.1). If we choose especially the Feynman gauge ( $\xi = 1$ ) the propagator becomes very simple, however new considerations must be taken into account. When Goldstone bosons emerge, despite being unphysical states, as virtual particles they can interact like other particles. The new  $G^0$  implies new contributions to the processes at one loop and they will be present in our calculations.

In the upper left panel of Fig. 2.1, we find the loop diagram with the neutral scalar particles, Higgs ( $H$ ) and Goldstone Boson ( $G^0$ ). Firstly we will calculate the contribution from the Higgs Boson, in this context we present the interaction Lagrangian of the neutral

scalars in the following expression:

$$\begin{aligned}
-\mathcal{L}_\nu^Y \supset & \frac{1}{2} \bar{\nu}_i P_R \left[ U_{ai}^*(Y_\nu)_{as} U_{sj}^* + U_{si}^*(Y_\nu)_{as} U_{aj}^* \right] N_j \phi_0^* \\
& + \frac{1}{2} \bar{\nu}_i P_L \left[ U_{si}(Y_\nu^*)_{as} U_{aj} + U_{ai}(Y_\nu^*)_{as} U_{sj} \right] N_j \phi_0
\end{aligned} \tag{2.27}$$

If we define  $\Lambda_{ij}$  as:

$$\Lambda_{ij} = \sum_{a,s} U_{si}(Y_\nu^*)_{as} U_{aj} + U_{ai}(Y_\nu^*)_{as} U_{sj}, \tag{2.28}$$

with this we can write the self-energy as:

$$-i\Sigma_{ij}^H = \sum_n \int \frac{d^d k}{(2\pi)^d} \left( \frac{i}{\sqrt{2}} \right) \Lambda_{in} (S_F)_n \left( \frac{i}{\sqrt{2}} \right) \Lambda_{nj} S_H \tag{2.29}$$

where  $S_F$  and  $S_H$  are the Fermion and Higgs propagators respectively. Our objective is to calculate the Higgs contribution to  $B_L$ , so we follow the same procedure that was done for  $B_L^{Z^0}$ :

$$(B_L^H)_{ij} = \frac{i}{2} \sum_n \Lambda_{in} m_n I(M_H^2, m_n^2) \Lambda_{nj}, \tag{2.30}$$

where  $M_H$  is the mass of SM Higgs Boson and  $I(M_H^2, m_n^2)$  is defined in the Eq. (2.13).

Solving the loop integral gives:

$$(B_L^H)_{ij} = \frac{1}{32\pi^2} \sum_n \Lambda_{in} m_n \left[ \tilde{k} - 1 + \ln \frac{m_n^2}{Q^2} + \left( \frac{m_n^2}{M_H^2} - 1 \right)^{-1} \ln \frac{m_n^2}{M_H^2} \right] \Lambda_{nj}. \tag{2.31}$$

For the Goldstone loop diagram the contribution is obtained using the interaction vertex  $\Lambda_{ij} \rightarrow -i\Lambda_{ij}$  in Eq. (2.29) and changing the propagator  $S_H$  to  $S_{G^0}$ , this leads us to have:

$$(B_L^{G^0})_{ij} = -\frac{1}{32\pi^2} \sum_n \Lambda_{in} m_n \left[ \tilde{k} - 1 + \ln \frac{m_n^2}{Q^2} + \left( \frac{m_n^2}{M_{Z^0}^2} - 1 \right)^{-1} \ln \frac{m_n^2}{M_{Z^0}^2} \right] \Lambda_{nj} \tag{2.32}$$

The sum of the Higgs and Goldstone contributions algebraically cancels the divergence  $\tilde{k}$ . Due to the type of gauge used, this instance is a coincidence. For example, as described in [30], the Z boson, Goldstone, and scalar contributions are each gauge-dependent. In such instances, the Z and Goldstone contributions combined cancel the divergence, preserving the gauge invariance of  $\delta M_L^{Z+G^0}$ . The full neutral scalar contribution  $B_L$  is expressed as:

$$(B_L^{H+G^0})_{ij} = \frac{1}{32\pi^2} \sum_n \Lambda_{in} m_n \left[ \left( \frac{m_n^2}{M_H^2} - 1 \right)^{-1} \ln \frac{m_n^2}{M_H^2} - \left( \frac{m_n^2}{M_{Z^0}^2} - 1 \right)^{-1} \ln \frac{m_n^2}{M_{Z^0}^2} \right] \Lambda_{nj} \tag{2.33}$$

with this last result, we can calculate  $\delta M_L$  from the Eq. (2.8):

$$\begin{aligned}
(\delta M_L^{H+G^0})_{aa'} = & \frac{1}{32\pi^2} \sum_{n,i,j} U_{ai}^* \Lambda_{in} m_n \left[ \left( \frac{m_n^2}{M_H^2} - 1 \right)^{-1} \ln \frac{m_n^2}{M_H^2} \right. \\
& \left. - \left( \frac{m_n^2}{M_{Z^0}^2} - 1 \right)^{-1} \ln \frac{m_n^2}{M_{Z^0}^2} \right] \Lambda_{nj} U_{a'j}^* \tag{2.34}
\end{aligned}$$

Similar to Eq. (2.20), we can express the last relation as a function the Yukawa couplings where we again get a suppression of  $\mathcal{O}(Y_\nu^2)$ .

$$\begin{aligned}
(\delta M_L^{H+G^0})_{aa'} &= \frac{1}{32\pi^2} \sum_{n,s,s'} (Y_\nu^*)_{as} U_{sn} m_n \left[ \left( \frac{m_n^2}{M_H^2} - 1 \right)^{-1} \ln \frac{m_n^2}{M_H^2} \right. \\
&\quad \left. - \left( \frac{m_n^2}{M_{Z^0}^2} - 1 \right)^{-1} \ln \frac{m_n^2}{M_{Z^0}^2} \right] U_{s'n} (Y_\nu^*)_{a's'}
\end{aligned} \tag{2.35}$$

For  $\delta M_D$ , obtained from Eq. (2.9), the corrections from Higgs and Goldstone bosons are:

$$\begin{aligned}
(\delta M_D^{H+G^0})_{as} &= \frac{1}{32\pi^2} \sum_{n,i,j} U_{ai}^* \Lambda_{in} m_n \left[ \left( \frac{m_n^2}{M_H^2} - 1 \right)^{-1} \ln \frac{m_n^2}{M_H^2} \right. \\
&\quad \left. - \left( \frac{m_n^2}{M_{Z^0}^2} - 1 \right)^{-1} \ln \frac{m_n^2}{M_{Z^0}^2} \right] \Lambda_{nj} U_{sj}^* \tag{2.36} \\
&= \frac{1}{32\pi^2} \sum_{n,a',s'} (Y_\nu^*)_{as'} U_{s'n} m_n \left[ \left( \frac{m_n^2}{M_H^2} - 1 \right)^{-1} \ln \frac{m_n^2}{M_H^2} \right. \\
&\quad \left. - \left( \frac{m_n^2}{M_{Z^0}^2} - 1 \right)^{-1} \ln \frac{m_n^2}{M_{Z^0}^2} \right] U_{a'n} (Y_\nu^*)_{a's} \tag{2.37}
\end{aligned}$$

For the Higgs and neutral Goldstone contribution we have again a  $Y_\nu^2$  factor and additional  $U_{an}$  suppression. This indicates this term will be numerically smaller than the corresponding correction to  $\delta M_L$ . Finally, for  $\delta M_R$

$$\begin{aligned}
(\delta M_R^{H+G^0})_{ss'} &= \frac{1}{32\pi^2} \sum_{n,i,j} U_{si}^* \Lambda_{in} m_n \left[ \left( \frac{m_n^2}{M_H^2} - 1 \right)^{-1} \ln \frac{m_n^2}{M_H^2} \right. \\
&\quad \left. - \left( \frac{m_n^2}{M_{Z^0}^2} - 1 \right)^{-1} \ln \frac{m_n^2}{M_{Z^0}^2} \right] \Lambda_{nj} U_{s'j}^* \tag{2.38} \\
&= \frac{1}{32\pi^2} \sum_{n,a,a'} (Y_\nu^*)_{as} U_{an} m_n \left[ \left( \frac{m_n^2}{M_H^2} - 1 \right)^{-1} \ln \frac{m_n^2}{M_H^2} \right. \\
&\quad \left. - \left( \frac{m_n^2}{M_{Z^0}^2} - 1 \right)^{-1} \ln \frac{m_n^2}{M_{Z^0}^2} \right] U_{a'n} (Y_\nu^*)_{a's'} \tag{2.39}
\end{aligned}$$

Here, the suppression is of order  $(Y_\nu U_{an})^2$ , so this term is the smallest of them all.

## 2.3 Charged Scalar Contribution

With the Lagrangian for the charged part, we can write the appropriate vertices to construct the  $\Sigma$  function.

$$-\mathcal{L}_\nu^\pm \supset \bar{e}_a [P_R(Y_\nu)_{as} U_{si}^* - P_L(Y_e)_{aa} U_{ai}] \nu_i \phi^- - \bar{\nu}_i [P_L U_{si}(Y_\nu^*)_{as} - P_R U_{si}^*(Y_e^*)_{aa}] e_a \phi^+ \quad (2.40)$$

The self-energy due to the charged Goldstone boson is given by:

$$-i\Sigma_{ij}^- = \int \frac{d^d k}{(2\pi)^d} i [P_L U_{si}(Y_\nu^*)_{as} - P_R U_{ai}^*(Y_e^*)_{aa}] (S_F)_a i [P_R (Y_\nu)_{as'} U_{s'i}^* - P_L (Y_e)_{aa} U_{ai}] S_- \quad (2.41)$$

where  $S_F$  and  $S_-$  are the fermion and charged scalar propagators. It is easy to get  $B_L$

$$(B_L^-)_{ij} = -i \sum_{a,s} m_a [(Y_e)_{aa} U_{ai}(Y_\nu^*)_{as} U_{sj} + U_{si}(Y_\nu^*)_{as} (Y_e)_{aa} U_{aj}] I(M_W^2, m_a^2) \quad (2.42)$$

In the last expression,  $I(M_W^2, m_a^2)$  is the scalar loop function that has been defined in Eq. (2.13), where  $M_W$  and  $m_a = (v_{\text{SM}}/\sqrt{2})(Y_e)_{aa}$  are the  $W$  Boson and charged lepton masses respectively. Furthermore, with Eq. (1.19) and replacing the expression for the Yukawa coupling of the leptons we have the following:

$$\begin{aligned} (B_L^-)_{ij} &= -i \left( \frac{g}{\sqrt{2}M_W} \right)^2 \sum_a m_a^2 [U_{ai} U_{aj}^* m_j + U_{ai}^* U_{aj} m_i] I(M_W^2, m_a^2) \\ &= -\frac{g^2}{32\pi^2 M_W^2} \sum_a m_a^2 [U_{ai} U_{aj}^* m_j + U_{ai}^* U_{aj} m_i] \left( \tilde{k} - 1 + \ln \frac{m_a^2}{Q^2} + \left( \frac{m_a^2}{M_W^2} - 1 \right)^{-1} \ln \frac{m_a^2}{M_W^2} \right) \end{aligned} \quad (2.43)$$

For  $\delta M_L$ :

$$\begin{aligned} (\delta M_L^-)_{aa'} &= -\frac{g^2}{32\pi^2 M_W^2} \sum_{a'',i,j} U_{ai}^* m_{a''}^2 [U_{a''i} U_{a''j}^* m_j + U_{a''i}^* U_{a''j} m_i] \\ &\quad \times \left( \tilde{k} - 1 + \ln \frac{m_{a''}^2}{Q^2} + \left( \frac{m_{a''}^2}{M_W^2} - 1 \right)^{-1} \ln \frac{m_{a''}^2}{M_W^2} \right) U_{a'j}^* \quad (2.44) \\ &= -\frac{g^2}{32\pi^2 M_W^2} \sum_{i,j} \left[ m_i m_{a'}^2 U_{ai}^* U_{a'i} \left( \tilde{k} - 1 + \ln \frac{m_{a'}^2}{Q^2} + \left( \frac{m_{a'}^2}{M_W^2} - 1 \right)^{-1} \ln \frac{m_{a'}^2}{M_W^2} \right) \right. \\ &\quad \left. + m_j m_a^2 U_{aj}^* U_{a'j} \left( \tilde{k} - 1 + \ln \frac{m_a^2}{Q^2} + \left( \frac{m_a^2}{M_W^2} - 1 \right)^{-1} \ln \frac{m_a^2}{M_W^2} \right) \right] \end{aligned} \quad (2.45)$$

With this we get the structure  $\sum_i U_{ai}^* m_i U_{a'i} = 0$ , which leads us to have to  $(\delta M_L^-)_{aa'} = 0$ . Using Eq. (2.9) we get the contribution to  $\delta M_D$

$$\begin{aligned}
(\delta M_D^-)_{as} &= -\frac{g^2}{32\pi^2 M_W^2} \sum_{a',i,j} U_{ai}^* m_{a'}^2 [U_{a'i} U_{a'j}^* m_j + U_{a'i}^* U_{a'j} m_i] \\
&\quad \times \left( \tilde{k} - 1 + \ln \frac{m_{a'}^2}{Q^2} + \left( \frac{m_{a'}^2}{M_W^2} - 1 \right)^{-1} \ln \frac{m_{a'}^2}{M_W^2} \right) U_{sj}^* \\
&= -\frac{g^2}{32\pi^2 M_W^2} \sum_j m_a U_{aj}^* U_{sj}^* m_j \left( \tilde{k} - 1 + \ln \frac{m_a^2}{Q^2} + \left( \frac{m_a^2}{M_W^2} - 1 \right)^{-1} \ln \frac{m_a^2}{M_W^2} \right)
\end{aligned} \tag{2.46}$$

Rewriting this last expression including Yukawa couplings,

$$(\delta M_D^-)_{as} = -\frac{1}{16\pi^2} m_a (Y_e)_{aa} \left( \tilde{k} - 1 + \ln \frac{m_a^2}{Q^2} + \left( \frac{m_a^2}{M_W^2} - 1 \right)^{-1} \ln \frac{m_a^2}{M_W^2} \right) (Y_\nu^*)_{as} \tag{2.47}$$

The charged Goldstone contribution is suppressed by  $(Y_e Y_\nu)$  factor, so in principle can be numerically relevant, particularly for  $a = \tau$ . Nevertheless it can be ignored, as it is always included with an additional  $Y_\nu$  (See Eq. 2.2).

We can calculate the  $\delta M_R$  expression

$$\begin{aligned}
(\delta M_R^-)_{ss'} &= -\frac{g^2}{32\pi^2 M_W^2} \sum_{a,i,j} U_{si}^* m_a^2 [U_{ai} U_{aj}^* m_j + U_{ai}^* U_{aj} m_i] \\
&\quad \times \left( \tilde{k} - 1 + \ln \frac{m_a^2}{Q^2} + \left( \frac{m_a^2}{M_W^2} - 1 \right)^{-1} \ln \frac{m_a^2}{M_W^2} \right) U_{s'j}^*
\end{aligned} \tag{2.48}$$

$$(\delta M_R^-)_{ss'} = 0 \tag{2.49}$$

Finally, we quantify the contribution from the charged Goldstone boson. Since this affects  $M_D$ , it is necessary to specify how we renormalize the fields and couplings. If we denote the diagonalized mass matrix at tree level by  $M_\nu^{\text{diag}}$ , the renormalized self-energy  $\tilde{\Sigma}$  is:

$$\begin{aligned}
\tilde{\Sigma}(p) &= \Sigma(p) - \frac{1}{2}(\delta_\nu + \delta_\nu^\dagger) \not{p} P_L - \frac{1}{2}(\delta_\nu^* + \delta_\nu^T) \not{p} P_R \\
&\quad + \left( \delta m + \frac{1}{2} M_\nu^{\text{diag}} \delta_\nu + \frac{1}{2} \delta_\nu^T M_\nu^{\text{diag}} \right) P_L + \left( \delta m + \frac{1}{2} M_\nu^{\text{diag}} \delta_\nu + \frac{1}{2} \delta_\nu^T M_\nu^{\text{diag}} \right)^* P_R,
\end{aligned} \tag{2.50}$$

Here,  $\delta_\nu$  and  $\delta m$  are the field strength and mass counterterms:

$$M_\nu^{\text{diag}} = \tilde{M}_\nu^{\text{diag}} + \delta m \tag{2.51}$$

$$\begin{pmatrix} \nu_\ell \\ N_h \end{pmatrix}_L = \left( 1 + \frac{1}{2} \delta_\nu \right) \begin{pmatrix} \tilde{\nu}_\ell \\ \tilde{N}_h \end{pmatrix}_L \tag{2.52}$$



We follow the  $\overline{\text{MS}}$  prescription, which effectively removes the  $\tilde{k}$  divergence in Eq. (2.47). Inspecting this equation, we find a correction to  $M_D$  that does not explicitly depend on the heavy neutrino masses, but does depend on  $Y_\nu$ . Thus, if the latter are enhanced, these contributions could be large, and would not be avoided by taking degenerate masses.

We will show that this is not the case. As reported earlier, we expect this correction to affect light neutrino masses via the following term:

$$\begin{aligned}
& - \left( \delta M_D^- M_R^{-1} M_D^T + M_D M_R^{-1} \delta M_D^{-T} \right)_{aa'} \\
& \approx - \frac{g}{16\pi^2 \sqrt{2}} (Y_e)_{aa} \frac{m_a}{M_W} \left[ \ln \frac{m_a^2}{Q^2} + \left( \frac{m_a^2}{M_W^2} - 1 \right)^{-1} \ln \frac{m_a^2}{M_W^2} - 1 \right] \left( U_{\text{PMNS}}^* \hat{m}_\ell U_{\text{PMNS}}^\dagger \right)_{aa'} + (a \leftrightarrow a')
\end{aligned} \tag{2.53}$$

where we have used Eqs. (1.28) and (1.30), with the approximation where  $H = \bar{H} = I$ , and neglected light neutrino masses in front of the heavy ones. Thus, we find that the charged Goldstone contribution is proportional to light neutrino masses, and thus under control. We have checked numerically that this is the case, by adding  $\delta M_D^-$  to the full neutrino mass matrix, and diagonalizing.

Each contribution has now been described analytically. Out of all of these, we are primarily interested in  $\delta M_L$ . With what we have found, in the following section we will attempt to explain how these contributions affect the masses of light neutrinos.

## 2.4 Numerical Evaluation

Since in Eq. (2.2) only terms up to  $\mathcal{O}(Y_\nu^2)$  are included, the most important terms are:

$$M_\nu^{\text{full}} = M_\nu^{\text{tree}} + \left( \delta M_L^{Z^0} + \delta M_L^{H+G^0} \right) - \left( \delta M_D^- M_R^{-1} M_D^T + M_D M_R^{-1} \delta M_D^{-T} \right) \tag{2.54}$$

As we have seen, the  $\delta M_D^-$  term has an additional  $Y_e$  suppression (See Eq. (2.47)), so it can be neglected. The total contribution to the active-active region of the full neutrino mass matrix is given by the sum of  $\delta M_L^{Z^0}$  and  $\delta M_L^{H+G^0}$ .

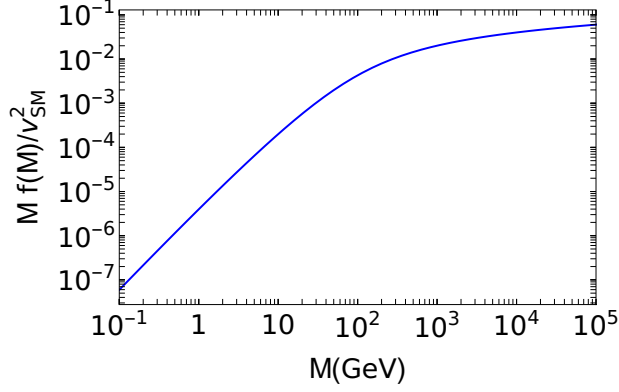


Figure 2.2: Dependence of loop function, conveniently normalized, with respect to  $v_{\text{SM}}^2/M$ .

$$\begin{aligned}
 (\delta M_L^{Z^0+H+G^0})_{aa'} &= \frac{1}{32\pi^2} \sum_{n,s,s'} (Y_\nu)_{as}^* U_{sn} m_n \left[ \left( \frac{m_n^2}{M_H^2} - 1 \right)^{-1} \ln \frac{m_n^2}{M_H^2} \right. \\
 &\quad \left. + 3 \left( \frac{m_n^2}{M_{Z^0}^2} - 1 \right)^{-1} \ln \frac{m_n^2}{M_{Z^0}^2} \right] U_{s'n} (Y_\nu)_{a's'}^*
 \end{aligned} \tag{2.55}$$

We define the loop function as:

$$f(m_n) = \frac{m_n}{16\pi^2} \left[ \left( \frac{m_n^2}{M_H^2} - 1 \right)^{-1} \ln \frac{m_n^2}{M_H^2} + 3 \left( \frac{m_n^2}{M_{Z^0}^2} - 1 \right)^{-1} \ln \frac{m_n^2}{M_{Z^0}^2} \right] \tag{2.56}$$

The function  $f(M)$  normalized by the factor  $v_{\text{SM}}^2/M$  is dependent on the mass of the heavy neutrino as we can see in Figure 2.2<sup>1</sup>. The behavior of this function is increasing with the mass, around  $M \sim 100$  GeV there is a change in the slope of the curve. The growth is caused by logarithms in Eq. (2.56), and the factors that accompany these change the slope of the curve.

The total contribution taking the heavy states can be written as :

$$(\delta M_L^{Z^0+H+G^0})_{aa'} \approx \frac{1}{2} \sum_{h,s,s'} (Y_\nu)_{as}^* U_{sh} f(m_h) U_{s'h} (Y_\nu)_{a's'}^* \tag{2.57}$$

Let us now understand how the  $\delta M_L$  loop corrections affect light neutrino eigenvalues. We shall take a specific choice of parameters for Eq. (1.27), in the case of normal ordering of light neutrino masses. By taking only  $\rho_{56}$ ,  $\gamma_{56}$  different from zero, and  $\gamma_{56}$  relatively large,

<sup>1</sup>This normalization factor comes from a typical seesaw, so the comparison of this loop function would apparently indicate the variation with respect to the tree-level light neutrino masses.

we can write the  $U_{ah}$  mixing as [26], [39]:

$$U_{a4} = i (U_{\text{PMNS}})_{a1} \sqrt{\frac{m_1}{M_4}} \quad (2.58)$$

$$U_{a5} = z_{56} Z_a \sqrt{\frac{m_3}{M_5}} \cosh \gamma_{56} e^{i z_{56} \rho_{56}} \quad (2.59)$$

$$U_{a6} = i Z_a \sqrt{\frac{m_3}{M_6}} \cosh \gamma_{56} e^{i z_{56} \rho_{56}} \quad (2.60)$$

$$Z_a = (U_{\text{PMNS}})_{a3} + i z_{56} \sqrt{\frac{m_2}{m_3}} (U_{\text{PMNS}})_{a2} \quad (2.61)$$

Here,  $z_{56}$  is the sign of  $\gamma_{56}$ , and we have approximated  $H = \bar{H} = I$ . The Yukawa coupling in this approximation takes the following expression  $Y_\nu^* = U_{ah}^* M_h / v_{\text{SM}}$ . We see that both  $U_{a5}$  and  $U_{a6}$  can be enhanced [40]–[42], in this case by a factor  $\cosh \gamma_{56}$ , while  $U_{a4}$  remains small. Thus, by taking a very large  $M_4$  we can decouple this heavy neutrino, leaving us with an effective  $3 + 2$  seesaw model. Note that this possibility of enhancing the active-heavy mixing while keeping acceptable light neutrino masses can be attributed to a slightly broken lepton number symmetry [43]–[45]. Combining Eqs. (2.59) and (2.60) with Eqs. (1.28) and (1.30), the full neutrino mass matrix can be reconstructed at tree-level as [1]:

$$M_\nu = \begin{pmatrix} 0 & M_D & \varepsilon \\ M_D^T & \mu' & M_R \\ \varepsilon^T & M_R & \mu \end{pmatrix} \quad (2.62)$$

For the  $3+2$  model, one can look for certain configurations of the mass matrix in order to be able to achieve some experimentally verifiable process. These configurations are usually called textures and they depend on the Lepton Number Violation (LNV) parameters,  $\mu$ ,  $\mu'$  and  $\varepsilon$ . If  $\mu = \mu' = 0$ , it leads to the familiar Linear Seesaw [46]. Setting  $\varepsilon = \mu' = 0$  yields the Inverse Seesaw [47], [48]. As seen in [1], the parameters  $\mu, \mu'$  contribute to the splitting of heavy states.

Neglecting the contribution of  $N_4$ , we have:

$$U_{a5}^* U_{a'5}^* = z_{56}^2 \frac{m_3}{M_5} Z_a^* Z_{a'}^* \cosh^2 \gamma_{56} e^{-2i z_{56} \rho_{56}} \quad (2.63)$$

$$U_{a6}^* U_{a'6}^* = -\frac{m_3}{M_6} Z_a^* Z_{a'}^* \cosh^2 \gamma_{56} e^{-2i z_{56} \rho_{56}} \quad (2.64)$$

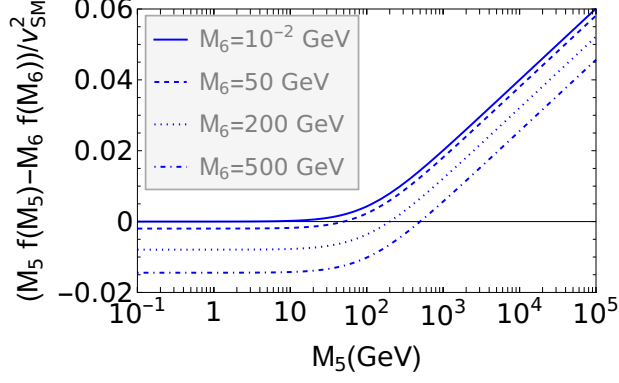


Figure 2.3: Flavour-independent behaviour of  $\delta M_L$  on  $M_5$ , fixing  $M_6$  for different values.

$$\begin{aligned}
(\delta M_L^{Z^0+H+G^0})_{aa'} &\approx \frac{1}{v_{\text{SM}}^2} (U_{a5}^* f(m_5) m_5^2 U_{a'5}^* + U_{a6}^* f(m_6) m_6^2 U_{a'6}^*) \\
&= \frac{m_3}{v_{\text{SM}}^2} Z_a^* Z_{a'}^* [M_5 f(M_5) - M_6 f(M_6)] \cosh^2 \gamma_{56} e^{-2iz_{56}\rho_{56}}
\end{aligned}
\tag{2.65}$$

In Eq. (2.65), the flavor structure is contained in the  $Z_a Z_{a'}$  term, we also note that the term in the square brackets is dependent on the mass of heavy neutrinos. The hyperbolic cosine is a term that enhances the correction, leading to very large matrix elements.

We show in Fig. 2.3 the full mass dependence of the loop correction, that is, the term in square brackets of Eq. (2.65), normalized with respect to  $v_{\text{SM}}^2$ . We fix  $M_6 = \{10^{-2}, 50, 200, 500\}$  GeV, and vary  $M_5$ . For lower  $M_5$ , the contribution from  $N_6$  dominates, and the curve is flat and negative. For larger masses, the contribution from  $N_5$  is more significant, leading to a change in sign. We find a well-known cancellation whenever  $M_5 = M_6$ . Thus, unless the masses are degenerate, the loop correction will be dominated by the heaviest neutrino with couplings enhanced by  $\gamma_{56}$ .

In Fig. 2.4, we show the matrix elements for  $\gamma_{56} = 5$ , fixing  $M_6 = \{10^{-1}, 10^3\}$  GeV. In the upper panels, with small  $M_6$ , we find that the matrix elements exhibit values close to zero for small values of  $M_5$ . The slopes of each curve undergo a noticeable change around  $M_6 \sim 100$  GeV, followed by a substantial increase. As evident in Eq. (2.65), in this scenario, the dominance of the term  $M_5 f_5$  arises from the negligible value of  $M_6$ . The corrections are somewhat larger for the  $\mu$  and  $\tau$  flavors, which are attributed to the smaller  $Z_e$ . In the lower panels, which take a larger value of  $M_6$ , each curve is initially

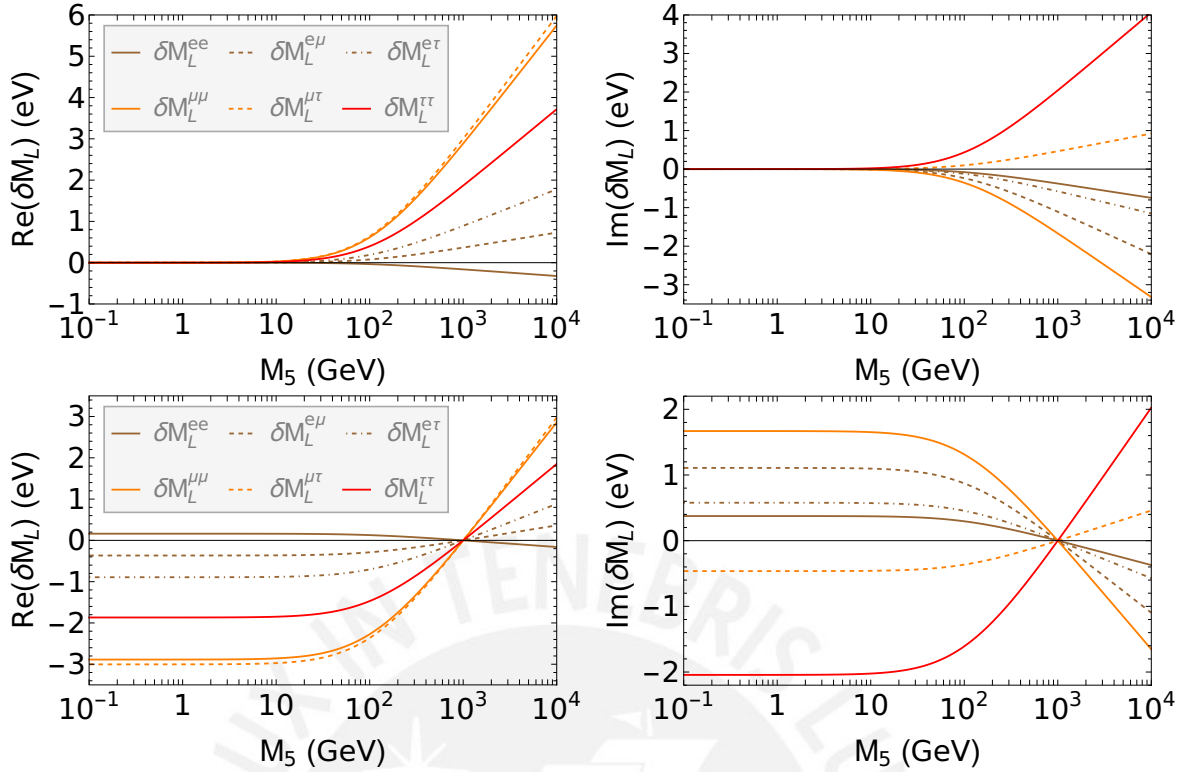


Figure 2.4: Real (left) and imaginary (right) part of the matrix elements of  $\delta M_L$ , setting  $\gamma_{56} = 5$ . The upper(lower) panels have  $M_6 = 10^{-1}(10^3)$  GeV.

flat but nonzero, and once again, the change in slope occurs around the same value as in the upper panel. Moreover, there is a cancellation of the contribution that arises from the term within the brackets in Eq. (2.65).

Let us now add the loop correction to the neutrino mass matrix and find the eigenvalues corresponding to the lightest neutrinos.

The eigenvalue dependence on  $\gamma_{56}$  is shown in the Upper and Lower panels of Figure 2.5, allowing only  $M_5$  or  $M_6$  to be large, and fixing the other mass at 100 MeV. In both panels we find that the two largest tree-level eigenvalues are affected by the loop corrections. For large  $M_5$  (upper panels), we see that an increase in  $\gamma_{56}$  generates a distancing between the second and third mass eigenvalues. The second eigenvalue eventually becomes smaller than the first one, switching places. The situation is similar for large  $M_6$  (lower panels). Here, increasing  $\gamma_{56}$  leads the second and third eigenvalues to initially decrease their splitting, intersecting, and then spreading apart.

As can be observed, varying  $\gamma_{56}$  beyond a certain threshold causes the eigenvalues for the masses of light neutrinos ( $m_i$ ) to be excessively large in comparison to the value at

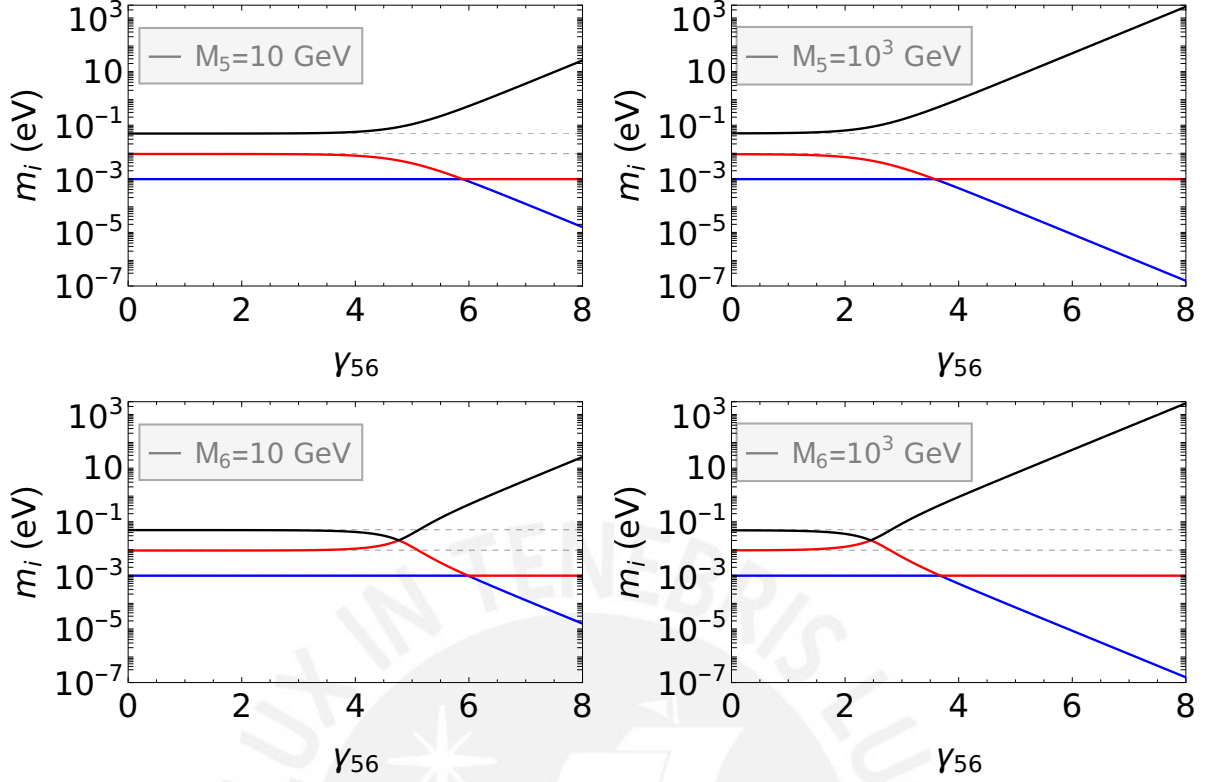


Figure 2.5: The light mass behaviour respect to variation of  $\gamma_{56}$ , for fixed heavy masses. The dashed gray horizontal lines denote the neutrino masses at tree level. Largest, intermediate and smallest eigenvalues are shown in black, red and blue, respectively.

the tree-level. This is an undesirable situation, meaning that in order to reproduce the observed neutrino masses, one would need to tune the three-level masses so that they cancel part of the loop correction.

In Figure 2.6, the light neutrino masses are shown by varying  $M_5$ , fixing  $\gamma_{56}$  to different values, and  $M_6 = \{10^{-1}, 10^2, 10^3\}$  GeV. In the left column, we fix  $\gamma_{56} = 2$ , in the small mass range of  $M_5$ , the corrections do not considerably affect the tree-level values, as seen in the upper and middle panels for  $M_6 = 10^{-1}$  and  $10^2$  GeV respectively. A small difference is seen for  $M_6 = 10^3$  GeV, mainly in  $m_2$  and  $m_3$ . For large values of  $M_5$ , it can be seen that the behavior of the eigenvalues  $m_2$  and  $m_3$  departs from the tree-level values and is therefore slightly affected by the quantum corrections. In the right column, when  $\gamma_{56} = 8$ , the corrections affect the eigenvalues substantially, increasing and decreasing in some cases. We can also see the evident cancellation for specific values of  $M_6$ .

Given the large corrections in  $\delta M_L$ , it is possible to put bounds on  $\gamma_{56}$ . If this is possible then we can extract limits on the mixings, in this case  $|U_{ah}|^2$  for a given mass of

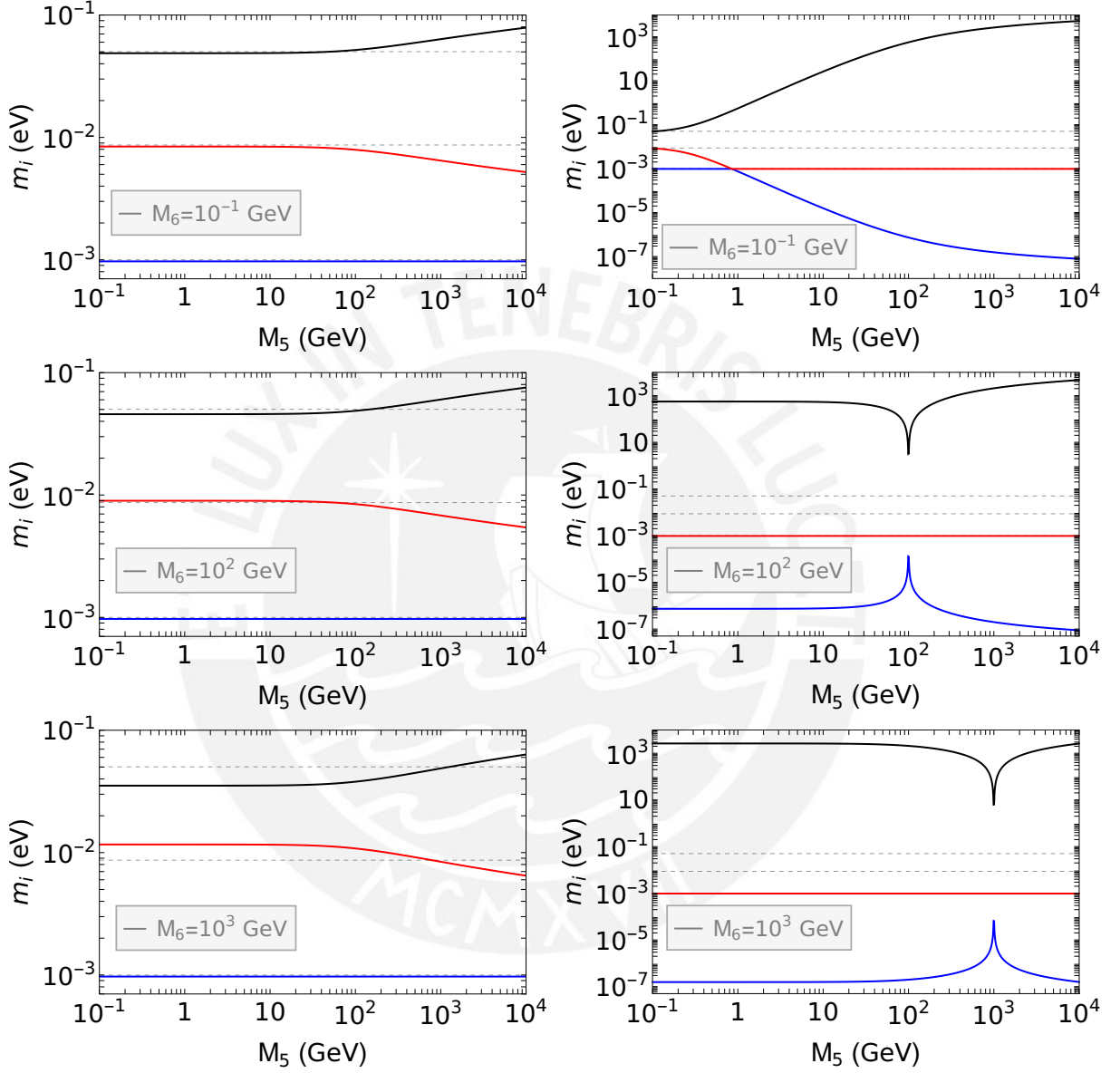


Figure 2.6: The blue, red and black lines represent the eigenvalues  $m_1$ ,  $m_2$  and  $m_3$  respectively for  $\gamma_{56} = 2$  (Left column) and  $\gamma_{56} = 8$  (Right column). The dashed horizontal lines represent the masses of light neutrinos at tree level.

$M_6$ (GeV)	$M_5$ (GeV)	$\gamma_{56}$	$ U_{e5} ^2$	$ U_{\mu5} ^2$	$ U_{\tau5} ^2$
10	1	6.59	$4.89 \times 10^{-7}$	$3.99 \times 10^{-6}$	$3.31 \times 10^{-6}$
	500	2.49	$2.69 \times 10^{-13}$	$2.15 \times 10^{-12}$	$1.79 \times 10^{-12}$
	$10^3$	2.32	$9.72 \times 10^{-14}$	$7.74 \times 10^{-13}$	$6.45 \times 10^{-13}$
100	1	2.94	$3.30 \times 10^{-10}$	$2.68 \times 10^{-9}$	$2.23 \times 10^{-9}$
	500	2.67	$3.82 \times 10^{-13}$	$3.08 \times 10^{-12}$	$2.57 \times 10^{-12}$
	$10^3$	2.45	$1.24 \times 10^{-13}$	$9.93 \times 10^{-13}$	$8.28 \times 10^{-13}$

Table 2.1: Maximum values of  $\gamma_{56}$  and  $U_{a5}$  allowed without exceeding corrections to the neutrino masses by 50%.

heavy neutrinos  $M_h$ . We will require that the corrections do not exceed 50% of the value at tree-level. These limits for  $|U_{a5}|^2$  are shown in the upper panels of Fig. 2.7, setting  $M_6 = \{10^{-1}, 100\}$  GeV. Limits for specific values of  $M_5, M_6$  are shown in Table 2.1.

Note that the apparent stronger bounds on  $|U_{e5}|^2$  are really due to the correlations existing between the mixings such that, given some value for  $|U_{\mu h}|^2$  or  $|U_{\tau h}|^2$ , the different  $Z_a$  terms make  $|U_{eh}|^2$  smaller. From this result, it is clear that one heavy neutrino with mass  $\gtrsim 1$  GeV cannot have its mixing enhanced by too much, so is unlikely to appear at collider searches. We can see that these limits are relaxed considerably when the heavy neutrino masses are degenerate. If  $M_5 \rightarrow M_6$  we have the cancellations between the contributions of  $N_5$  and  $N_6$ . This can be seen in the upper right panel of Figure 2.7 for  $M_5 = M_6 = 10^2$  GeV.

In the lower panel of the Figures 2.7, we show the values of  $\gamma_{56}$  that maximize  $|U_{a5}|^2$  when the mass of the heavy neutrino  $M_5$  is being varied. When the contribution is dominated by a single neutrino (dotdashed line) it is possible to have large  $\gamma_{56}$  for small  $M_5$  and thus a large  $|U_{a5}|^2$ . For the other cases when  $M_6 = \{10^2, 10^3\}$  GeV, the limits in  $U_{a5}$  are much more stringent, but can be relaxed when masses are degenerate.

The cancellation between heavy neutrino contributions can again be attributed to the slightly broken lepton number symmetry, which guarantees that loop corrections are kept small [49], [50]. The maximum size of allowed non-degeneracy is critically dependent on the value of  $|U_{ah}|^2$  and the average mass, as was shown in [1].

Even though our results have been presented for a specific scenario, given in Eqs (2.58)-



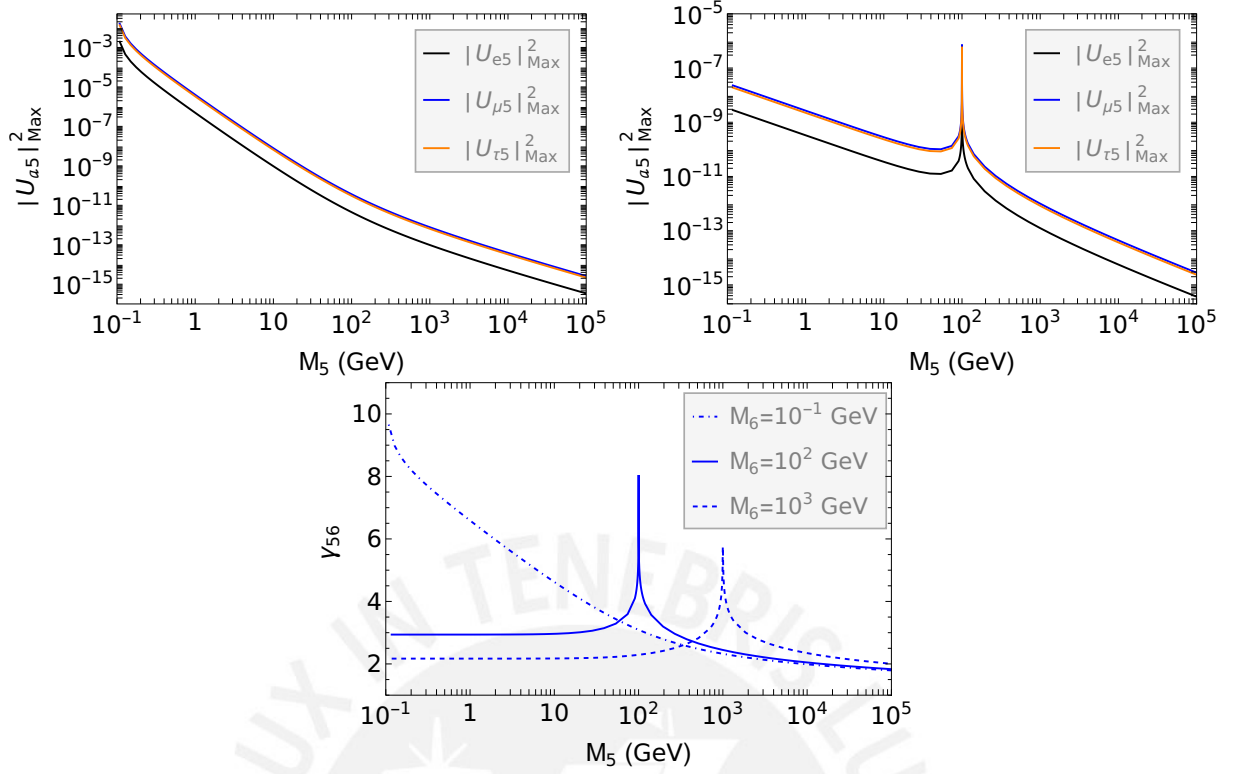


Figure 2.7: Upper panel: Maximum value of  $|U_{a5}|^2$  as a function of  $M_5$ , for  $M_6 = \{10^{-1}, 10^2\}$  GeV. Lower panel: values of  $\gamma_{56}$  that maximize  $|U_{a5}|^2$ . Specific values for  $M_5$  and  $M_6$  are shown in Table 2.1.

(2.60), we expect them to hold qualitatively whenever one has enhanced mixing. As one can see in the Appendix of [26], in most of such scenarios the structure of the Yukawas and mixing matrices are similar, with two sets of mixings being larger than the third.

# ONE LOOP CORRECTIONS IN THE $\nu_R$ MSSM

Supersymmetry (SUSY) is a popular theoretical model that tries to solve some problems in particle physics, such as the hierarchy problem, and also proposes a dark matter candidate. The theory associates the fermions and bosons of the Standard Model with particles with different spin, in other words, it causes an increase in particle content. Despite the promising implications, experimentally, no evidence for these new particles has yet been found. In addition, the wide spectrum of new parameters complicates the situation when performing numerical analyses.

The simplest SUSY extension of the standard seesaw model involves introducing  $\hat{\nu}_R^c$  superfields to the Minimal Supersymmetric Standard Model (MSSM). This implies the presence of new scalar partners, the R-sneutrinos  $\tilde{\nu}_R^c$ , in addition to the sterile neutrinos. This model also includes the particle content shown in Table 3.1 and 3.2. In particular, there are two Higgs doublets,  $H_u$  and  $H_d$ , both of which acquire vev's.

Apart from the R-sneutrinos, and the new Higgs doublet, we also have Binos, winos, and Higgsinos—the states in the interaction base. The combination of these fields forms the mass states known as neutralinos and charginos, which will be crucial in the next sections.

Chiral superfield	Notation	Spin 0	Spin 1/2	$SU(3)_c \times SU(2)_L \times U(1)_Y$
squarks, quarks	$\hat{Q}$	$\tilde{Q}$	$(u_L, d_L)$	$(3, 2, 1/6)$
	$\hat{u}_R^c$	$\tilde{u}_R^c$	$u_R^c$	$(\bar{3}, 1, -2/3)$
	$\hat{d}_R^c$	$\tilde{d}_R^c$	$d_R^c$	$(\bar{3}, 1, 1/3)$
sleptons, leptons	$\hat{L}$	$\tilde{L}$	$(\nu_L, e_L)$	$(1, 2, -1/2)$
	$\hat{e}_R^c$	$\tilde{e}_R^c$	$e_R^c$	$(1, 1, 1)$
	$\hat{\nu}_R^c$	$\tilde{\nu}_R^c$	$\nu_R^c$	$(1, 1, 0)$
higgs, higgsinos	$\hat{H}_u$	$H_u$	$\tilde{H}_u$	$(1, 2, 1/2)$
	$\hat{H}_d$	$H_d$	$\tilde{H}_d$	$(1, 2, -1/2)$

Table 3.1: Fields and superpartners in the model. To clarify,  $\hat{\nu}_R^c$  appears only in the MSSM extension, hence the name  $\nu_R$ MSSM .

Superfield	Notation	Spin 1	Spin 1/2	$SU(3)_c \times SU(2)_L \times U(1)_Y$
gluinos, gluons	$\hat{g}$	$g$	$\tilde{g}$	$(8, 1, 0)$
winos, W bosons	$\hat{W}$	$W^\pm, W^0$	$\tilde{W}^\pm, \tilde{W}^0$	$(1, 3, 0)$
binos, B bosons	$\hat{B}$	$B^0$	$\tilde{B}^0$	$(1, 1, 0)$

Table 3.2: Gauge supermultiplets in the MSSM.

### 3.1 Lagrangian in the $\nu_R$ MSSM extension

The most general Lagrangian for chiral superfields  $\Phi_i$  can be written as:

$$\mathcal{L} = \underbrace{K(\Phi_i, \Phi_i^\dagger)}_{\text{Kähler-potential}} \Big|_D + \left( \underbrace{\mathcal{W}(\Phi_i)}_{\text{Superpotential}} \Big|_F + h.c. \right) \quad (3.1)$$

The sneutrino scalar potential is determined by F-terms from the Superpotential  $\mathcal{W}(\Phi)$

$$F_i = \frac{\partial \mathcal{W}^*}{\partial \Phi_i^*} \quad (3.2)$$

where the the scalar potential is calculated as  $V_F = \sum_i |F_i|^2$ . The D-terms from the Kähler potential, give a further contribution to the scalar potential:

$$D_a = \sum_i g_a \phi_i^* T_a \phi_i. \quad (3.3)$$

where  $T_a$  are the generators of the gauge group  $G$  that make up the representation to which the chiral superfields belong and  $g_a$  is the associated coupling constant. The scalar potential for the D-terms could be written as  $V_D = \frac{1}{2} \sum_a D_a D_a$ .

The superpotential is a mathematical tool that describes supersymmetric mass terms and Yukawa interactions and is invariant under gauge symmetry transformations.  $\mathcal{W}(\Phi)$  is a holomorphic function of  $\Phi$ , which we will write as:

$$\mathcal{W} = \mathcal{W}_{\text{MSSM}} + (Y_\nu^*)_{as} \widehat{L}_a \cdot \widehat{H}_u \widehat{\nu}_{Rs}^c + \frac{1}{2} (M_R)_{ss'} \widehat{\nu}_{Rs}^c \widehat{\nu}_{Rs'}^c \quad (3.4)$$

where  $\widehat{L}$ ,  $\widehat{H}$  and  $\widehat{\nu}_R^c$  are the chiral superfields. The MSSM superpotential is defined as:

$$\mathcal{W}_{\text{MSSM}} = \mu \widehat{H}_u \cdot \widehat{H}_d + \widehat{u}_R^c Y_u \widehat{Q} \cdot \widehat{H}_u - \widehat{d}_R^c Y_d \widehat{Q} \cdot \widehat{H}_d - \widehat{e}_R^c Y_e \widehat{L} \cdot \widehat{H}_d \quad (3.5)$$

It is important to define  $A.B = A^\alpha \epsilon_{\alpha\beta} B^\beta$  where the  $\alpha$  and  $\beta$  indices of  $SU(2)_L$  are contracted by the  $\epsilon$  term. Its representation is given by:

$$\epsilon^{\alpha\beta} = \begin{pmatrix} 0 & 1 \\ -1 & 0 \end{pmatrix} = -\epsilon_{\alpha\beta} \quad (3.6)$$

The relevant SUSY-Breaking terms that will be included to form the Lagrangian are:

$$\mathcal{V}^{\text{soft}} = \mathcal{V}_{\text{MSSM}}^{\text{soft}} + (m_{\tilde{\nu}_R}^2)_{ss'} \tilde{\nu}_{Rs}^{c*} \tilde{\nu}_{Rs'}^c + \left( \frac{1}{2} (B_\nu)_{ss'} \tilde{\nu}_{Rs}^c \tilde{\nu}_{Rs'}^c + (T_\nu^*)_{as} \tilde{L}_a \cdot H_u \tilde{\nu}_{Rs}^c + \text{H.c.} \right) \quad (3.7)$$

To explicitly break SUSY, introduce the soft-breaking terms described by the following Lagrangian:

$$\begin{aligned} \mathcal{L}_{\text{SOFT}} = & -\frac{1}{2} (M_3 \tilde{g}\tilde{g} + M_2 \tilde{W}\tilde{W} + M_1 \tilde{B}\tilde{B} + h.c.) \\ & -\tilde{Q}_i^* (m_{\tilde{Q}}^2)_{ij} \tilde{Q}_j - \tilde{u}_{Ri}^{c*} (m_{\tilde{u}}^2)_{ij} \tilde{u}_{Rj}^c - \tilde{d}_{Ri}^{c*} (m_{\tilde{d}}^2)_{ij} \tilde{d}_{Rj}^c \\ & -\tilde{L}_i^* (m_{\tilde{L}}^2)_{ij} \tilde{L}_j - \tilde{e}_{Ri}^{c*} (m_{\tilde{e}}^2)_{ij} \tilde{e}_{Rj}^c \\ & -m_{H_u}^2 H_u^\dagger \cdot H_u - m_{H_d}^2 H_d^\dagger \cdot H_d - (B_\mu H_u \cdot H_d + h.c.) \\ & -\tilde{Q}_i (T_u)_{ij} \tilde{u}_{Rj}^c H_u - \tilde{Q}_i (T_d)_{ij} \tilde{d}_{Rj}^c H_d - \tilde{L}_i (T_e)_{ij} \tilde{e}_{Rj}^c H_d + h.c. \end{aligned} \quad (3.8)$$

where  $M_1$ ,  $M_2$  and  $M_3$  are the masses for the binos, winos and gluinos, respectively. It is important to note that additional terms appear that contribute to the Higgs potential, such as  $m_{H_u}^2$ ,  $m_{H_d}^2$  and  $B_\mu$ .

### Neutral Higgs masses

Since there are two scalar doublets,  $H_u$  and  $H_d$ , we may construct the Higgs scalar potential, which only includes neutral fields [51], [52].

$$\begin{aligned} V_{H_{u,d}^0} = & (|\mu| + m_{H_u}^2) |H_u^0|^2 + (|\mu| + m_{H_d}^2) |H_d^0|^2 + (-B_\mu H_u^0 H_d^0 + h.c.) \\ & + \frac{1}{8} (g_1^2 + g_2^2) (|H_u^0|^2 - |H_d^0|^2)^2 \end{aligned} \quad (3.9)$$

where the gauge constant couplings of the symmetry groups  $SU(2)_L$  and  $U(1)_Y$  are  $g_2$  and  $g_1$ , respectively. The  $U(1)_{EM}$  symmetry, which remains after the SSB, requires us to have a vanishing VEV for a charged scalar. We have these for the neutral scalars as follows:

$$\langle H_u \rangle = \begin{pmatrix} 0 \\ v_u \end{pmatrix}, \quad \langle H_d \rangle = \begin{pmatrix} v_d \\ 0 \end{pmatrix} \quad (3.10)$$

As can be observed, each doublet acquires a VEV that is related to a common parameter in SUSY,  $\tan \beta = v_u/v_d$ . Additionally, the standard model VEV is related to the two found in the 2HDM, as given by  $v_{SM} = \sqrt{v_u^2 + v_d^2}$ .

The minimization conditions are:

$$\frac{\partial V}{\partial H_u} = 2(|\mu|^2 + m_{H_u^0}^2)v_u - B_\mu v_d - M_Z^2 \cos(2\beta) v_u = 0 \quad (3.11)$$

$$\frac{\partial V}{\partial H_d} = 2(|\mu|^2 + m_{H_d^0}^2)v_u - B_\mu v_u + M_Z^2 \cos(2\beta) v_d = 0 \quad (3.12)$$

The mass matrix for CP even higgs bosons is:

$$M_{even}^2 = \begin{pmatrix} -B_\mu \tan \beta + M_Z^2 \cos^2 \beta & B_\mu - M_Z^2 \sin \beta \cos \beta \\ B_\mu M_Z^2 \sin \beta \cos \beta & -B_\mu \cot \beta + M_Z^2 \sin^2 \beta \end{pmatrix} \quad (3.13)$$

while in the case for CP-odd higgs:

$$M_{odd}^2 = \begin{pmatrix} -B_\mu \tan \beta & B_\mu \\ B_\mu & -B_\mu \cot \beta \end{pmatrix} \quad (3.14)$$

The eigenvalues derived from these matrices are displayed below. There are two states for the CP-odd case: a Goldstone boson  $G^0$  with zero mass and a different boson known as a pseudoscalar  $A^0$ .

$$M_{G^0}^2 = 0, \quad M_A^2 = \frac{2B_\mu}{\sin 2\beta} \quad (3.15)$$

The eigenvalues obtained from the mass matrix for CP-even Higgs are:

$$M_{H_1^0, H_2^0}^2 = \frac{1}{2} \left( M_A^2 + M_Z^2 \pm ((M_A^2 + M_Z^2)^2 - 4M_Z^2 M_A^2 \cos^2 2\beta)^{1/2} \right), \quad (3.16)$$

where  $M_{H_2^0} > M_{H_1^0}$ .

## Charged Higgs

The scalar potential for the charged part can be written as [51], [52]:

$$V_{H_{u,d}^\pm} = (m_{H_u}^2 + |\mu|^2)|H_u^+|^2 + (m_{H_d}^2 + |\mu|^2)|H_d^-|^2 + B_\mu(H_u^+ H_d^- + h.c.) + \frac{g_1^2 + g_2^2}{4} (|H_u^0|^2 - |H_d^0|^2)(|H_u^+|^2 - |H_d^-|^2) + \frac{g_2^2}{2} |H_u^+ H_d^{0*} + H_u^0 H_d^{-*}| \quad (3.17)$$

then we can write the mass matrix for the charged higgses as:

$$\mathcal{L}_{H^\pm} = - \begin{pmatrix} H_d^\mp & H_u^{\pm*} \end{pmatrix} M_{H^\pm}^2 \begin{pmatrix} H_d^{\mp*} \\ H_u^\pm \end{pmatrix} \quad (3.18)$$

One of the eigenvalues obtained corresponds to the massless Goldstone bosons that are "absorbed" by the massive  $W$  bosons. Two massive charged Higgs bosons  $H^\pm$  are also obtained.

$$M_{H^\pm}^2 = \begin{pmatrix} m_{H_d}^2 + |\mu|^2 + \frac{g_1^2 + g_2^2}{4}(v_d^2 - v_u^2) + \frac{g_2^2}{2}v_u^2 & B_\mu + \frac{g_2^2}{2}v_u v_d \\ B_\mu + \frac{g_2^2}{2}v_u v_d & m_{H_u}^2 + |\mu|^2 - \frac{g_1^2 + g_2^2}{4}(v_d^2 - v_u^2) + \frac{g_2^2}{2}v_d^2 \end{pmatrix} \quad (3.19)$$

The eigenvalues after diagonalization of this matrix can be written as:

$$M_{G^\pm}^2 = 0 \quad M_{H^\pm}^2 = M_A^2 + M_W^2 \quad (3.20)$$

where  $M_A$  and  $M_W$  are the masses of the pseudoscalar  $A^0$  and  $W$  boson respectively.

### Sneutrino mass

We know that the sneutrinos are scalars, and as for the Higgs boson, we can separate the real and imaginary parts. In the MSSM, the scalar and pseudoscalar parts have the same mass matrices. In the SUSY seesaw, the lepton number violation terms may contribute differently to the mass matrices. We can write sneutrino mass matrix by separating the  $\tilde{\nu}_L$  and  $\tilde{\nu}_R^c$  fields into their real and imaginary parts as follows:

$$\tilde{\nu}_L = \frac{1}{\sqrt{2}}(\phi_{LS} + i\phi_{LP}) \quad \tilde{\nu}_R^c = \frac{1}{\sqrt{2}}(\phi_{RS} - i\phi_{RP}) \quad (3.21)$$

where  $\phi_{LS,LP}$  and  $\phi_{RS,RP}$  are the real and imaginary components for the fields of the L and R sneutrinos respectively. The mass Lagrangian can be written as:

$$\mathcal{L}_{\tilde{\nu}} = \frac{1}{2} \begin{pmatrix} \tilde{\phi}_S^T & \tilde{\phi}_P^T \end{pmatrix} \begin{pmatrix} M_{SS}^2 & M_{SP}^2 \\ M_{PS}^2 & M_{PP}^2 \end{pmatrix} \begin{pmatrix} \tilde{\phi}_S \\ \tilde{\phi}_P \end{pmatrix} \quad (3.22)$$

with the scalar and pseudoscalar vectors represented by:

$$\tilde{\phi}_S = (\phi_{LS}, \phi_{RS})^T, \quad \tilde{\phi}_P = (\phi_{LP}, \phi_{RP})^T \quad (3.23)$$

We have four  $2 \times 2$  blocks

$$M_{SS}^2, \quad M_{PP}^2, \quad M_{PS}^2, \quad M_{SP}^2 \quad (3.24)$$

where  $SS$ ,  $PP$  and  $SP$  describe the scalar, pseudoscalar and scalar-pseudoscalar mixture respectively, which are defined as:

$$M_{SS}^2 = \begin{pmatrix} \Re \left[ m_L^2 + \frac{v_u^2}{2} Y_\nu Y_\nu^\dagger + \frac{1}{2} m_Z^2 \cos 2\beta \right] & \Re \left[ \frac{v_u}{\sqrt{2}} (T_\nu^* + Y_\nu^* M_R^* - \mu^* Y_\nu^* \cot \beta) \right] \\ \Re \left[ \frac{v_u}{\sqrt{2}} (T_\nu^\dagger + M_R^\dagger Y_\nu^\dagger - \mu^* Y_\nu^\dagger \cot \beta) \right] & \Re \left[ m_{\tilde{\nu}_R}^2 + \frac{v_u^2}{2} Y_\nu^T Y_\nu^* + M_R^\dagger M_R + B_\nu \right] \end{pmatrix} \quad (3.25)$$

$$M_{PP}^2 = \begin{pmatrix} \Re \left[ m_L^2 + \frac{1}{2} v_u^2 Y_\nu Y_\nu^\dagger + \frac{1}{2} m_Z^2 \cos 2\beta \right] & \Re \left[ \frac{v_u}{\sqrt{2}} (T_\nu^* - Y_\nu^* M_R^\dagger - \mu^* Y_\nu^* \cot \beta) \right] \\ \Re \left[ \frac{v_u}{\sqrt{2}} (T_\nu^\dagger - M_R^* Y_\nu^\dagger - \mu^* Y_\nu^\dagger \cot \beta) \right] & \Re \left[ m_{\tilde{\nu}_R}^2 + \frac{1}{2} v_u^2 Y_\nu^T Y_\nu^* + M_R^\dagger M_R - B_{\tilde{\nu}} \right] \end{pmatrix} \quad (3.26)$$

$$M_{SP}^2 = \begin{pmatrix} -\Im \left[ m_L^2 + \frac{1}{2} v_u^2 Y_\nu Y_\nu^\dagger \right] & \Im \left[ \frac{v_u}{\sqrt{2}} (T_\nu^* - Y_\nu^* M_R^\dagger - \mu^* Y_\nu^* \cot \beta) \right] \\ -\Im \left[ \frac{v_u}{\sqrt{2}} (T_\nu^\dagger + M_R^* Y_\nu^\dagger - \mu^* Y_\nu^\dagger \cot \beta) \right] & \Im \left[ m_{\tilde{\nu}_R}^2 + \frac{1}{2} v_u^2 Y_\nu^T Y_\nu^* + M_R^\dagger M_R + B_{\tilde{\nu}} \right] \end{pmatrix} \quad (3.27)$$

$$M_{PS}^2 = (M_{SP}^2)^T \quad (3.28)$$

One can tell apart the LNV terms, as they carry opposite signs in  $M_{SS}$  and  $M_{PP}$ . In [53]–[55] the mass matrix was simplified in order to avoid the splitting of  $\tilde{\nu}_L$  and  $\tilde{\nu}_R^c$  into  $\tilde{\phi}_{LS,LP}$  and  $\tilde{\phi}_{RS,RP}$ . This is possible by neglecting the  $B_\nu$  and  $Y_\nu^* M_R^*$  terms, which violate lepton number and the conservation of CP was also assumed. However, in this work we will not assume these terms can be neglected.

## Neutralinos

As commented earlier, in supersymmetry theory, there are hypothetical fields called neutral higgsinos ( $\tilde{H}_u$  and  $\tilde{H}_d$ ) and gauginos ( $\tilde{B}^0$  and  $\tilde{W}^0$ ). The linear combination of these particles forms four mass eigenstates known as neutralinos,  $\tilde{\chi}_i^0$  ( $i = 1, 2, 3, 4$ ) [51]. The complete neutralino mass matrix is described as follows:

$$M_{\tilde{\chi}^0} = \begin{pmatrix} M_1 & 0 & -g_1 v_d / \sqrt{2} & g_1 v_u / \sqrt{2} \\ 0 & M_2 & g_2 v_d / \sqrt{2} & -g_2 v_u / \sqrt{2} \\ -g_1 v_d / \sqrt{2} & g_2 v_d / \sqrt{2} & 0 & -\mu \\ g_1 v_u / \sqrt{2} & -g_2 v_u / \sqrt{2} & -\mu & 0 \end{pmatrix} \quad (3.29)$$

The soft masses of the Bino ( $\tilde{B}^0$ ), Wino ( $\tilde{W}^0$ ) and Higgsino, denoted as  $M_1$ ,  $M_2$  and  $\mu$  respectively, originate from the Lagrangian ( $\mathcal{L}_{soft}$ ). To obtain the real and positive eigenvalues  $m_{\tilde{\chi}_i}$ , the mass matrix is diagonalized by means of a unitary matrix  $O$ .

$$O^* M_{\tilde{\chi}^0} O^{-1} = \begin{pmatrix} m_{\tilde{\chi}_1} & 0 & 0 & 0 \\ 0 & m_{\tilde{\chi}_2} & 0 & 0 \\ 0 & 0 & m_{\tilde{\chi}_3} & 0 \\ 0 & 0 & 0 & m_{\tilde{\chi}_4} \end{pmatrix} \quad (3.30)$$

## Charginos

There are charged wino states  $\tilde{W}^+$  and  $\tilde{W}^-$  as well as charged Higgsinos  $\tilde{H}_u^+$  and  $\tilde{H}_d^-$ , which are analogous to the previously described states in the preceding paragraph. These combine to produce new states with charge  $\pm 1$  that are referred to as charginos. In the interaction base  $\psi^\pm = (\tilde{W}^+, \tilde{H}_u^+, \tilde{W}^-, \tilde{H}_d^-)$ , the chargino mass lagrangian is:

$$\mathcal{L}_{\tilde{\chi}^\pm} = -\frac{1}{2}(\psi^\pm)^T M_{\tilde{\chi}^\pm} \psi^\pm + c.c \quad (3.31)$$

where

$$M_{\tilde{\chi}^\pm} = \begin{pmatrix} 0 & X^T \\ X & 0 \end{pmatrix} \quad (3.32)$$

and

$$X = \begin{pmatrix} M_2 & g_2 v_u \\ g_2 v_d & \mu \end{pmatrix} \quad (3.33)$$

The mass eigenstates described are related to gauge eigenstates via unitary matrices  $\mathbf{U}$  and  $\mathbf{V}$  as [51] :

$$\begin{pmatrix} \tilde{\chi}_1^+ \\ \tilde{\chi}_2^+ \end{pmatrix} = \mathbf{V} \begin{pmatrix} \tilde{W}^+ \\ \tilde{H}_u^+ \end{pmatrix}, \quad \begin{pmatrix} \tilde{\chi}_1^- \\ \tilde{\chi}_2^- \end{pmatrix} = \mathbf{U} \begin{pmatrix} \tilde{W}^- \\ \tilde{H}_d^- \end{pmatrix} \quad (3.34)$$

The mass matrix can be diagonalized as

$$\mathbf{U}^* X \mathbf{V}^{-1} = \begin{pmatrix} \tilde{\chi}_1 & 0 \\ 0 & \tilde{\chi}_2 \end{pmatrix} \quad (3.35)$$

with the real diagonal elements  $\tilde{\chi}_{1,2}$ . It is relatively easy to get the eigenvalue because it is a  $2 \times 2$  matrix.

$$m_{\tilde{\chi}_1, \tilde{\chi}_2}^2 = \frac{1}{2} \left[ |M_2|^2 + |\mu|^2 + 2M_W^2 \mp \left( (|M_2|^2 + |\mu|^2 + 2M_W^2)^2 - 4|\mu M_2 - M_W^2 \sin 2\beta|^2 \right)^{1/2} \right]. \quad (3.36)$$



We now know a little bit more about the model particle composition and interactions. As a starting step, we will investigate the non-SUSY loop contributions, which are similar to those of a two-Higgs doublet model (2HDM). We shall go through these terms in depth here. Then we will observe what occurs with the contributions from supersymmetric particles.

## 3.2 One loop corrections to neutrinos mass of non-SUSY contributions

The  $\nu_R$ MSSM adds two Higgs doublets, the non-SUSY phenomenology resembles that of 2HDM, although this is a simpler theory than the supersymmetric one. The relevant Yukawa interactions are described by this Lagrangian:

$$-\mathcal{L} \supset -(Y_e)_{aa} \bar{L}_a \cdot H_d e_{R_a} + (Y_\nu)_{as} \bar{L}_a \cdot H_u \nu_{R_s} + \text{H.c.} \quad (3.37)$$

Each Higgs doublet is responsible for giving masses to the up and down type fermions, so, as we will show later, the Dirac mass term must also be redefined. The two doublets in this model can be parameterized as follows.

$$H_u = \begin{pmatrix} H_u^+ \\ H_u^0 \end{pmatrix}, \quad H_d = \begin{pmatrix} H_d^0 \\ H_d^- \end{pmatrix}, \quad (3.38)$$

where the neutral components are defined as:

$$H_u^0 = \frac{1}{\sqrt{2}} (v_u + \eta_u + i\omega_u), \quad H_d^0 = \frac{1}{\sqrt{2}} (v_d + \eta_d + i\omega_d) \quad (3.39)$$

In this model, the mass eigenstates can be described in terms of interaction eigenstates:

$$\begin{pmatrix} H_1^0 \\ H_2^0 \end{pmatrix} = \begin{pmatrix} c_\alpha & -s_\alpha \\ s_\alpha & c_\alpha \end{pmatrix} \begin{pmatrix} \eta_u \\ \eta_d \end{pmatrix}, \quad \begin{pmatrix} G^0 \\ A^0 \end{pmatrix} = \begin{pmatrix} s_\beta & -c_\beta \\ c_\beta & s_\beta \end{pmatrix} \begin{pmatrix} \omega_u \\ \omega_d \end{pmatrix} \quad (3.40)$$

It is possible to express the neutral component of the  $H_u$  field as a function of the mass eigenstates as:

$$H_u^0 = \frac{1}{\sqrt{2}} (v_u + c_\alpha H_1^0 + s_\alpha H_2^0 + i(s_\beta G^0 + c_\beta A^0)) \quad (3.41)$$

moreover, for the charged scalar states.

$$\begin{pmatrix} G^- \\ H^- \end{pmatrix} = \begin{pmatrix} s_\beta & -c_\beta \\ c_\beta & s_\beta \end{pmatrix} \begin{pmatrix} H_u^- \\ H_d^- \end{pmatrix} \quad (3.42)$$

Where  $s_\alpha$ ,  $c_\alpha$ ,  $s_\beta$  and  $c_\beta$  are the sines and cosines of the mixing angles  $\alpha$  and  $\beta$  obtained by diagonalizing Eqs. (3.13), (3.14) and (3.19). The angle  $\alpha$  is fixed at tree level by  $\tan \beta$  and  $M_A$ :

$$\alpha = \frac{1}{2} \arctan \left[ (\tan 2\beta) \frac{M_A^2 + M_Z^2}{M_A^2 - M_Z^2} \right] \quad (3.43)$$

It is well known that at the tree level, the lightest Higgs mass cannot exceed  $\sim M_Z$ , which is in clear contradiction with experimental observations. However, this issue can be addressed by considering quantum corrections to the Higgs scalar potential, which can raise the mass of the lightest Higgs to the observable value. In our case, we will stick with the value of the masses at tree-level. We see in [9] that the quartic coupling is modified to increase the mass of the Higgs. However, there are cancellations at the tree level that must be taken into account between the  $H_2^0$  and  $A^0$  contributions, which are lost if only the masses of the scalars are modified. Therefore, the mass matrix of the pseudoscalars would also have to be modified, but we do not do that in this work.

### 3.2.1 Neutral and charged scalar contributions

The Lagrangian that describes the interactions of the neutral fields in this model is:

$$\begin{aligned} -\mathcal{L}_{\nu R 2\text{HDM}}^Y &\supset \frac{1}{2} \bar{\nu}_i P_R \Lambda_{ij}^* N_j H_u^0 + \frac{1}{2} \bar{\nu}_i P_L \Lambda_{ij} N_j H_u^{0*} \\ &\supset \frac{c_\alpha}{2\sqrt{2}} \bar{\nu}_i (\Lambda_{ij}^* P_R + \Lambda_{ij} P_L) N_j H_1^0 + \frac{s_\alpha}{2\sqrt{2}} \bar{\nu}_i (\Lambda_{ij}^* P_R + \Lambda_{ij} P_L) N_j H_2^0 \\ &\quad + \frac{is_\beta}{2\sqrt{2}} \bar{\nu}_i (\Lambda_{ij}^* P_R - \Lambda_{ij} P_L) N_j G^0 - \frac{ic_\beta}{2\sqrt{2}} \bar{\nu}_i (\Lambda_{ij}^* P_R - \Lambda_{ij} P_L) N_j A^0 \end{aligned} \quad (3.44)$$

where  $\Lambda_{ij}$  was defined in Eq. (2.28).

Firstly, we will illustrate the contributions made by the neutral scalar fields, which are presented in Figure 3.1.

We can use the vertices presented in Eq. (3.44) of the Yukawa lagrangian to write the self-energy of each diagram. The self-energy function for each diagram can be expressed as follows:

$$-i\Sigma_{ij}^x = \sum_n \int \frac{d^d k}{(2\pi)^d} \rho_x \left( \frac{i}{\sqrt{2}} \Lambda_{in} \right) (S_F)_n \left( \frac{i}{\sqrt{2}} \Lambda_{nj} \right) S_x \quad (3.45)$$

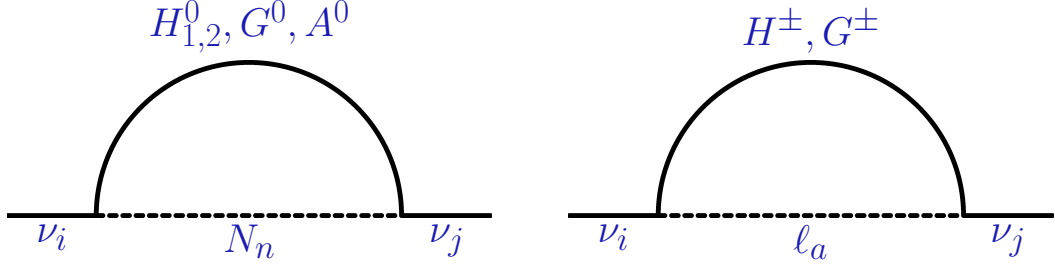


Figure 3.1: The one-loop contributions involving neutral (Left) and charged scalar (Right) fields in the context of non-supersymmetric model.

where we defined  $\rho_x = \{\cos^2 \alpha, \sin^2 \alpha, -\sin^2 \beta, -\cos^2 \beta\}$  for  $x = \{H_1^0, H_2^0, G^0, A^0\}$  respectively. The additional terms the appear in Eq. (3.45) are the fermion ( $S_F$ ) and scalar boson ( $S_x$ ) propagator.

We may utilize the formulas from Appendix B to solve the integral. The same steps as in Chapter 2 were used to obtain  $B_L$ :

$$\begin{aligned}
(B_L^x)_{ij} &= \frac{i}{2} \sum_n \rho_x \Lambda_{in} m_n I_2(M_x^2, m_n^2) \Lambda_{nj} \\
&= \frac{\rho_x}{32\pi^2} \sum_n \Lambda_{in} m_n \left( \tilde{k} - 1 + \ln \frac{m_n^2}{Q^2} + \left( \frac{m_n^2}{M_x^2} - 1 \right)^{-1} \ln \frac{m_n^2}{M_x^2} \right) \Lambda_{nj} \quad (3.46)
\end{aligned}$$

where  $\tilde{k}$  was defined in the  $Z^0$  one loop contribution to neutrino mass in Eq. (2.16). The contribution to  $\delta M_L$  using Eq. (2.8)

$$\begin{aligned}
\left( \delta M_L^{H_{1,2}^0 + G^0 + A^0} \right)_{aa'} &= \sum_x \sum_{i,j} U_{ai}^* (B_L^x)_{ij} U_{a'j}^* \\
&= \frac{1}{32\pi^2} \sum_x \sum_{n,s,s'} \rho_x (Y_\nu)_{as}^* U_{sn} m_n \left( \frac{m_n^2}{M_x^2} - 1 \right)^{-1} \ln \frac{m_n^2}{M_x^2} U_{s'n} (Y_\nu)_{a's'}^* \quad (3.47)
\end{aligned}$$

The structure obtained is very similar to the result of Eq. (2.35), in addition, it also reflects again the suppression by the Yukawas. Just as in Chapter 2 for the  $\nu_R$ SM, each part of the mass matrix receives corrections, so we will follow those same steps here. In

the case of  $\delta M_D$ :

$$\begin{aligned}
(\delta M_D^{H_{1,2}^0+G^0+A^0})_{as} &= \sum_x \sum_{i,j} U_{ai}^* (B_L^x)_{ij} U_{sj}^* \\
&= \frac{1}{32\pi^2} \sum_x \sum_{n,s,s'} \rho_x(Y_\nu)_{as'}^* U_{s'n} m_n \left( \frac{m_n^2}{M_x^2} - 1 \right)^{-1} \ln \frac{m_n^2}{M_x^2} U_{a'n} (Y_\nu)_{a's}^*
\end{aligned} \tag{3.48}$$

In the same way we do the calculation for  $\delta M_R$ :

$$\begin{aligned}
(\delta M_R^{H_{1,2}^0+G^0+A^0})_{ss'} &= \sum_x \sum_{i,j} U_{si}^* (B_L^x)_{ij} U_{s'j}^* \\
&= \frac{1}{32\pi^2} \sum_x \sum_{n,a,a'} \rho_x(Y_\nu)_{as}^* U_{an} m_n \left( \frac{m_n^2}{M_x^2} - 1 \right)^{-1} \ln \frac{m_n^2}{M_x^2} U_{a'n} (Y_\nu)_{a's'}^*
\end{aligned} \tag{3.49}$$

Both corrections have a similar structure to the expressions in Eqs. (2.36) and (2.38), the difference appears in the additional scalars in the 2HDM, i.e., the sum over  $x$  and the factor  $\rho_x$ . Similar to the Standard Seesaw, the divergence  $\tilde{k}$  is exactly canceled by the sum of the neutral scalar, Goldstone, and pseudoscalar contributions.

In the sector of charged scalars, we calculate the contributions to  $B_L$  as:

$$\begin{aligned}
(B_L^{H^-})_{ij} &= \frac{\sin 2\beta}{32\pi^2} \sum_{a,s} m_a \left( \tilde{k} - 1 + \ln \frac{m_a^2}{Q^2} + \left( \frac{m_a^2}{M_{H^-}^2} - 1 \right)^{-1} \ln \frac{m_a^2}{M_{H^-}^2} \right) \\
&\quad \times [U_{si} (Y_\nu)_{as}^* (Y_e^*)_{aa} U_{aj} + U_{ai} (Y_e^*)_{aa} (Y_\nu)_{as}^* U_{sj}]
\end{aligned} \tag{3.50}$$

$$\begin{aligned}
(B_L^{G^-})_{ij} &= -\frac{\sin 2\beta}{32\pi^2} \sum_a m_a^2 \left( \tilde{k} - 1 + \ln \frac{m_a^2}{Q^2} + \left( \frac{m_a^2}{M_{W^-}^2} - 1 \right)^{-1} \ln \frac{m_a^2}{M_{W^-}^2} \right) \\
&\quad \times [U_{ai} m_j U_{aj}^* + U_{ai}^* m_i U_{aj}]
\end{aligned} \tag{3.51}$$

Using (1.19) in Eq. (3.51) and combining it with the charged Higgs, the divergence cancels, similar to what happens with the neutral scalar contribution.

$$\begin{aligned}
(B_L^{H^-+G^-})_{ij} &= \frac{\sin 2\beta}{32\pi^2} \sum_{a,s} m_a \left( \left( \frac{m_a^2}{M_{H^-}^2} - 1 \right)^{-1} \ln \frac{m_a^2}{M_{H^-}^2} + \left( \frac{m_a^2}{M_{W^-}^2} - 1 \right)^{-1} \ln \frac{m_a^2}{M_{W^-}^2} \right) \\
&\quad \times [U_{si} (Y_\nu)_{as}^* (Y_e^*)_{aa} U_{aj} + U_{ai} (Y_e^*)_{aa} (Y_\nu)_{as}^* U_{sj}]
\end{aligned} \tag{3.52}$$

For  $\delta M_L$ ,

$$(\delta M_L^{H^-+G^-})_{aa'} = \sum_{i,j} U_{ai}^* (B_L^{H^-+G^-})_{ij} U_{aj}^* \tag{3.53}$$

$$= 0 \tag{3.54}$$

This is because the structure provided in Eq. (3.52) is cancelled by the properties of the mixing matrices shown in Eq.(1.18). According to Eq. (1.16) for  $\delta M_D$ ,

$$(\delta M_D^{H^-+G^-})_{as} = \sum_{(i,j)} U_{ai}^* (B_L^{H^-+G^-})_{ij} U_{sj}^* \quad (3.55)$$

$$= \frac{\sin 2\beta}{32\pi^2} (Y_e^*)_{aa} m_a \left[ \left( \frac{m_a^2}{M_{H^-}^2} - 1 \right)^{-1} \ln \frac{m_a^2}{M_{H^-}^2} - \left( \frac{m_a^2}{M_W^2} - 1 \right)^{-1} \ln \frac{m_a^2}{M_W^2} \right] (Y_\nu^*)_{as} \quad (3.56)$$

There is the suppression by the terms  $Y_e$  and  $Y_\nu$  as in Eq. (2.47), an additional difference is the  $\sin 2\beta$  term and the absence of the divergence. For  $\delta M_R$ ,

$$(\delta M_R^{H^-+G^-})_{ss'} = \sum_{i,j} U_{si}^* (B_L^{H^-+G^-})_{ij} U_{s'j}^* \quad (3.57)$$

$$= 0 \quad (3.58)$$

This situation is similar to  $\delta M_L^{H^-+G^-}$ , the result is due to the mixing matrices properties. The procedure for calculating the contribution of the  $Z^0$  boson is the same as in the  $\nu_R$ SM in Section 2.1, but we must also take into account the redefinition of the Dirac mass,  $M_D = \frac{v_{SM}}{\sqrt{2}} Y_\nu^* \sin \beta$ .

$$(\delta M_L^{Z^0})_{aa'} = \frac{\sin^2 \beta}{8\pi^2} \sum_{n,s,s'} (Y_\nu^*)_{as} U_{sn} m_n \left( \frac{m_n^2}{M_Z^2} - 1 \right)^{-1} \ln \frac{m_n^2}{M_Z^2} U_{s'n} (Y_\nu^*)_{a's'} \quad (3.59)$$

The contribution  $\delta M_D^{H^-+G^-}$  depends on  $Y_\nu$  and  $Y_e$ , which can be neglected when inserted into Eq. (2.2). Therefore, like in the Standard Seesaw, only the  $\delta M_L$  correction needs to be considered.

Finally, the complete neutral contribution can be expressed as follows:

$$(\delta M_L)^{2\text{HDM}} = \delta M_L^{H^0,2^+G^0+A^0} + \delta M_L^{Z^0} \quad (3.60)$$

### 3.3 One loop corrections to neutrino mass in SUSY

SUSY contributions to light neutrino masses lead to different types of loops, with the most relevant particles inside these loops being sneutrinos and neutralinos. We will focus on the  $\hat{\nu}_R^c$  sector, where terms involving lepton number violation (LNV) appear and modify each component of the neutrino mass matrix.

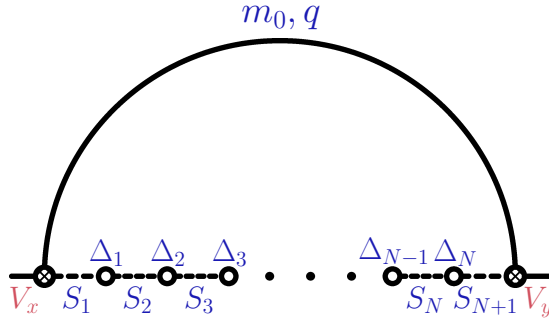


Figure 3.2: General one loop Feynman diagram including the mass insertions  $\Delta_N$ .

Before calculating loop diagrams, we need to define the mass insertion approximation method. Our objective in this section is to take this approximation to calculate the general expressions that we will use in the numerical analysis in the final chapter.

### 3.3.1 The Mass Insertion Approximation (MIA)

There are many parameters in SUSY, most of which are used to calculate physical quantities through masses and mixing angles. The latter are obtained by diagonalizing the corresponding mass matrices. However, the role of each parameter is not always clear in the analysis. In order to fully understand the physics behind the model, it is helpful to demonstrate the effect of each parameter. By doing so, the phenomenology of the model becomes more interesting to study [56] [57].

In SUSY, the Mass Insertion technique is a powerful method that allows for the consideration of off-diagonal elements in sfermion matrices as interactions that change the particle type. With this approach, it is not necessary to have diagonal sfermion matrices, making Mass Insertion a useful tool for SUSY research.

The mass insertion technique has many applications and variants, depending on where the Mass insertions are located. In our particular case, they will only appear in the scalar line. Let us examine loop diagrams involving neutralinos and sneutrinos. The scalar line in these diagrams can contain  $N$  mass insertions, as illustrated in Figure 3.2. A general expression for this diagram, including vertices and propagators of the particles involved, is:

$$-i\Sigma^{\text{SUSY}} = \int \frac{d^d k}{(2\pi)^d} (i V_x) S_F(i V_y) S_1(i \Delta_1) S_2(i \Delta_2) \dots (i \Delta_N) S_{N+1} \quad (3.61)$$

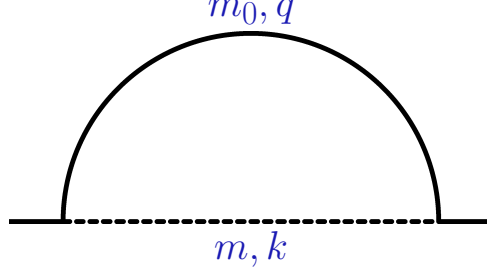


Figure 3.3: One loop diagram with two propagators that allows to form the  $I_2(m_0^2, m^2)$  expression.

Here,  $S_F$  and  $S_i$  are the propagators of the fermions and scalars respectively. We also identify the vertices of the loop as  $V_x$  and  $V_y$  which we will specify later. Thus, the expression for the correction to neutrino mass can be written :

$$\Sigma^{\text{SUSY}} \supset V_x V_y m_0 (\Delta_1 \Delta_2 \dots \Delta_N) I_{N+2}(m_0^2, m_1^2, m_2^2, \dots, m_{N+1}^2) \quad (3.62)$$

where the loop integral is expressed as follows:

$$I_{N+2}(m_0^2, m_1^2, m_2^2, \dots, m_{N+1}^2) = \int \frac{d^d k}{(2\pi)^d} \frac{1}{(q^2 - m_0^2)(k^2 - m_1^2)(k^2 - m_2^2) \dots (k^2 - m_{N+1}^2)} \quad (3.63)$$

In this expression,  $q$  and  $k$  are the momentum on the fermionic and scalar lines respectively. We showed the general expressions in the MIA, so in principle it is difficult to know how they work. In order to clarify it, consider the loop integral with two scalar propagators (see Figure 3.3). The solution to this loop integral can be found in the literature (the complete solution can be found in Appendix B).

$$I_2(m_0^2, m^2) = \int \frac{d^d k}{(2\pi)^d} \frac{1}{(q^2 - m_0^2)(k^2 - m^2)} \quad (3.64)$$

$$= -\frac{i}{16\pi^2} \left( \tilde{k} + \ln \frac{m^2}{Q^2} + \left( \frac{m^2}{m_0^2} - 1 \right)^{-1} \ln \frac{m^2}{m_0^2} \right) \quad (3.65)$$

In the loop integral,  $m_0$  and  $m$  represent the masses of the particles inside the loop. As we will see, the solution in Eq. (3.65) is important for generating a recurrence expression for one-loop diagrams with more than two propagators. Notice, this result has been used in the one-loop corrections in Chapter 2.

As first example, illustrated in Figure 3.4, we have the case where one line has one or two mass insertions represented, by a black dot. In the left panel, the mass Insertion leads to a loop integral with three propagators, which implies that three particles are involved in the final solution.

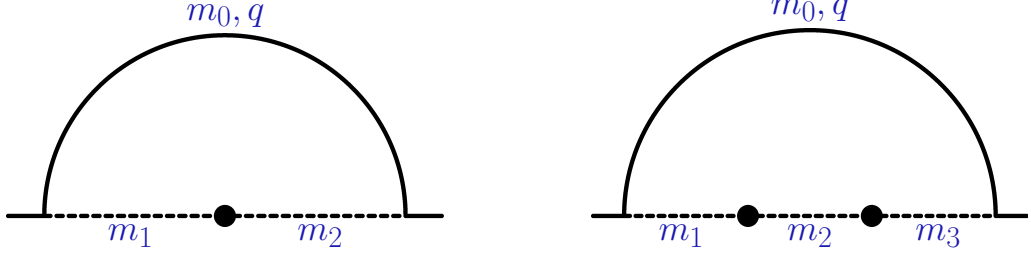


Figure 3.4: One loop diagram with one (Left) and two (Right) mass insertions.

$$I_3(m_0^2, m_1^2, m_2^2) = \int \frac{d^d k}{(2\pi)^d} \frac{1}{(q^2 - m_0^2)(k^2 - m_1^2)(k^2 - m_2^2)} \quad (3.66)$$

We get this expression when  $N = 1$  in Eq. (3.63). A simple procedure to evaluate  $I_3$  is to use the partial fractions of the terms that have the same momentum.

$$\frac{1}{(k^2 - m_1^2)(k^2 - m_2^2)} = \frac{1}{m_1^2 - m_2^2} \left( \frac{1}{k^2 - m_1^2} - \frac{1}{k^2 - m_2^2} \right) \quad (3.67)$$

Then, plugging this into Eq. (3.66) and separating the integrals, we have two functions like Eq. (3.64).

$$I_3(m_0^2, m_1^2, m_2^2) = \frac{1}{m_1^2 - m_2^2} \left( \int \frac{d^d k}{(2\pi)^d} \frac{1}{(q^2 - m_0^2)(k^2 - m_1^2)} - \int \frac{d^d k}{(2\pi)^d} \frac{1}{(q^2 - m_0^2)(k^2 - m_2^2)} \right) \quad (3.68)$$

This allows us to write  $I_3$  as a function of  $I_2$  :

$$I_3(m_0^2, m_1^2, m_2^2) = \frac{1}{m_1^2 - m_2^2} [I_2(m_0^2, m_1^2) - I_2(m_0^2, m_2^2)] \quad (3.69)$$

From this, it is convenient to define a dimensionless function  $f_3$ :

$$f_3(m_0^2, m_1^2, m_2^2) \equiv i m_0^2 I_3(m_0^2, m_1^2, m_2^2) \quad (3.70)$$

This function  $f_3(m_0^2, m_1^2, m_2^2)$  is symmetric under the exchange of  $m_1$  and  $m_2$ , and will appear in our calculation of loop correction [58]. In the right panel in Fig. 3.4, a similar procedure can be followed for a diagram with two mass insertions ( $N = 2$ ).

$$I_4(m_0^2, m_1^2, m_2^2, m_3^2) = \int \frac{d^d k}{(2\pi)^d} \frac{1}{(q^2 - m_0^2)(k^2 - m_1^2)(k^2 - m_2^2)(k^2 - m_3^2)} \quad (3.71)$$

Using Eq. (3.67):

$$I_4(m_0^2, m_1^2, m_2^2, m_3^2) = \frac{1}{m_1^2 - m_2^2} \left( \int \frac{d^d k}{(2\pi)^d} \frac{1}{(q^2 - m_0^2)(k^2 - m_1^2)(k^2 - m_3^2)} - \int \frac{d^d k}{(2\pi)^d} \frac{1}{(q^2 - m_0^2)(k^2 - m_2^2)(k^2 - m_3^2)} \right) \quad (3.72)$$

$$= \frac{1}{m_1^2 - m_2^2} [I_3(m_0^2, m_1^2, m_3^2) - I_3(m_0^2, m_2^2, m_3^2)] \quad (3.73)$$



Notice that, in the same way as for  $f_3$ , we can write  $f_4$  as:

$$f_4(m_0^2, m_1^2, m_2^2, m_3^2) = i m_0^4 I_4(m_0^2, m_1^2, m_2^2, m_3^2) \quad (3.74)$$

We wrote the full loop integral in Eq. (3.63), and can express it in terms of the adimensional function  $f_{N+2}$  as:

$$I_{N+2}(m_0^2, m_1^2, m_2^2, \dots, m_{N+1}^2) = -\frac{i}{m_0^{2N}} f_{N+2}(m_0^2, m_1^2, m_2^2, \dots, m_{N+1}^2) \quad (3.75)$$

where the function  $f_{N+2}$  is defined as

$$f_{N+2}(m_0^2, m_1^2, m_2^2, \dots, m_{N+1}^2) = \frac{m_0^2}{m_1^2 - m_2^2} \left[ f_{N+1}(m_0^2, m_1^2, m_3^2, \dots, m_{N+1}^2) - f_{N+1}(m_0^2, m_2^2, m_3^2, \dots, m_{N+1}^2) \right] \quad (3.76)$$

In Fig. 3.5, the normalized loop functions  $f_3$  and  $f_4$  are shown. This way of presenting this function is due to the fact that these will appear in the supersymmetric contributions. In the upper left panel, the function is large for small values of  $m_0$  and  $m_1$  when  $m_2 = 10$  (blue) and 600 (red) GeV. In the upper right panel, we can see the symmetry of  $f_3$  to the exchange of  $m_1 \leftrightarrow m_2$ . In the lower left panel, the  $f_4$  function is shown for fixed values of  $m_2$  and  $m_3$ . The contour for this function is large for small values of  $m_0$  and  $m_1$  with  $m_2 = m_3 = 600$  GeV, instead with 10 GeV (blue) the range for  $m_0$  and  $m_1$  increases. In the lower right panel, we can see the symmetry of  $f_4$  to the exchange of  $m_1 \leftrightarrow m_3$ . These symmetry conditions are important for the calculation of the contributions to a loop in the MI.

### 3.3.2 Conventions for lepton number violation and conserving mass insertions

The mass Lagrangian obtained from the  $F$  and  $D$  terms can be classified into two categories: those that preserve lepton number and those that violate it.

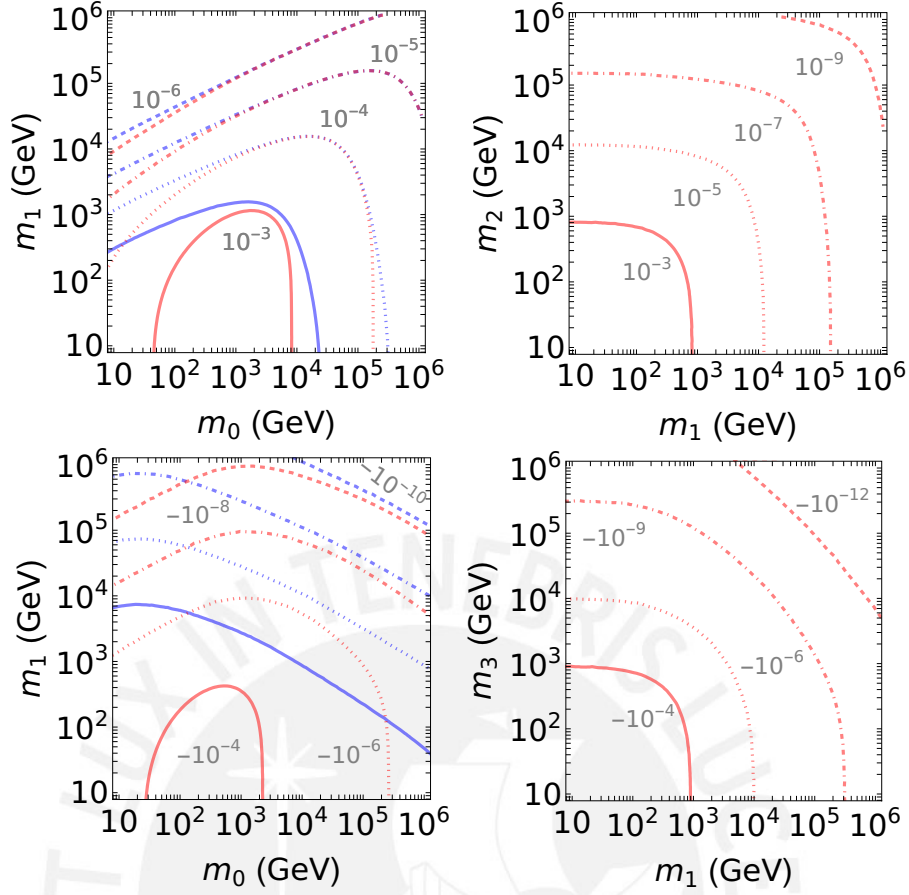


Figure 3.5: Upper panel:  $(v_{SM}/m_0)f_3(m_0^2, m_1^2, m_2^2)$  is shown for fixed  $m_2 = 10(600)$  GeV in blue (red) lines (left). For  $m_0 = 100$  GeV, the symmetry of  $f_3$  with respect to  $m_1$  and  $m_2$  appears (right). Lower panel: we have  $(v_{SM}^3/m_0^3)f_4(m_0^2, m_1^2, m_2^2, m_3^2)$  for fixed  $m_2 = m_3 = 10(600)$  GeV in blue (red) lines (left). The symmetry of this function by setting  $m_0 = m_2 = 100$  GeV is shown on the right

$$\begin{aligned}
\mathcal{L}_{\tilde{\nu}}^{\text{mass}} &= \mathcal{L}_{\tilde{\nu}}^{\text{LNC}} + \mathcal{L}_{\tilde{\nu}}^{\text{LNV}} \tag{3.77} \\
-\mathcal{L}_{\tilde{\nu}}^{\text{LNC}} &= \tilde{\nu}_{La}^* \underbrace{\left( m_L^2 + \frac{v_u^2}{2} Y_\nu Y_\nu^\dagger + \frac{1}{2} m_Z^2 \cos 2\beta \mathbb{1}_{3 \times 3} \right)}_{m_{\tilde{\nu}_L}^2} \tilde{\nu}_{La'} \\
&\quad + \tilde{\nu}_{Rs}^c \underbrace{\left( m_{\tilde{\nu}}^{2T} + \frac{v_u^2}{2} Y_\nu^\dagger Y_\nu + M_R M_R^* \right)}_{m_{\tilde{\nu}_R}^2} \tilde{\nu}_{Rs'}^c \\
&\quad + \tilde{\nu}_{Rs}^c \left( \frac{v_u}{\sqrt{2}} T_\nu^\dagger - \frac{v_d}{\sqrt{2}} \mu^* Y_\nu^\dagger \right)_{sa} \tilde{\nu}_{La} + \tilde{\nu}_{La}^* \left( \frac{v_u}{\sqrt{2}} T_\nu - \frac{v_d}{\sqrt{2}} \mu Y_\nu \right)_{as} \tilde{\nu}_{Rs}^c \tag{3.78}
\end{aligned}$$

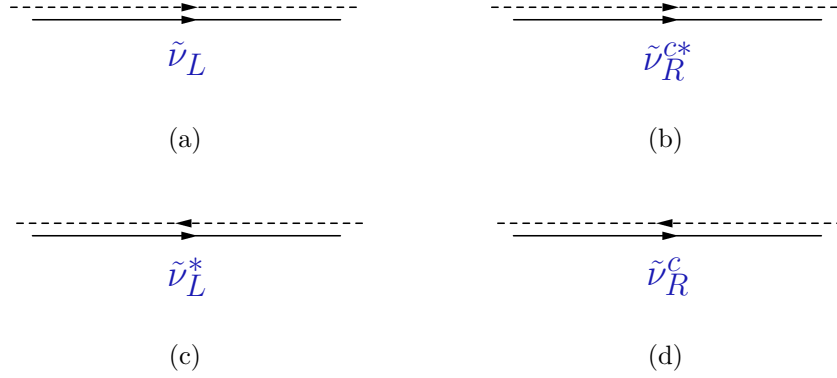


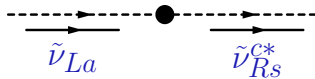
Figure 3.6: Lepton number convention for the scalar fields  $\tilde{\nu}_L$  and  $\tilde{\nu}_R^c$ .

$$-\mathcal{L}_{\tilde{\nu}}^{\text{LNV}} = \tilde{\nu}_{Rs}^c \left( \frac{1}{2} B_\nu \right)_{ss'} \tilde{\nu}_{Rs'}^c + \tilde{\nu}_{La}^* \left( \frac{v_u}{\sqrt{2}} Y_\nu M_R \right)_{as} \tilde{\nu}_{Rs}^c + \tilde{\nu}_{La} \left( \frac{v_u}{\sqrt{2}} Y_\nu^* M_R^* \right)_{as} \tilde{\nu}_{Rs}^{c*} \quad (3.79)$$

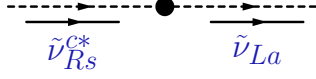
For simplicity, it will be assumed that  $m_L^2$  and  $m_\nu^2$  will be diagonal. Then  $m_{\tilde{\nu}_L}^2$  and  $m_{\tilde{\nu}_R}^2$  can be taken as diagonals in a reasonable approximation, given that we also have  $Y_\nu^2$  terms. While the terms mentioned above will be part of the sneutrino propagators in the loops, the terms that change flavor will be those described by the mass insertions. In addition, we can also specify if they violate lepton number or not in the lagrangian. As we can see, the terms shown in Eqs. (3.78) and (3.79) will help us to define the interactions in the diagrams involving loops.

Figure 3.6 shows the lines for scalar fields involved in this work. The arrow in the dotted line indicates the lepton number flux, and the arrow in the solid line represents the direction of momentum. In our convention, when both arrows are in the same direction, we assign a Lepton Number of +1 (as seen in 3.6a and 3.6b) flowing in the direction of momentum. Conversely, when the arrows have opposite directions, we assign a Lepton Number of  $-1$  (as shown in 3.6c and 3.6d).

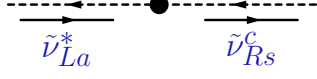
We have mass insertions with lepton number conservation and violation. The LNC terms depend on the trilinear  $T_\nu$ , Yukawa coupling and the parameters  $\mu$ ,  $\tan \beta$  and  $v_u$  (See Eq. (3.80) - (3.83)).



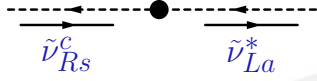
$$\Delta_{sa}^{\text{LNC}} = \frac{v_u}{\sqrt{2}} (T_\nu - \mu \cot \beta Y_\nu)_{as}^* \quad (3.80)$$



$$\Delta_{as}^{\text{LNC}} = \frac{v_u}{\sqrt{2}}(T_\nu - \mu \cot \beta Y_\nu)_{as} \quad (3.81)$$

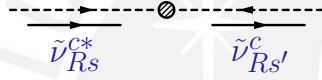


$$\Delta_{sa}^{\text{LNC}} = \frac{v_u}{\sqrt{2}}(T_\nu - \mu \cot \beta Y_\nu)_{as} \quad (3.82)$$



$$\Delta_{as}^{\text{LNC}} = \frac{v_u}{\sqrt{2}}(T_\nu - \mu \cot \beta Y_\nu)_{as}^* \quad (3.83)$$

In the LNV mass insertions, we have two types of interactions. The first type depends only on  $B_\nu$ , as seen in Equations (3.84) and (3.85).

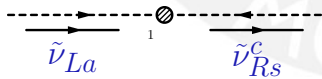


$$\Delta_{s's}^{\text{LNV}} = (B_\nu)_{s's}^* \quad (3.84)$$

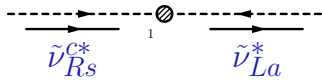


$$\Delta_{s's}^{\text{LNV}} = (B_\nu)_{s's} \quad (3.85)$$

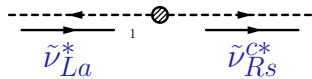
and the second by the factor  $M_R Y_\nu$  (See Eqs. (3.86)-(3.89)).



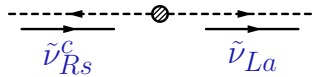
$$\Delta_{sa}^{\text{LNV}} = \frac{v_u}{\sqrt{2}}(Y_\nu)_{as'}^*(M_R^*)_{s's} \quad (3.86)$$



$$\Delta_{as}^{\text{LNV}} = \frac{v_u}{\sqrt{2}}(Y_\nu)_{as'}^*(M_R^*)_{s's} \quad (3.87)$$



$$\Delta_{sa}^{\text{LNV}} = \frac{v_u}{\sqrt{2}}(Y_\nu)_{as'}(M_R)_{s's} \quad (3.88)$$



$$\Delta_{as}^{\text{LNV}} = \frac{v_u}{\sqrt{2}}(Y_\nu)_{as'}(M_R)_{s's} \quad (3.89)$$

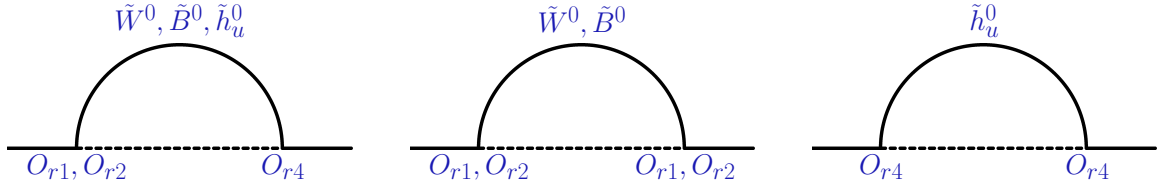


Figure 3.7: Three types of Feynman diagrams in which MI will be included, where  $O_{rb}$  are the neutralino mixing matrix elements.

### 3.3.3 Reducible and Irreducible contributions to one loop to the neutrino masses in SUSY

In the loop diagrams, we have fermionic and scalar lines inside the loop. In the fermionic line, we consider all states in the mass base, therefore it is necessary to include the mixing matrices  $O_{rb}$  in each vertex for neutralinos, where  $r$  is the index of the mass eigenstates for the neutralinos, and  $b$  indicates the type of gaugino involved.

In general, we have three different kinds of loop diagrams involving the SUSY particles: the Mixed, pure Gaugino and Higgsino case that are shown in the left, medium and right respectively in Fig. 3.7.

We need to define the expressions for the vertices  $V_{x,y}$  that will appear in the diagrams we will develop (See Eq. (3.61)). If the interaction involves a bino or wino eigenstate, the vertex will be determined by the neutralino matrix elements  $O_{rb}$ , where  $g_b$  is the gauge constant coupling and  $b = 1, 2$ .

$$V_{rb} = \frac{(-1)^b}{\sqrt{2}} g_b O_{rb}. \quad (3.90)$$

However, if higgsino-like neutralinos ( $b = 4$ ) are involved, the matrix element will change, and the Yukawa coupling will also come into play:

$$V_{asr} = (Y_\nu)_{as} O_{r4}. \quad (3.91)$$

So, in some cases, Yukawa couplings may appear in the vertices along with some additional ones due to mass insertions.

In the scalar line we will include the mass insertions taking LNV and LNC terms, in this case we will look for diagrams where the LNV mass insertions are relevant.

From Eq. (3.62), the expression for the correction to the neutrino mass can be written as follows:

$$\delta M_L^{\text{irr,red}} = \frac{1}{m_0^{2N-1}} V_x V_y (\Delta_1 \Delta_2 \dots \Delta_N) f_{N+2}(m_0^2, m_1^2, m_2^2, \dots, m_{N+1}^2) \quad (3.92)$$

where  $m_0$  is the neutralino mass and  $\delta M_L^{\text{irr}}$  and  $\delta M_L^{\text{red}}$  refer to the reducible (red) and irreducible (irr) contributions in SUSY. We will recognize reducible and irreducible contributions among those where the term  $B_\nu$  appears. Therefore, when  $B_\nu = 0$  the contributions that remain will be called irreducible, otherwise reducible. Additionally, the loop function for  $N$  mass insertions is described in Eq.(3.76). The total contribution to  $\delta M_L$  in SUSY is defined as:

$$(\delta M_L)^{\text{SUSY}} = (\delta M_L^{\text{irr}})^{gg} + (\delta M_L^{\text{irr}})^{gh} + (\delta M_L^{\text{red}})^{gg} + (\delta M_L^{\text{red}})^{gh} + (\delta M_L^{\text{red}})^h \quad (3.93)$$

where  $(\delta M_L^{\text{irr,red}})^{gg}$ ,  $(\delta M_L^{\text{irr,red}})^{gh}$  and  $(\delta M_L^{\text{red}})^h$  are the Gaugino-Gaugino, Gaugino-Higgsino and Higgsino-Higgsino contributions respectively.

One of the main restrictions on the number of diagrams is determined by the order of the Yukawa couplings in each correction of a loop. In Equation (3.92),  $\delta M_L$  can be proportional up to  $\mathcal{O}(Y_\nu^2)$ , beyond which the contributions become negligible. In the next sections, we will explicitly show each contribution.

### 3.3.4 Irreducible contributions

We have a set of diagrams that arise from the considerations in the previous section. The special case in this context is when  $B_\nu = 0$ , the non-zero contributions that remain are referred to as irreducible. Before starting with the calculation of these contributions, we need to keep in mind the Yukawa suppression up to  $\mathcal{O}(Y_\nu^2)$ . This statement is very important because it puts limits on the number of loop diagrams in this work. We showed previously the kinds of mass insertions with LNV and LNC terms that will contribute to the development of contributions. In pure-Higgsino diagrams, there are already two Yukawas at each vertex, and LNV insertions like  $Y_\nu M_R$  produce further suppression. For this diagram, if we only include LR insertions, more Yukawas will appear and suppression will increase, so this type of contribution here is insignificant.

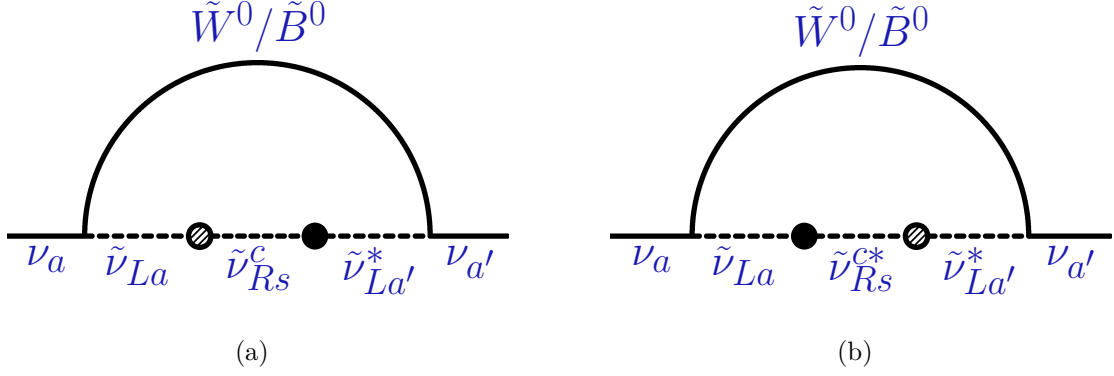


Figure 3.8: Pure gaugino one loop diagrams. In all diagrams the shaded (black) blobs indicate LNV (LNC) insertions.

### Pure gaugino case

There is no  $Y_\nu$  suppression in the vertices in the pure Gaugino case, allowing us to have more than one MI, which can be LNV or LNC-like. In order to obtain a suitable diagram, LR transitions are required. We have SM neutrinos as external particles with left chirality; in this case, one MI is not possible, therefore an additional insertion is required.

In this case (See Fig. 3.8a), all of the diagrams will come from the two mass insertions ( $N = 2$ ), more than this would lead to negligible contributions. Based on what was found in Eq. (3.92), we can write the expression for the correction to the mass as:

$$(\delta M_L^{\text{irr}})^{gg}_{aa'} = \sum_{r,s} \frac{1}{m_{\tilde{\chi}_r^0}^3} V_{rb}^g V_{rb'}^g \Delta_{sa}^{\text{LNV}} \Delta_{a's}^{\text{LNC}} f_4(m_{\tilde{\chi}_r^0}^2, m_{\tilde{\nu}_{La}}^2, m_{\tilde{\nu}_{Rs}}^2, m_{\tilde{\nu}_{La'}}^2) \quad (3.94)$$

We have the gauge vertices  $V_{rb}^g$  and  $V_{rb'}^g$  with  $r = \{1, 2, 3, 4\}$  denote the neutralino mass eigenstate and  $b, b' = \{1, 2\}$  for the type of gaugino under consideration. The expression in Eq. (3.94) is for the diagram in Fig. (3.8a). A similar procedure is done for the other diagram in the right panel (Fig. (3.8b)).

$$(\delta M_L^{\text{irr}})^{gg}_{aa'} = \sum_{r,s} \frac{1}{m_{\tilde{\chi}_r^0}^3} V_{rb}^g V_{rb'}^g \Delta_{sa}^{\text{LNC}} \Delta_{a's}^{\text{LNV}} f_4(m_{\tilde{\chi}_r^0}^2, m_{\tilde{\nu}_{La}}^2, m_{\tilde{\nu}_{Rs}}^2, m_{\tilde{\nu}_{La'}}^2) \quad (3.95)$$

In these contributions, we have one<sup>1</sup>LNV term like  $Y_\nu M_R$  and one with LNC insertion<sup>1</sup>. The total contribution for both diagrams can be written as:

$$(\delta M_L^{\text{irr}})^{gg}_{aa'} = \frac{v_u^2}{4} (-1)^{b+b'} g_b g_{b'} \sum_{r=1}^4 \sum_{s,s'=1}^3 \frac{1}{m_{\tilde{\chi}_r^0}^3} O_{rb} O_{rb'} \left[ (Y_\nu^* M_R^*)_{as} (T_\nu - \mu \cot \beta Y_\nu)_{a's}^* + (T_\nu - \mu \cot \beta Y_\nu)_{as}^* (Y_\nu^* M_R^*)_{a's} \right] f_4(m_{\tilde{\chi}_r^0}^2, m_{\tilde{\nu}_{La}}^2, m_{\tilde{\nu}_{Rs}}^2, m_{\tilde{\nu}_{La'}}^2) \quad (3.96)$$

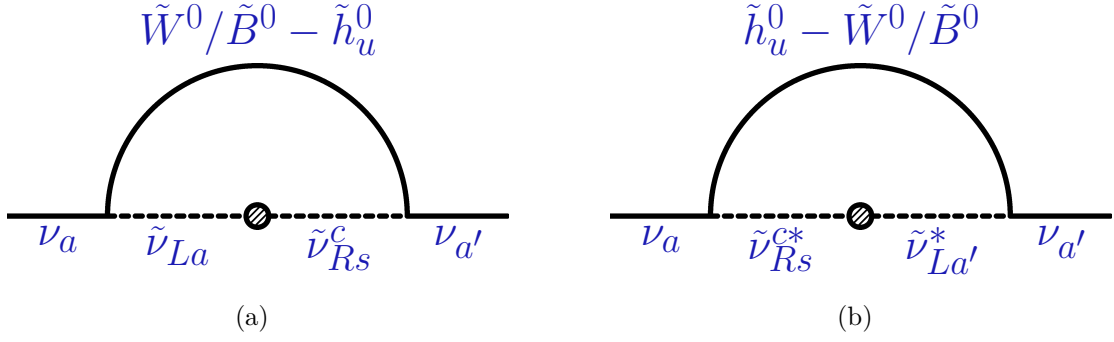


Figure 3.9: Mixed diagrams with one LNV mass insertion.

where  $m_{\tilde{\nu}_L}^2$  and  $m_{\tilde{\nu}_R}^2$  were defined in Eq. (3.78).

### Gaugino-Higgsino case

We will have gaugino/higgsino-type neutralinos participating in loop diagrams, as shown in Fig. 3.9. The vertices for gauginos are represented by  $V_{rb}$  and for higgsinos by  $V_{a'sr}$ . As we can see, there is a Yukawa coupling ( $Y_\nu$ ) in one of the vertices. In order to not exceed the number of  $Y_\nu$ , only one mass insertion is allowed. In the Eq. (3.92) when  $N = 1$  the one loop correction expression is:

$$(\delta M_L^{\text{irr}})^{gh} = \sum_{r,s} \frac{1}{m_{\tilde{\chi}_r^0}} V_{rb}^g V_{a'sr}^h \Delta_{sa}^{\text{LNV}} f_3(m_{\tilde{\chi}_r^0}^2, m_{\tilde{\nu}_{Rs}}^2, m_{\tilde{\nu}_{La}}^2) \quad (3.97)$$

The full expression found for this case is:

$$(\delta M_L^{\text{irr}})^{gh} = \frac{v_u}{2} (-1)^b g_b \sum_{r=1}^4 \sum_{s=1}^3 \frac{1}{m_{\tilde{\chi}_r^0}} O_{rb} O_{r4} \left[ (Y_\nu)^*_{a's} (Y_\nu^* M_R^*)_{as} f_3(m_{\tilde{\chi}_r^0}^2, m_{\tilde{\nu}_{La}}^2, m_{\tilde{\nu}_{Rs}}^2) \right. \\ \left. + (Y_\nu)^*_{as} (Y_\nu^* M_R^*)_{a's} f_3(m_{\tilde{\chi}_r^0}^2, m_{\tilde{\nu}_{Rs}}^2, m_{\tilde{\nu}_{La'}}^2) \right] \quad (3.98)$$

### 3.3.5 Reducible contributions

When  $B_\nu \neq 0$ , there are additional contributions with more mass insertions in the scalar line for both the pure-gaugino and mixed cases. This  $B_\nu$  term is important because the suppression is not as strong as the one from  $Y_\nu$ , allowing diagrams with a larger number of insertions. In the next section, we will provide the analytic expressions for each contribution.



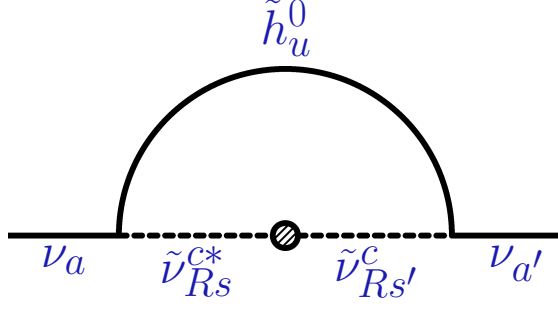


Figure 3.10: Pure-higgsino diagram with one LNV mass insertion.

### Pure Higgsino case

We start with the pure Higgsino case in Fig. (3.10). Previously, for the irreducible part, this was negligible. In this scenario, there is already a  $Y_\nu$  suppression in each vertex. Therefore, we need to identify mass insertions that do not depend on this term. By using the  $B_\nu$  term, we can obtain a non-suppressed contribution, which implies that  $N = 1$  in Eq. (3.92). This leads to the following expression:

$$(\delta M_L^{\text{red}})_{aa'}^h = \sum_{r,s,s'} \frac{1}{m_{\tilde{\chi}_r^0}} V_{asr}^h V_{a's'r}^h \Delta_{s's}^{\text{LNV}} f_3(m_{\tilde{\chi}_r^0}^2, m_{\tilde{\nu}_{Rs}}^2, m_{\tilde{\nu}_{Rs'}}^2) \quad (3.99)$$

As we can see, unlike the other cases, this expression is not dependent on the masses of the L sneutrinos.

$$(\delta M_L^{\text{red}})_{aa'}^h = \sum_{r=1}^4 \sum_{s,s'=1}^3 \frac{1}{m_{\tilde{\chi}_r^0}} O_{r4}^2 (Y_\nu)_{as}^* (Y_\nu)_{a's'}^* (B_\nu)_{ss'}^* f_3(m_{\tilde{\chi}_r^0}^2, m_{\tilde{\nu}_{Rs}}^2, m_{\tilde{\nu}_{Rs'}}^2) \quad (3.100)$$

This entire expression has suppression up to order  $\mathcal{O}(Y_\nu^2)$  and varies linearly with  $B_\nu$ . The behavior of the loop function is shown in Fig. 3.5.

### Pure gaugino case

As it was seen in the irreducible part, there is no suppression by the Yukawas in the vertices. This allowed for two insertions, avoiding a negligible contribution. We have two LR transitions; now, in order to avoid another type of suppression, we can incorporate insertions with the new term  $B_\nu$ . The diagrams that exhibit these characteristics are displayed in Figure 3.11. When  $N = 3$  in Eq. (3.92), we obtain the subsequent expression:

$$(\delta M_L^{\text{red}})_{aa'}^{gg} = \sum_{r,s,s'} \frac{1}{m_{\tilde{\chi}_r^0}^5} V_{rb}^g V_{r'b'}^g \Delta_{sa}^{\text{LNV}} \Delta_{ss'}^{\text{LNV}} \Delta_{s'a'}^{\text{LNV}} f_5(m_{\tilde{\chi}_r^0}^2, m_{\tilde{\nu}_{La}}^2, m_{\tilde{\nu}_{Rs}}^2, m_{\tilde{\nu}_{Rs'}}^2, m_{\tilde{\nu}_{La'}}^2) \quad (3.101)$$

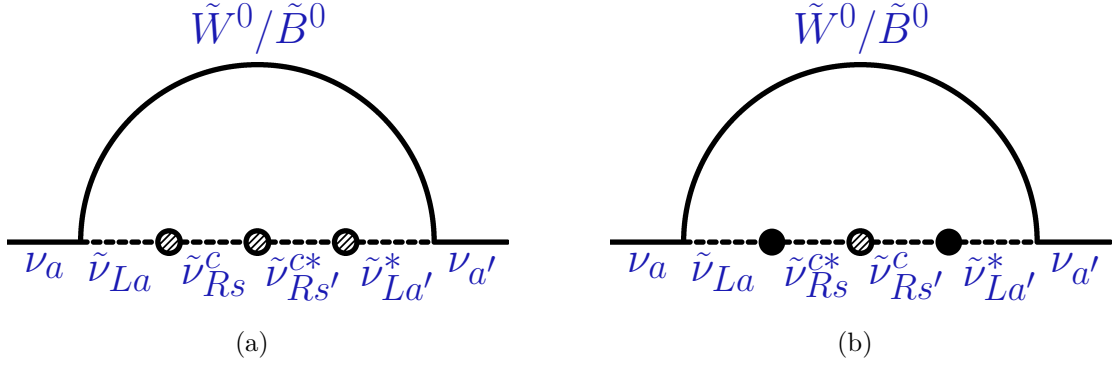


Figure 3.11: One loop diagrams with three mass insertion. a) Three LNV insertions. b) Two LNC and one LNV insertion.

and for the second diagram (Fig. 3.11b)

$$(\delta M_L^{\text{red}})_{aa'}^{gg} = \sum_{r,s,s'} \frac{1}{m_{\tilde{\chi}_r^0}^5} V_{rb}^g V_{rb'}^g \Delta_{sa'}^{\text{LNC}} \Delta_{s's}^{\text{LNV}} \Delta_{a's'}^{\text{LNC}} f_5(m_{\tilde{\chi}_r^0}^2, m_{\tilde{\nu}_{La'}}^2, m_{\tilde{\nu}_{Rs}}^2, m_{\tilde{\nu}_{Rs'}}^2, m_{\tilde{\nu}_{La'}}^2) \quad (3.102)$$

The sum of both contributions can be expressed as:

$$\begin{aligned} (\delta M_L^{\text{red}})_{aa'}^{gg} &= \frac{v_u^2}{8} (-1)^{b+b'} g_b g_{b'} \sum_{r=1}^4 \sum_{s,s'=1}^3 \frac{1}{m_{\tilde{\chi}_r^0}^5} O_{rb} O_{rb'} \left[ (Y_\nu^* M_R^*)_{as} (B_\nu)_{ss'} (Y_\nu^* M_R^*)_{a's'} \right. \\ &\quad \left. + (T_\nu - \mu \cot \beta Y_\nu)_{as}^* (B_\nu)_{ss'}^* (T_\nu - \mu \cot \beta Y_\nu)_{a's'}^* \right] f_5(m_{\tilde{\chi}_r^0}^2, m_{\tilde{\nu}_{La'}}^2, m_{\tilde{\nu}_{Rs}}^2, m_{\tilde{\nu}_{Rs'}}^2, m_{\tilde{\nu}_{La'}}^2) \end{aligned} \quad (3.103)$$

where we define the function  $f_5$  as:

$$f_5(m_0^2, m_1^2, m_2^2, m_3^2, m_4^2) = \frac{m_0^2}{m_1^2 - m_2^2} \left[ f_4(m_0^2, m_1^2, m_3^2, m_4^2) - f_4(m_0^2, m_2^2, m_3^2, m_4^2) \right] \quad (3.104)$$

### Gaugino-Higgsino case

In this case, there is already a  $Y_\nu$  on a vertex, which limits the number of additional insertions. One of these is the LR transition, which is LNC, and the other, which includes the RR insertion,  $B_\nu$ . By considering the appropriate mass insertions, we are led to consider  $N = 2$  in Eq. (3.92). With this, the following expression is obtained:

$$(\delta M_L^{\text{irr}})_{aa'}^{gh} = \sum_{r,s,s'} \frac{1}{m_{\tilde{\chi}_r^0}^3} V_{rb}^g V_{ra's'}^h \Delta_{as}^{\text{LNC}} \Delta_{ss'}^{\text{LNV}} f_4(m_{\tilde{\chi}_r^0}^2, m_{\tilde{\nu}_{La'}}^2, m_{\tilde{\nu}_{Rs}}^2, m_{\tilde{\nu}_{Rs'}}^2) \quad (3.105)$$

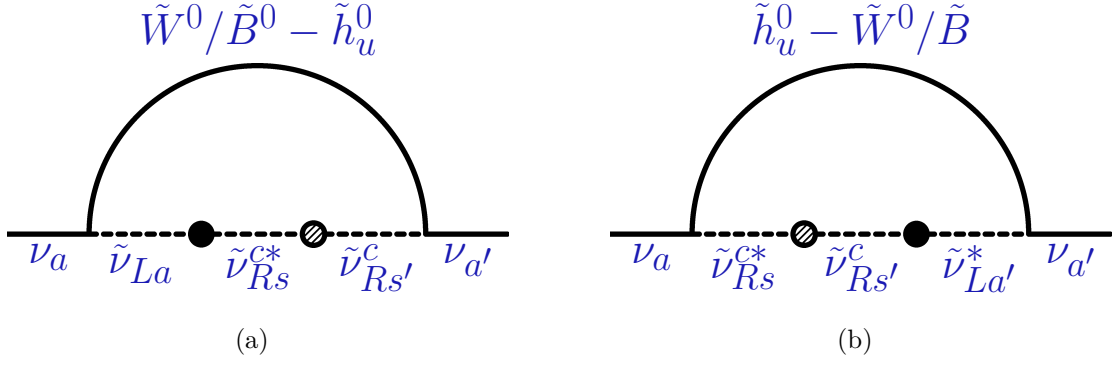


Figure 3.12: Mixed one loop diagram with two mass insertion. Shaded(black) blobs indicate LNV(LNC) insertions

The total contribution from the diagrams in Fig. 3.12 can be written as:

$$\begin{aligned}
(\delta M_L^{\text{red}})_{aa'}^{gh} &= \frac{v_u}{4} (-1)^b g_b \sum_{r=1}^4 \sum_{s,s'=1}^3 \frac{1}{m_{\tilde{\chi}_r^0}^3} O_{rb} O_{r4} \\
&\times \left[ (Y_\nu)_{a's'}^* (T_\nu - \mu \cot \beta Y_\nu)_{as}^* (B_\nu)_{ss'} f_4(m_{\tilde{\chi}_r^0}^2, m_{\tilde{\nu}_{La}}^2, m_{\tilde{\nu}_{Rs}}^2, m_{\tilde{\nu}_{Rs'}}^2) \right. \\
&\quad \left. + (Y_\nu)_{as}^* B_{ss'} (T_\nu - \mu \cot \beta Y_\nu)_{a's}^* f_4(m_{\tilde{\chi}_r^0}^2, m_{\tilde{\nu}_{Rs}}^2, m_{\tilde{\nu}_{Rs'}}^2, m_{\tilde{\nu}_{La'}}^2) \right] \quad (3.106)
\end{aligned}$$

The sum of the reducible and irreducible contributions computed with the mass insertion contributes to  $(\delta M_L)^{\text{SUSY}}$ .

$$\delta M_L = (\delta M_L)^{\text{2HMD}} + (\delta M_L)^{\text{SUSY}} \quad (3.107)$$

It is important for the following sections to consider the total contribution, which will be the sum of the supersymmetric and non-supersymmetric contributions.

# SEARCHING FOR CANCELLATIONS

Before starting the numerical analysis, it is important to remind the reader that our objective is to keep the one loop corrections to neutrino masses under control, avoiding fine-tuning in the neutrino sector, while allowing large contributions from the LNV terms. Furthermore, as seen in Chapter 2, the quantum corrections in the  $\nu_R$ SM are very large, and, since we know that the non-supersymmetric contributions are similar to these, therefore, we hope to find a region in  $\nu_R$ MSSM parameter space where cancellations between SUSY and non-SUSY contributions can exist. In this section of the work, we will show this with the equations presented in Chapter 3.

As described in Chapter 3, we have the complete contributions for  $(\delta M_L)^{\text{SUSY}}$  and  $(\delta M_L)^{2\text{HDM}}$ . Nevertheless, using these full expressions makes the analysis not very transparent for our purposes. The parametrization used in Eqs. (1.28), (1.30), (2.59) and (2.60) is thus helpful to demonstrate the role of each term in the contributions found in the Eq. (3.60) for non-SUSY and Eqs. (3.96), (3.98), (3.100), (3.103) and (3.106) for irreducible and reducible SUSY contributions, respectively. In what follows, we will use this to elucidate the relevance of each expression in the loop-corrected masses.

## 4.1 Non-SUSY contributions in benchmark scenario

We show the full non-SUSY contribution in Eq. (3.60). Expressing it in terms of our effective 3+2 seesaw, we simplify and get:

$$(\delta M_L)_{aa'}^{2\text{HDM}} = \frac{1}{2} \sum_{h,s,s'} (Y_\nu)_{as}^* U_{sh} (Y_\nu)_{a's'}^* U_{s'h} g(M_h, M_A, \tan \beta) \quad (4.1)$$

$$= K_{aa'} \underbrace{[M_5 g(M_5, M_A, \tan \beta) - M_6 g(M_6, M_A, \tan \beta)]}_{G_{2\text{HDM}}} \quad (4.2)$$

In the limit when  $M_5 \rightarrow M_6$ , degenerate heavy neutrinos, this contribution vanishes. The flavour factor  $K_{aa'}$  is defined as:

$$K_{aa'} = \frac{m_3}{v_u^2} \cosh^2 \gamma_{56} Z_{a'}^* Z_a^* e^{-2iz_{56}\rho_{56}} \quad (4.3)$$

This will be a common factor that can also be factored out of the supersymmetric contributions. The constant  $Z_a$  was defined in Eq. (2.61). Also, the loop function is defined as:

$$g(M, M_A, \tan \beta) = \frac{M}{16\pi^2} \left[ 3 \sin^2 \beta \left( \frac{M^2}{M_Z^2} - 1 \right)^{-1} \ln \frac{M^2}{M_Z^2} + \cos^2 \alpha \left( \frac{M^2}{M_{H_1^0}^2} - 1 \right)^{-1} \ln \frac{M^2}{M_{H_1^0}^2} \right. \\ \left. + \sin^2 \alpha \left( \frac{M^2}{M_{H_2^0}^2} - 1 \right)^{-1} \ln \frac{M^2}{M_{H_2^0}^2} - \cos^2 \beta \left( \frac{M^2}{M_A^2} - 1 \right)^{-1} \ln \frac{M^2}{M_A^2} \right] \quad (4.4)$$

In the decoupling limit, when  $M_A$  is very large, the mass of the states  $H_{1,2}^0, H^\pm$  are also large. Then the tree-level prediction for the lighter neutral scalar is  $m_h^2 = M_Z^2 \cos^2 2\beta$ , also the angle  $\alpha$  approaches the value  $\beta - \pi/2$  [51], [62]. Thus, in this case the expression for the loop function can be written as  $g(M, M_A \rightarrow \infty, \tan \beta) \approx \sin^2 \beta f(M)$ , where  $f(M)$  was defined in Eq. (2.56), which serves as a consistency check.

The  $g$  function is compared with the one found in Chapter 2 for the Seesaw, in Fig. 4.1. We find the function  $g(M, M_A, \tan \beta)$  does not depend strongly on  $M_A$  and  $\tan \beta$ , in fact, it reflects numerically similar values with  $f(M)$ . We can see that for the masses of the heavy neutrinos  $M_h = 40$  and 200 GeV, a reduction of less than 80% is not observed.

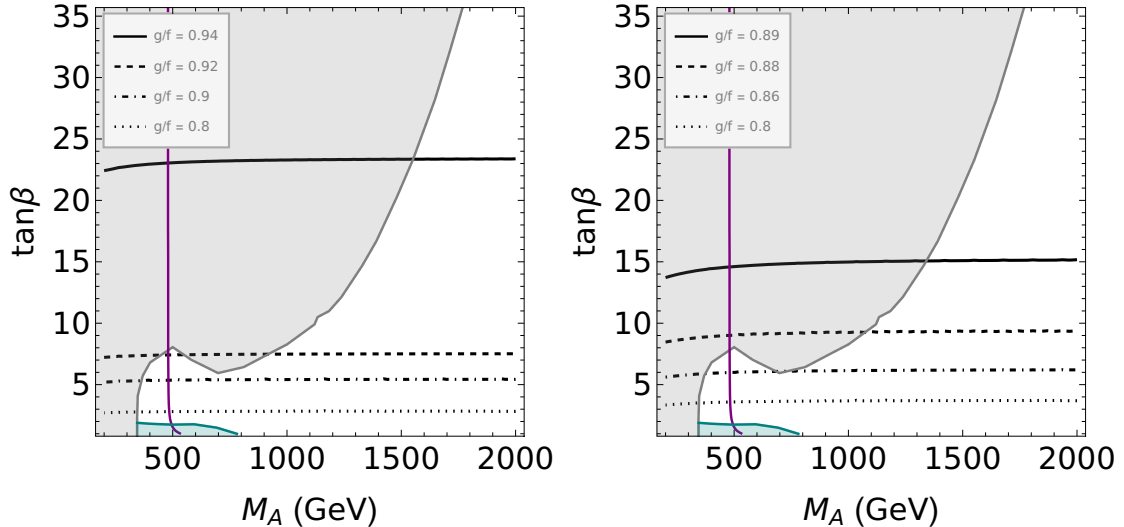


Figure 4.1: Ratio between loop functions,  $g(M_h, M_A, \tan \beta)/f(M_h)$ . Gray (dark green) region is excluded by  $H/A \rightarrow \tau^+\tau^-$  [59] ( $H^\pm \rightarrow tb$  [60]) searches. The region to the left of the purple curve is excluded, as here the light Higgs boson couplings do not match with measurements [61]. We show results for  $M_h = 40(200)$  GeV on the left (right).

## 4.2 Irreducible SUSY contributions in benchmark scenario

By using the expressions of  $Y_\nu$  and  $M_R$  in the Casas-Ibarra parameterization, Eqs. (2.58)-(2.60), we can obtain simplified and suitable expressions for better analysis. In these calculations, to simplify, we use usual definitions in the literature for  $T_\nu$  and  $B_\nu$ .

$$T_\nu = a_\nu Y_\nu \quad (4.5)$$

$$B_\nu = b_\nu M_R \quad (4.6)$$

where  $a_\nu$  and  $b_\nu$  are real numbers.

Our work will focus on analyzing the interference between SUSY and non-SUSY contributions. It is important to understand the new LNV terms that have been included in the loop diagrams in order to get a greater contribution from them. Moreover, at the same time, it is necessary to check that the full loop corrections are kept under control, avoiding the need for fine-tuning in the neutrino sector.

We want to quantify this interference in order to understand the impact of supersymmetric contributions on light neutrino masses. We introduce  $R^{\text{csusy}}$  as the variable that

represents the ratio between SUSY and Non-SUSY:

$$R^{c_{\text{susy}}} = 1 + \frac{(\delta M_L^{c_{\text{susy}}})^{\text{SUSY}}}{(\delta M_L)^{2\text{HDM}}} \quad (4.7)$$

where  $c_{\text{susy}} = \text{irr}, \text{red}, \text{irr} + \text{red}$  represent the irreducible, reducible and irreducible + reducible contributions. The flavor structure, Eq. (4.3), for  $(\delta M_L)^{\text{SUSY}}$  and  $(\delta M_L)^{2\text{HDM}}$  is cancelled, therefore  $R^{c_{\text{susy}}}$  is a real value with no indices. What remains after factoring the flavour structure are the functions  $G^{\text{SUSY}}$  and  $G_{2\text{HDM}}$ , which, through  $R^{c_{\text{susy}}}$ , will show us the amount of cancellation that can be obtained. In Eq. (4.2) we defined  $G_{2\text{HDM}}$ , for  $G^{\text{SUSY}}$  we will have the following expression.

$$G^{\text{SUSY}} = \underbrace{G_{\text{red}}}_{\text{Reducible contributions}} + \underbrace{G_{\text{irr}}}_{\text{Irreducible contributions}} \quad (4.8)$$

We will also assume in the rest of the work that the L sneutrinos will always be degenerate, allowing these functions without the flavor indices. According to the expression in Eq. (4.7), if  $R^{c_{\text{susy}}} > 1$ , this suggests that the supersymmetric and non-supersymmetric contributions have the same sign, whereas  $0 < R^{c_{\text{susy}}} < 1$  implies that the contributions have opposite signs and lead to destructive interference. If  $R^{c_{\text{susy}}} < 0$ , the supersymmetric contributions are greater than the non-susy, and these have opposite signs.

#### a) Pure gaugino

According to the definitions found above, Eq. (3.96) can be written like this:

$$(\delta M_L^{\text{irr}})^{gg} = K_{aa'} G_{\text{irr}}^{gg} \quad (4.9)$$

where the function  $G_{\text{irr}}^{gg}$  is defined as:

$$G_{\text{irr}}^{gg} = (-1)^{b+b'} v_u^2 g_b g_{b'} (a_\nu - \mu \cot \beta) \sum_{r=1}^4 \frac{1}{m_{\tilde{\chi}_r^0}^3} O_{rb} O_{rb'} \\ \times \left[ M_5^2 f_4(m_{\tilde{\chi}_r^0}^2, m_{\tilde{\nu}_L}^2, m_{\tilde{\nu}_{R5}}^2, m_{\tilde{\nu}_L}^2) - M_6^2 f_4(m_{\tilde{\chi}_r^0}^2, m_{\tilde{\nu}_L}^2, m_{\tilde{\nu}_{R6}}^2, m_{\tilde{\nu}_L}^2) \right] \quad (4.10)$$

We have a linear dependence with respect to  $a_\nu$ . The mass insertion also has a linear dependence on  $\mu \cot \beta$ , these parameters also enter the neutralino masses and mixing.

Observing the last expression, we can identify different scenarios that depend on the supersymmetric particle masses in the loop functions. If in Eq. (4.10),  $m_{\tilde{\nu}_{R5}} = m_{\tilde{\nu}_{R6}} = m_{\tilde{\nu}_R}$  (degenerate R sneutrinos), we can write the next expression:

$$G_{\text{irr}}^{gg} = (-1)^{b+b'} v_u^2 g_b g_{b'} (a_\nu - \mu \cot \beta) \Delta M_{56} (M_5 + M_6) \\ \times \sum_{r=1}^4 \frac{1}{m_{\tilde{\chi}_r^0}^3} O_{rb} O_{rb'} f_4(m_{\tilde{\chi}_r^0}^2, m_{\tilde{\nu}_L}^2, m_{\tilde{\nu}_R}^2, m_{\tilde{\nu}_L}^2) \quad (4.11)$$

where  $\Delta M_{56} = M_5 - M_6$  represents the splitting of heavy neutrino masses. This indicates that in the limit of degenerate masses,  $G_{\text{irr}}^{gg}$  tends to zero.

### b) Gaugino-Higgsino

In this case, we follow a similar procedure as with pure gaugino. We simplify the expression in Eq. (3.98):

$$(\delta M_L^{\text{irr}})_{aa'}^{gh} = K_{aa'} G_{\text{irr}}^{gh} \quad (4.12)$$

where:

$$G_{\text{irr}}^{gh} = 2(-1)^b v_u g_b \sum_{r=1}^4 \frac{1}{m_{\tilde{\chi}_r^0}} O_{rb} O_{r4} \left[ M_5^2 f_3(m_{\tilde{\chi}_r^0}^2, m_{\tilde{\nu}_L}^2, m_{\tilde{\nu}_{R5}}^2) - M_6^2 f_3(m_{\tilde{\chi}_r^0}^2, m_{\tilde{\nu}_{R6}}^2, m_{\tilde{\nu}_L}^2) \right] \quad (4.13)$$

We have the dependence on the heavy neutrino masses and the loop function  $f_3$ , which depend on the masses of the supersymmetric particles. There is implicitly a dependency on  $\mu$ ,  $\tan \beta$  through mixtures and supersymmetric masses.

When we have degenerate R sneutrinos, the contribution is simplified considerably.

$$G_{\text{irr}}^{gh} = 2(-1)^b v_u g_b \Delta M_{56} (M_5 + M_6) \sum_{r=1}^4 \frac{1}{m_{\tilde{\chi}_r^0}} O_{rb} O_{r4} f_3(m_{\tilde{\chi}_r^0}^2, m_{\tilde{\nu}_R}^2, m_{\tilde{\nu}_L}^2) \quad (4.14)$$

Once again, the dependence on the splitting of the heavy neutrino masses appears. The behavior of  $f_3$  has already been analyzed in Fig. 3.5.

In the development of the numerical analysis of the irreducible part, as shown in this Section, the contributions are considerably simplified, showing an appropriate and transparent situation to work with.

In order to understand how these corrections affect the neutrino masses, we will first assume the degenerate states for the R sneutrinos. If neutrinos and sneutrinos are independently degenerate, we find that the corrections disappear. This is because there is a cancellation of the LNV terms in the neutrino sector (Sec. 2.4 and 4.1), on the other side, in the unbroken SUSY limit, degenerate masses for neutrinos also imply degenerate masses for sneutrinos.

When  $\Delta M_{56} \neq 0$ , we have large contributions for the SUSY and non-SUSY parts. In the SUSY-conserving limit where  $M_{\text{SUSY}}, \mu \rightarrow 0$  and  $\tan \beta \rightarrow 1$  (this is a special limit and



$a_\nu = 0$	$M_5 > M_6$		$M_6 > M_5$		$a_\nu \neq 0$	$M_5 > M_6$		$M_6 > M_5$	
	$\mu < 0$	$\mu > 0$	$\mu < 0$	$\mu > 0$		$\mu < 0$	$\mu > 0$	$\mu < 0$	$\mu > 0$
$G_{\text{irr}}^{gg+gh}$	-	$\pm$	+	$\pm$	$G_{\text{irr}}^{gg+gh}$	-	$\pm$	+	$\pm$
$G_{2\text{HDM}}$	+	+	-	-	$G_{2\text{HDM}}$	+	+	-	-

Table 4.1: The signs for SUSY and Non-SUSY contributions when  $a_\nu = 0$  and  $a_\nu \neq 0$ .

it is not stable), it is observed that there is a cancellation between  $(\delta M_L)^{2\text{HDM}}$  and  $\delta M_L^{\text{irr}}$  (this confirms the result in [9]). Furthermore, we find that the pure gaugino  $(\delta M_L^{\text{irr}})^{gg}$  contribution is negligible, and the one that really achieves the cancellation is the gaugino-Higgsino  $(\delta M_L^{\text{irr}})^{gh}$ .

Nevertheless, SUSY is broken, so this cancellation can not be achieved, it is of interest, though, to search for other regions of the parameter space where cancellations can happen. We will begin by examining the irreducible contributions as defined previously for pure gaugino and mixed cases. In these cases, degenerate and non-degenerate R sneutrinos will be considered.

#### 4.2.1 Degenerate R sneutrino exploration

For this analysis, the supersymmetric parameters will be taken as random variables. For each choice of parameters, we can find the sign that the function  $G_{\text{irr}}$  will have and thus determine under what conditions interference is possible. We take  $\tan \beta = [5, 35]$ ,  $a_\nu = [100, 5000]$  GeV,  $M_A, M_1, M_2, M_{\tilde{L}} = [300, 5000]$  GeV and  $m_{\tilde{\nu}} = [10^{-1}, 5000]$ . For the heavy neutrino masses, we are considering the decoupling of neutrino  $N_4$ , and for  $N_{5,6} = [1, 10^3]$  GeV.

The irreducible contributions are described by  $G_{\text{irr}}$  and involve the diagrams of pure-gaugino ( $gg$ ) and gaugino-Higgsino ( $gh$ ), as we have previously examined. We show these results in Table 4.1, we have taken  $10^5$  different parameter combinations. Here are displayed the cases where  $a_\nu = 0$  and  $a_\nu \neq 0$ , with different scenarios depending on the signs of  $\Delta M_{56}$  and  $\mu$ . For example, if we take the case  $M_5 > M_6$  and  $\mu < 0$  for  $G_{\text{irr}}$ , the sign (-) indicates that all the values for that function are negative, otherwise, for this same case but with  $\mu > 0$ , where sign ( $\pm$ ) indicates that there are events with both positive and negative values.

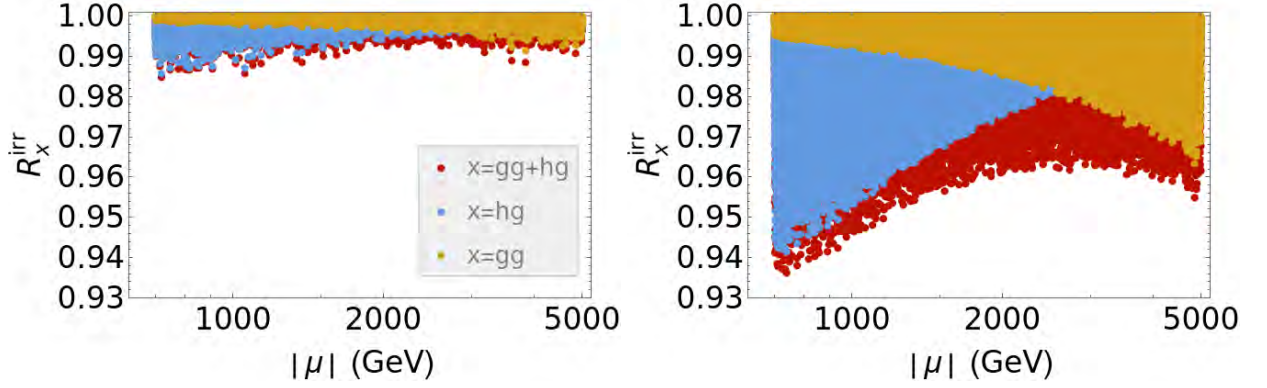


Figure 4.2: The left panel corresponds to the case where  $M_5 = 40$  GeV, while the right panel represents the scenario with  $M_5 = 200$  GeV. In both panels with  $\mu < 0$ , we have fixed values for  $\tan \beta = 8$ ,  $\gamma_{56} = 8$ , and  $M_A = 1100$  GeV.

We can observe that destructive interference is always achieved when  $\mu < 0$ , since  $G_{\text{irr}}^{gg+gh}$  and  $G_{2\text{HDM}}$  have opposite signs. This holds true for both cases where  $\Delta M_{56} > 0$  or  $\Delta M_{56} < 0$ . However, the interference is not as clear when  $\mu > 0$ . As can be seen in the Table, there are cases where the  $G_{\text{irr}}^{gg+gh}$  function is positive or negative, which does not allow us to have a clear idea when some type of interference occurs. In this scenario, we will need to examine the spectrum of parameters to determine if, and under what conditions, destructive interference can be achieved.

As mentioned before,  $R^{\text{csusy}}$  denotes the ratio of supersymmetric and non-supersymmetric contributions. We shall refer to this parameter as  $R^{\text{irr}}$ , and it will represent the ratio with only the irreducible contribution. In the left(right) panel of Fig. 4.2, the values derived from  $R^{\text{irr}}$  are displayed as a function of  $|\mu|$  for  $M_5 = 40(200)$  GeV, assuming that the variables  $-\mu$ ,  $M_2$ ,  $m_{\tilde{L}}$ , and  $m_{\tilde{\nu}}$  vary randomly.

In Fig. 4.2, the gaugino-gaugino ( $G_{\text{irr}}^{gg}$ ), gaugino-higgsino ( $G_{\text{irr}}^{gh}$ ) and total ( $G_{\text{irr}}^{gg+gh}$ ) contributions are shown with orange, blue and red dots respectively. For small  $\mu$ , it can be seen that  $G_{\text{irr}}^{gh}$  is the most relevant contribution for the destructive interference. For  $G_{\text{irr}}^{gg}$  the probability of getting cancellations increases as  $\mu$  grows. When analyzing the total contribution, we find that the region dominated by the  $G_{\text{irr}}^{gh}$  leads to a stronger cancellation. What we see is that larger  $M_h$  masses lead to stronger cancellations, but that is because the 2HDM part is smaller. It can be seen that this reduction of  $R_x^{\text{irr}}$  for  $M_5 = 40$  and 200 GeV is less than 1% and 6% respectively. It is evident that these results are not the best in order to achieve what is wanted ( $R_x^{\text{irr}} \approx 0\%$ ), but this allowed us to know how the

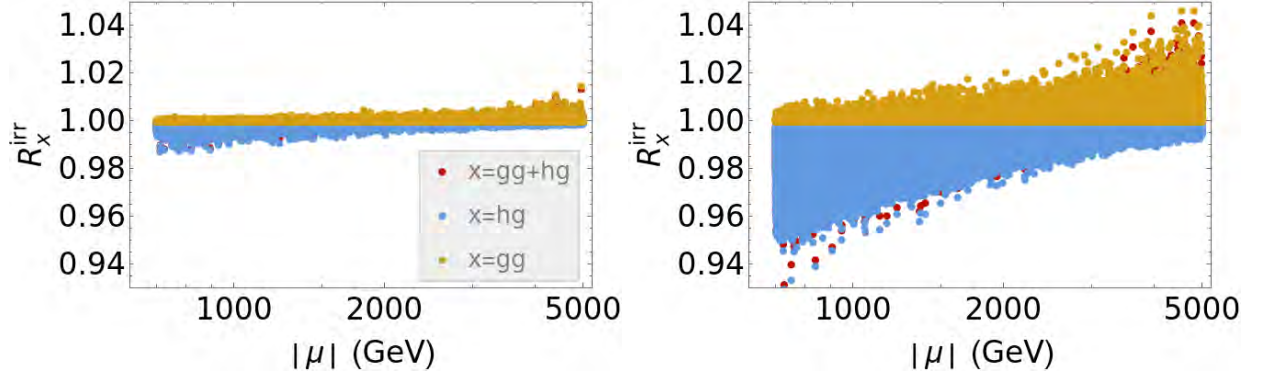


Figure 4.3: We show the scatter plot with the same parameters as in Fig. 4.2 but with  $\mu > 0$ .

parameters are working.

In Figure 4.3, we show the scatterplot for the scenario where  $\mu > 0$ ,  $a_\nu = 0$  with  $M_5 = 40(200)$  GeV in the left panel (right panel), following a similar approach as in the case where  $\mu < 0$ . The orange dots describe pure-gaugino contributions that result in values with  $R_{gg}^{\text{irr}} > 1$ , this indicates that  $G_{\text{irr}}^{gg}$  and  $G_{2\text{HDM}}$  have the same sign. When we have the gaugino-Higgsino contribution, we can see cancellations for small  $\mu$ , but they are not significant. As for the  $\mu < 0$  case, in the right panel, the aforementioned behavior is similar, but with larger  $R_x^{\text{irr}}$  values. The total irreducible contribution (red dots) generally leads to some cancellation (although not very significant) when  $\mu$  is small, i.e. the region dominated by the gaugino-Higgsino part. In contrast, large values of  $\mu$  usually lead to  $R_{gg+hg}^{\text{irr}} > 1$ , which is a region dominated by the pure gaugino contribution.

In this analysis, with  $\mu > 0$ , we find cases where  $R_x^{\text{irr}} > 1$  for all values of  $\mu$ . These are attributed to substantial irreducible contributions with the same sign as the 2HDM part. An extension of this analysis is then important to understand a little more about the behavior of each contribution. For this, we divide the spectrum of  $M_{1,2}$ ,  $\mu$ ,  $m_{\tilde{L}}$  into different hierarchies (see Table 4.2). This could allow us to identify how to avoid constructive interference.

In Fig. 4.4, we show the behavior of  $G_{\text{irr}}^{gg+gh}$  with respect to  $m_{\tilde{\nu}_R}$  for the different hierarchies described in Table 4.2. Since  $G_{2\text{HDM}}$  is negative cancellations are achieved when  $G_{\text{irr}}^{gg+gh}$  is positive. This occurs in the top panels of the Figure, where the sleptons are either the heaviest or second heaviest SUSY particles, since there is no change of sign in the irreducible contribution. This corresponds to the hierarchies *a* and *b* of the table. In

	$a$	$b$	$c$	$d$
—	$\mu < M_1 < M_2 < m_{\bar{L}}$	$\mu < M_1 < m_{\bar{L}} < M_2$	$\mu < m_{\bar{L}} < M_1 < M_2$	$m_{\bar{L}} < \mu < M_1 < M_2$
⋯	$\mu < M_2 < M_1 < m_{\bar{L}}$	$\mu < M_2 < m_{\bar{L}} < M_1$	$\mu < m_{\bar{L}} < M_2 < M_1$	$m_{\bar{L}} < \mu < M_2 < M_1$
—	$M_1 < \mu < M_2 < m_{\bar{L}}$	$M_1 < \mu < m_{\bar{L}} < M_2$	$M_1 < m_{\bar{L}} < \mu < M_2$	$m_{\bar{L}} < M_1 < \mu < M_2$
---	$M_2 < \mu < M_1 < m_{\bar{L}}$	$M_2 < \mu < m_{\bar{L}} < M_1$	$M_2 < m_{\bar{L}} < \mu < M_1$	$m_{\bar{L}} < M_2 < \mu < M_1$
—	$M_1 < M_2 < \mu < m_{\bar{L}}$	$M_1 < M_2 < m_{\bar{L}} < \mu$	$M_1 < m_{\bar{L}} < M_2 < \mu$	$m_{\bar{L}} < M_1 < M_2 < \mu$
---	$M_2 < M_1 < \mu < m_{\bar{L}}$	$M_2 < M_1 < m_{\bar{L}} < \mu$	$M_2 < m_{\bar{L}} < M_1 < \mu$	$m_{\bar{L}} < M_2 < M_1 < \mu$

Table 4.2: Hierarchies for  $\mu, M_1, M_2$  and  $m_{\bar{L}}$  which will be used to describe and identify the degree of interference with the irreducible and reducible contributions.

the lower panels, the function changes sign, causing  $R_{gg+gh}^{\text{irr}} > 1$ , which makes it impossible to guarantee that there is a cancellation.

During the development of this work, we found another contribution in the literature on this topic [9]. Here within the radiative inverse seesaw model, they show interesting results where they manage to optimize cancellations (referred to as "SUSY-screening") and thus relax the restrictions on the LNV parameters in that model. Although the setup is different from ours, it is possible to compare the results obtained since the cancellation mechanism is the same.

Since we are in the irreducible part, we will start with the results shown in [9] for  $\mu$  and  $a_\nu$ . In Figure 4.5, we show the maximum value of  $\Delta M_{65}$  allowed by one loop corrections without exceeding the value of 50% with respect to the light neutrino masses at tree level. We use the equations found in the Chapter 3 on the mass insertion framework and compare them with SPHeno [63], [64], which returns results using the exact calculations with the Higgs mass at the tree level. Considering the values in Table 4.3, we check that both results, SPHeno and mass insertions, agree very well for both  $\mu$  and  $a_\nu$ .

We find that for most values of  $\mu$  and  $a_\nu$  the mass difference  $\Delta M_{65}$  is constrained to very small values. We can find in both cases, fine-tuned values of  $\mu$  and  $a_\nu$  where the SUSY and 2HDM contributions cancel, leading to a peak. These values are in the ballpark of those found in [9]. In this case, the pure-gaugino contribution  $(\delta M_L^{\text{irr}})^{gg}$  dominates mainly due to its dependence on  $\mu$  and  $a_\nu$  in Eq. (3.96), as a result there is a cancellation with the contribution of  $(\delta M_L)^{2\text{HDM}}$ , relaxing the LNV restrictions on  $\Delta M_{65}$ . The peak of the

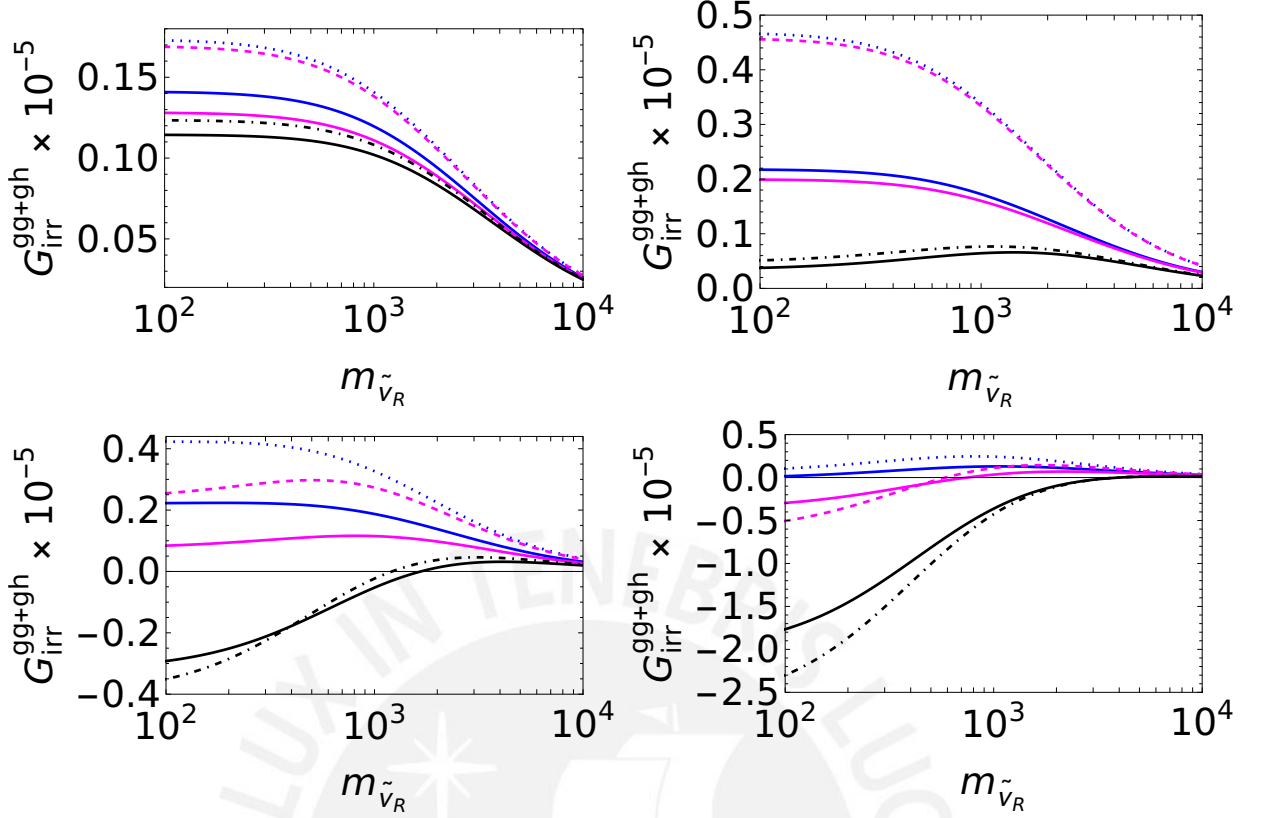


Figure 4.4: We show the behavior of  $G_{\text{irr}}^{gg+gh}$  for the order of the parameters shown in the table. There are four scenarios, see Table 4.2, that are identified as: upper left panel (a) and right (b), lower left panel (c) and right (d).

cancellation decreases, since from that point  $(\delta M_L^{\text{irr}})^{gg}$  no longer only cancels  $(\delta M_L)^{2\text{HDM}}$  but also exceeds it. Unfortunately, comparing this result with Figure 2.7, it can be argued that in this scenario the fine-tuning of the neutrino sector has been transferred to the SUSY sector, although this time without a symmetry such as LN to justify it.

In addition to this problem, we consider that the huge  $|\mu|$ ,  $a_\nu$  solutions have other issues that need to be resolved. The SUSY minimization constraints for  $|\mu|$  would result in a scenario with significant fine-tuning since the soft Higgs masses would need to have extremely specific values in order to cause electroweak symmetry breaking and replicate the observed Z mass at the same time. This would certainly result in a fine-tuning and probably very significant loop corrections to the light Higgs mass. On the other hand, it was argued for  $a_\nu$  in [54] that one had to satisfy the following conditions in order to avoid charge-breaking minima:

$$(a_\nu + M_R)^2 \leq 3(m_{H_u}^2 + |\mu|^2 + m_L^2 + m_{\tilde{V}_R}^2 + M_R^2 + B_\nu), \quad (4.15)$$

Parameter	Numerical value/interval
$\tan \beta$	2, 20
$\mu$	1200 GeV
$M_1$	1500 GeV
$M_2$	1500 GeV
$m_h$	$125.38 \pm 0.14$ GeV
$M_A$	5000 GeV
$m_H$	5002.8 GeV
$M_N$	500 GeV
$m_{\tilde{L}}^2$	$(3500 \text{ GeV})^2$
$\mu_R$	$[10^{-6}, 10^2]$ GeV

Table 4.3: Numerical values of the parameters used in [9].

Considering the benchmark spectrum, is unlikely to hold. The cancellations described in [9] are not seen as a generic property of the  $\nu_R$ MSSM, but rather as requiring additional ingredients beyond the basic structure of the model.

#### 4.2.2 Non-degenerate R sneutrinos exploration

Given the difficulty in achieving large cancellations, as demonstrated in the previous section, we will take into account the case when the masses of the sneutrinos  $\tilde{\nu}_5$  and  $\tilde{\nu}_6$  are non-degenerate. From the equations calculated for a loop, considering both the pure-gaugino and mixed contributions (See Eqs. (4.10) and (4.13)), it can be observed that the parts corresponding to  $\tilde{\nu}_{R5}$  and  $\tilde{\nu}_{R6}$  appear in different terms of the loop function with opposite signs. Based on the structure uncovered, when degeneracy occurs, the contribution becomes smaller.

In this analysis, we will suppose that one of the R sneutrino masses is very large which decouples the particle from the loop correction. This maximizes the total loop function and enhances the supersymmetric contribution. As for the scenario with degenerate R sneutrinos, we will assume  $\mu < 0$ . We found that the function  $G_{\text{irr}}^{gg+gh}$  is negative when  $\Delta M_{65} < 0$  and  $\Delta m_{\tilde{\nu}_{6,5}} > 0$ . On the other hand, if  $\Delta M_{65} > 0$  and  $\Delta m_{\tilde{\nu}_{6,5}} < 0$ ,  $G_{\text{irr}}^{gg+gh}$  is positive. This enables us to identify the correct spectrum that generates cancellations.

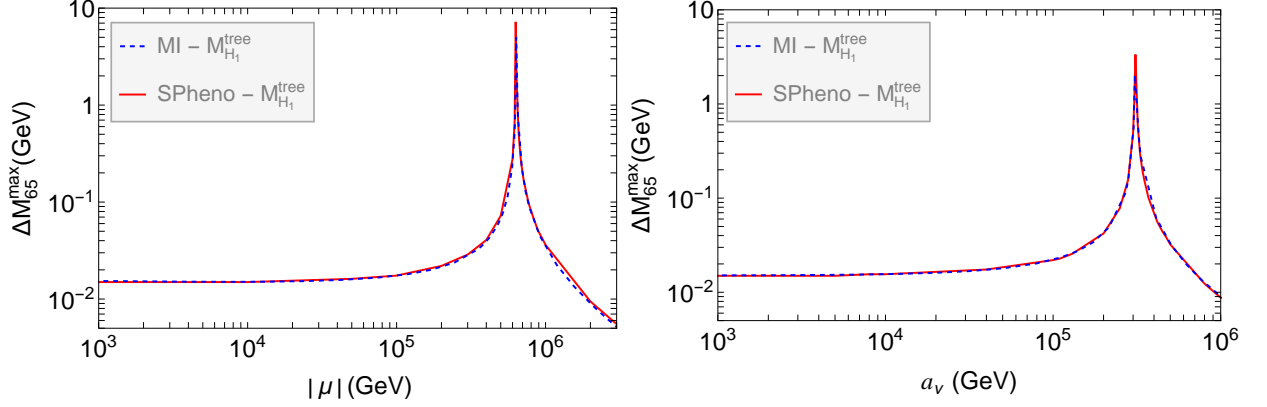


Figure 4.5: The maximum  $\Delta M_{65}$  allowed as a function of  $\mu$  (Left panel) and  $a_\nu$  (Right panel). Here we consider the spectrum of parameters in Table 4.3, with  $\gamma_{56}=8$  and  $|U_{\mu 5}| = 1.3 \times 10^{-7}$ .

In the left panel of Fig. 4.6, we set  $m_{\tilde{\nu}_{R5}}$  to a very large value with  $\Delta M_{65} > 0$ . We show that, for a given  $\Delta M_{65}$ , the value of  $R_{gh+gg}^{\text{irr}}$  increases with  $m_{\tilde{\nu}_{R6}}$ . Therefore, the cancellations are stronger for  $m_{\tilde{\nu}_{R6}}$  which is closer to its equivalent in heavy neutrino mass (ie, small soft masses). Furthermore, in contrast to the degenerate scenario, the cancellation efficiency depends on the splitting of the heavy neutrino mass, with smaller values of  $R_{gh+gg}^{\text{irr}}$  for smaller  $\Delta M_{65}$ . The reason for this is that the full SUSY contribution no longer depends on neutrino splitting, therefore lowering  $\Delta M_{65}$  merely lowers  $(\delta M_L)^{2HDM}$ , which in turn results in lower  $R_{gh+gg}^{\text{irr}}$ . Contrary to the degenerate case, the destructive interference this time can be significant for moderate values of  $|\mu|$ , with the SUSY contribution occasionally outweighing the non-SUSY component ( $R_{gh+gg}^{\text{irr}} < 0$ ).

In the right panel of Fig. 4.6, we have the maximum mixing versus  $\Delta M_{65}/M_5$ . The red curves represent the bounds coming from a standard seesaw, while the model of this work is shown in the blue curve. A relaxation of these limits is seen when  $\Delta M_{65}$  is small, apparently, it can be understood as a non-negligible effect, however, this vanishes when the splitting increases. So despite having a non-degenerate case, SUSY does not relax the fine-tuning associated with heavy neutrinos with large splitting and mixing. The gray curves shown for small splittings indicate tighter bounds than those of the standard seesaw, this is because the supersymmetric contribution is dominant, in other words, we have negative values of  $R_{gh+gg}^{\text{irr}}$ .

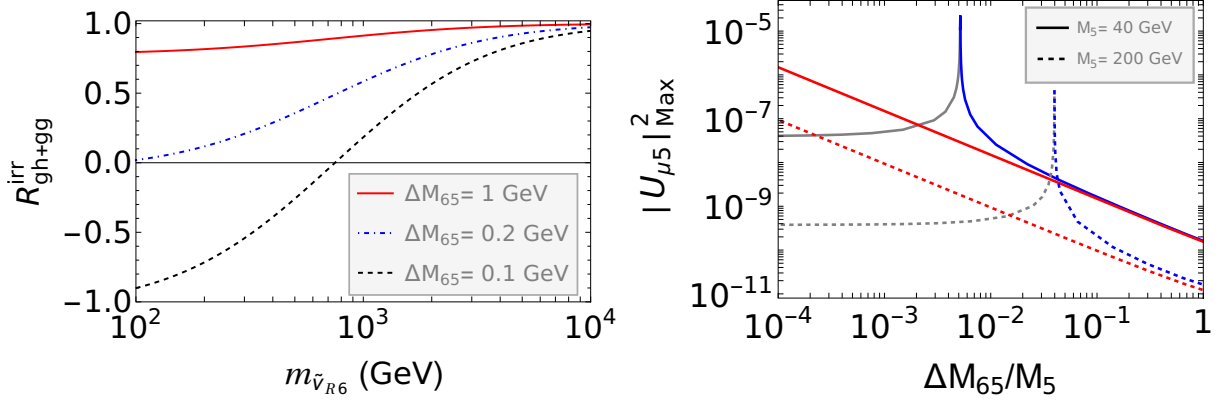


Figure 4.6: Left: Dependence of  $R_{gh+gg}^{\text{irr}}$  with  $m_{\tilde{\nu}_{R6}}$ , for several values of  $\Delta M_{65}$ . Heavy neutrino mass is set to  $M_5 = 40$  GeV. Right: Maximum allowed value of  $|U_{\mu 5}|^2$ , as a function of  $\Delta M_{65}/M_5$ , for two values of  $M_5$ . Limits on the Standard Seesaw are shown in red. Blue and gray lines show limits for the spectrum described in the text. For gray lines, the SUSY contribution is larger than the one from 2HDM.

### 4.3 Reducible SUSY contributions in Benchmark Scenario

A set of manageable expressions could be found for the three full contributions in Chapter 3. The new parameter  $b_\nu$  appears, and we need to examine its importance in the SUSY one-loop equations.

#### a) Pure higgsino

We follow the same treatment used to simplify the irreducible contributions. Consequently, for Eq. (3.100), we have the following expression:

$$(\delta M_L^{\text{red}})_{aa'}^h = K_{aa'} G_{\text{red}}^h \quad (4.16)$$

where

$$G_{\text{red}}^h = 2b_\nu \sum_{r=1}^4 \frac{1}{m_{\tilde{\chi}_r^0}} O_{r4}^2 \left[ M_5^2 f_3(m_{\tilde{\chi}_r^0}^2, m_{\tilde{\nu}_{R5}}^2, m_{\tilde{\nu}_{R5}}^2) - M_6^2 f_3(m_{\tilde{\chi}_r^0}^2, m_{\tilde{\nu}_{R6}}^2, m_{\tilde{\nu}_{R6}}^2) \right] \quad (4.17)$$

We see a linear dependence on  $b_\nu$  and no dependence on the mass of the L sneutrinos.

If we consider degenerate R sneutrinos, we can write that expression as:

$$G_{\text{red}}^h = 2b_\nu \sum_{r=1}^4 \frac{1}{m_{\tilde{\chi}_r^0}} O_{r4}^2 \Delta M_{56} (M_5 + M_6) f_3(m_{\tilde{\chi}_r^0}^2, m_{\tilde{\nu}_R}^2, m_{\tilde{\nu}_R}^2) \quad (4.18)$$



As in the irreducible case, it can be written in terms of the splitting of the heavy neutrino masses.

b) **Pure gaugino**

Once again, simplifying the expression in Eq. (3.103):

$$(\delta M_L^{\text{red}})_{aa'}^{gg} = K_{aa'} G_{\text{irr}}^{gg} \quad (4.19)$$

where:

$$\begin{aligned} G_{\text{red}}^{gg} &= \frac{(-1)^{b+b'}}{4} v_u^2 g_b g_{b'} b_\nu \sum_{r=1}^4 \frac{1}{m_{\tilde{\chi}_r^0}^5} O_{rb} O_{rb'} \\ &\times \left[ M_5^2 (M_5^2 + (a_\nu - \mu \cot \beta)^2) f_5(m_{\tilde{\chi}_r^0}^2, m_{\tilde{\nu}_L}^2, m_{\tilde{\nu}_{R5}}^2, m_{\tilde{\nu}_{R5}}^2, m_{\tilde{\nu}_L}^2) \right. \\ &\quad \left. - M_6^2 (M_6^2 + (a_\nu - \mu \cot \beta)^2) f_5(m_{\tilde{\chi}_r^0}^2, m_{\tilde{\nu}_L}^2, m_{\tilde{\nu}_{R6}}^2, m_{\tilde{\nu}_{R6}}^2, m_{\tilde{\nu}_L}^2) \right] \quad (4.20) \end{aligned}$$

The dependency is linear in  $b_\nu$  and quadratic in the  $(a_\nu - \mu \cot \beta)$  term. In what follows, the analysis will consider  $a_\nu = 0$ , which also indicates that a sign change in  $\mu$  would not lead to a global sign change in this expression, although it is possible to see a change in the sign due to the neutralino mixings. If the degenerate R sneutrinos are also considered, the expression can be written as:

$$\begin{aligned} G_{\text{red}}^{gg} &= \frac{(-1)^{b+b'}}{4} v_u^2 g_b g_{b'} b_\nu \Delta M_{56} (M_5 + M_6) (M_5^2 + M_6^2 + (a_\nu - \mu \cot \beta)^2) \\ &\times \sum_{r=1}^4 \frac{1}{m_{\tilde{\chi}_r^0}^5} O_{rb} O_{rb'} f_5(m_{\tilde{\chi}_r^0}^2, m_{\tilde{\nu}_L}^2, m_{\tilde{\nu}_R}^2, m_{\tilde{\nu}_R}^2, m_{\tilde{\nu}_L}^2) \quad (4.21) \end{aligned}$$

c) **Gaugino-Higgsino**

From Eq. (3.106):

$$(\delta M_L^{\text{red}})_{aa'}^{gh} = K_{aa'} G_{\text{red}}^{gh} \quad (4.22)$$

where:

$$\begin{aligned} G_{\text{red}}^{gh} &= (-1)^b v_u g_b (a_\nu - \mu \cot \beta) b_\nu \\ &\times \sum_{r=1}^4 \frac{1}{m_{\tilde{\chi}_r^0}^3} O_{rb} O_{r4} \left( M_5^2 f_4(m_{\tilde{\chi}_r^0}^2, m_{\tilde{\nu}_L}^2, m_{\tilde{\nu}_{R5}}^2, m_{\tilde{\nu}_{R5}}^2) - M_6^2 f_4(m_{\tilde{\chi}_r^0}^2, m_{\tilde{\nu}_L}^2, m_{\tilde{\nu}_{R6}}^2, m_{\tilde{\nu}_{R6}}^2) \right) \quad (4.23) \end{aligned}$$

There is a linear dependence on  $a_\nu$  and  $b_\nu$  and the behavior of the function  $f_4$  is described in Fig. 3.5. If we also have degenerate R sneutrinos:

$$G_{\text{red}}^{gh} = (-1)^b v_u g_b (a_\nu - \mu \cot \beta) b_\nu \Delta M_{56} (M_5 + M_6) \sum_{r=1}^4 \frac{1}{m_{\tilde{\chi}_r^0}^3} O_{rb} O_{r4} f_4(m_{\tilde{\chi}_r^0}^2, m_{\tilde{\nu}_L}^2, m_{\tilde{\nu}_R}^2, m_{\tilde{\nu}_R}^2) \quad (4.24)$$

$a_\nu = 0$	$M_5 > M_6$	$M_6 > M_5$
$b_\nu > 0$	$\mu < 0$	
$G_{\text{red}}^{gg+gh+hh}$	$\pm$	$\pm$
$G_{\text{red}}^{gg}$	$+$	$-$
$G_{\text{red}}^{gh}$	$+$	$-$
$G_{\text{red}}^{hh}$	$\pm$	$\pm$

Table 4.4: We show the signs for  $G_{\text{red}}$  fixing  $\tan\beta = 8$  and  $M_A = 1100$  GeV.

### 4.3.1 Degenerate R sneutrinos exploration

In Table 4.4, for the case with  $\Delta M_{56} < 0$ ,  $b_\nu > 0$  and  $\mu < 0$ , we find that  $G_{\text{red}}^{gg}$  and  $G_{\text{red}}^{gh}$  are negative while  $G_{\text{red}}^{hh}$  can take any sign. We can observe the typical values of  $G_{\text{red}}^{gg+gh}$  graphically in the scatter plot of Fig. 4.7 when the parameters  $M_2$ ,  $\mu$ ,  $b_\nu$ ,  $m_{\tilde{L}}$ ,  $m_{\tilde{\nu}}$  take the same values as those used in Sec. 4.2.1 and additionally  $b_\nu = [0, 35]$  GeV. No pattern is identified in the upper panels for  $M_2$  and  $b_\nu$  in the same way for  $\mu$  (lower panel). In the middle panels. For large  $m_{\tilde{\nu}_L}$  and  $m_{\tilde{\nu}_R}$ , we have  $R_{gg+gh}^{\text{red}} \rightarrow 1$ . A cancellation is never achieved with these contributions because the non-supersymmetric contribution also has the same sign as that for 2HDM, we always have  $R_{gg+gh}^{\text{red}} > 1$ . However, the supersymmetric functions will change sign if we take  $b_\nu \rightarrow -b_\nu$ , Eqs.(4.21) and (4.24), and this leads us to the scenario where destructive interference would be possible.

In Fig. 4.8, it is shown how  $R_{hh}^{\text{red}}$  varies with respect to  $\mu$ ,  $M_2$ ,  $m_{\tilde{\nu}_R}$  and  $b_\nu > 0$ . In the upper left panel, we analyze the case with  $b_\nu$ , here we can see that with the increase of this parameter, we usually have  $R_{hh}^{\text{red}} < 1$ , although it is also possible to have  $R_{hh}^{\text{red}} > 1$ . In the upper right panel, with small values of  $M_2$  it is possible to have constructive interference, with the increase of this parameter,  $R_{hh}^{\text{red}} < 1$  can be ensured. In the lower left panel, the preference arises for small values of  $\mu$  where cancellations occur, large values of  $\mu$  can lead to  $R_{hh}^{\text{red}} > 1$ . In the lower right panel, the largest cancellations are obtained when the masses for the R sneutrinos are small. In this scan, as shown for each parameter, the cancellations found are still very small.

In summary, to achieve cancellations with the gaugino-gaugino and gaugino-higgsino contributions, it is necessary to have  $b_\nu < 0$  with  $\Delta M_{56} < 0$ . On the other hand, for

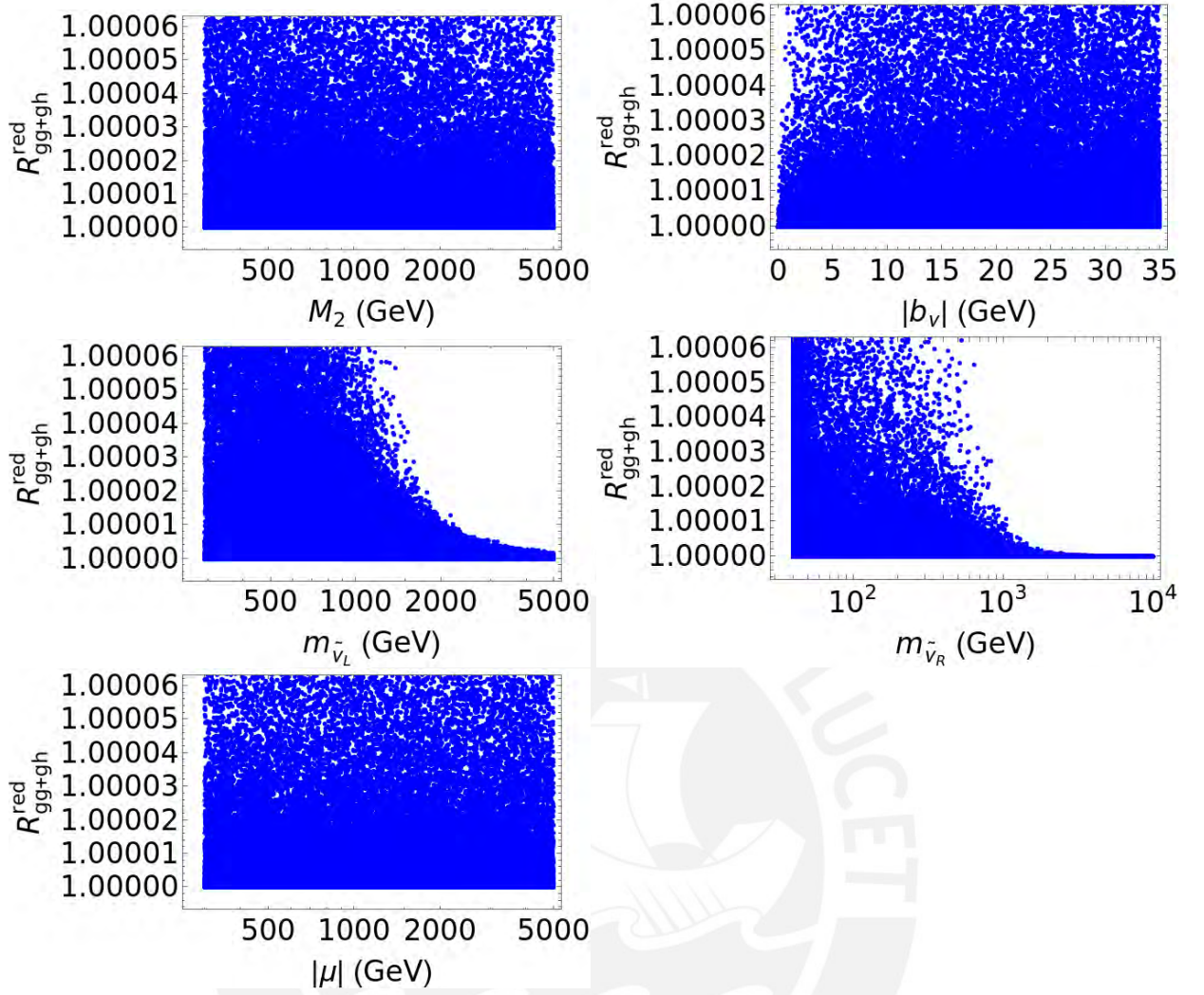


Figure 4.7: The  $R$  parameter is depicted considering the contributions from pure Gaugino and mixed terms for  $b_\nu > 0$  and  $\mu < 0$ . The parameters are being randomly varied for  $M_A = 1100$  GeV and  $\tan \beta = 8$ .

higgsino-higgsino contributions with  $b_\nu < 0$ , it is crucial to have a large  $|\mu|$  to avoid constructive interference. For  $b_\nu > 0$  is necessary to have small  $|\mu|$  values, however, this case is in conflict with the other reducible contributions.

If we combine the results from reducible and irreducible contributions, we confirm that the large  $\mu$  and negative  $b_\nu$  achieve the strongest cancellations. In Figure 4.9, we quantify this total supersymmetric contribution represented by  $R_{gg+gh+hh}^{\text{red}}$ . The parameters  $\mu$ ,  $M_1$ ,  $M_2$  and  $m_{\tilde{L}}$  are permuted around the test values to 500, 1000, 2000 and 5000 GeV. In order to quantify the behavior of  $R_{gg+gh+hh}^{\text{red}}$  we set  $b_\nu = -100$  GeV. In the upper panels of the Figure we show the hierarchies  $a$  (left) and  $b$  (right) of Table 4.2. Constructive interference between the reducible contribution and 2HDM ( $R_{gg+gh+hh}^{\text{red}} > 1$ ) is seen and therefore is

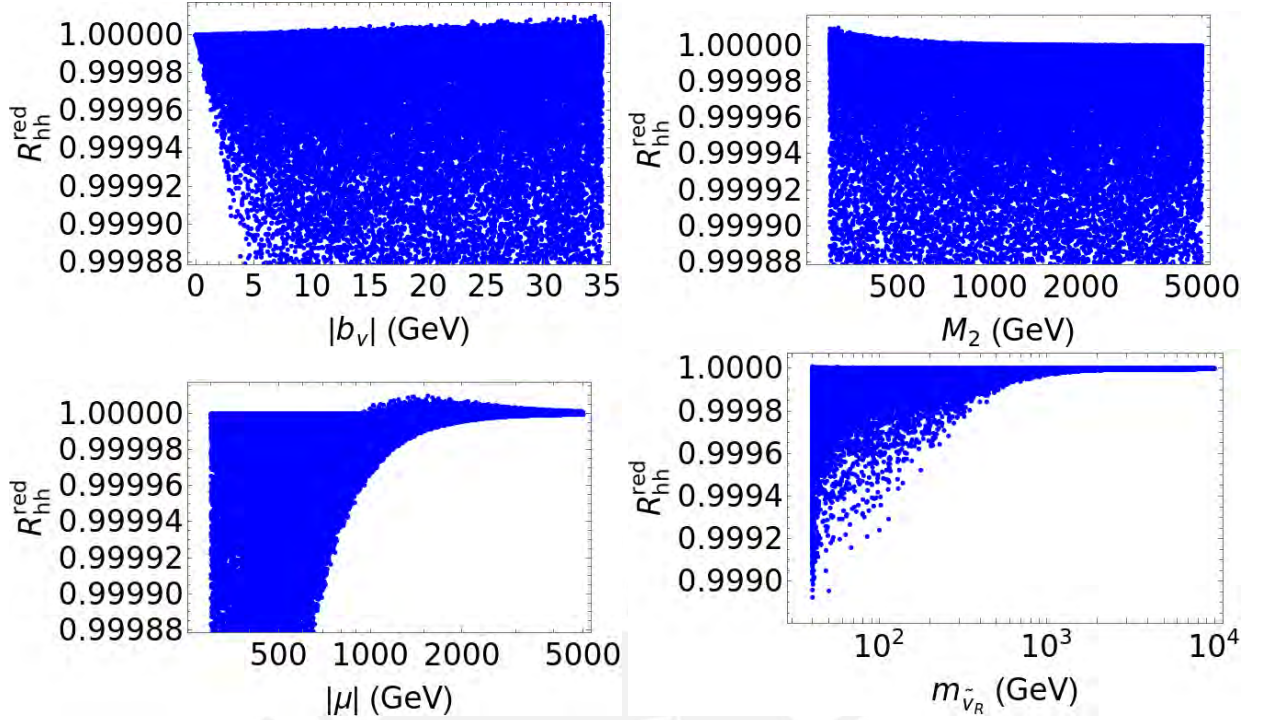


Figure 4.8: We show the higgsino-higgsino contribution for  $b_\nu > 0$  and  $\mu < 0$  with  $\tan \beta = 8$  and  $M_A = 1100$  GeV.

disfavoured. In the lower left and right panels we show hierarchies (c) and (d) respectively, we find that having a light  $m_{\tilde{L}}$  compared to  $m_{\tilde{\nu}_R}$  is important to get the cancellations. We need to know for which parameter hierarchy the largest cancellation is obtained. It can be seen that  $R_{gg+gh+hh}^{\text{red}} < 1$  is always achieved if  $|\mu| > M_1, M_2 > m_{\tilde{L}}$ .

We explore this situation in Fig. 4.10, where  $M_2 = 2M_1$  and vary between 700 and 5000 GeV, respecting the mentioned hierarchy. The effects are maximal for tiny values of  $m_{\tilde{\nu}}$ , which we set to 0.5 GeV in this example. We apply the following restriction  $b_\nu = M_5 - 5$  GeV. This arises due to the comparison of our numerical results with the simulation in SPheno in order to avoid tachyonic states.

In Fig. 4.10, it is found that the gaugino-gaugino contributions dominate the correction, followed by the gaugino-higgsino and the higgsino-higgsino. The strongest cancellations occur for large values of  $\mu$  and small  $m_{\tilde{L}}$  (green region). If we compare the left ( $M_5 = 40$  GeV) and right ( $M_5 = 200$  GeV) panels, we see that larger values of  $M_5$  somewhat favour the cancellations. Nevertheless, the value of  $R$  rarely becomes lower than 0.99. When compared with the corresponding irreducible contributions, we find that the reducible part never exceeds 0.6% of the latter. Therefore, considering reducible contributions does not

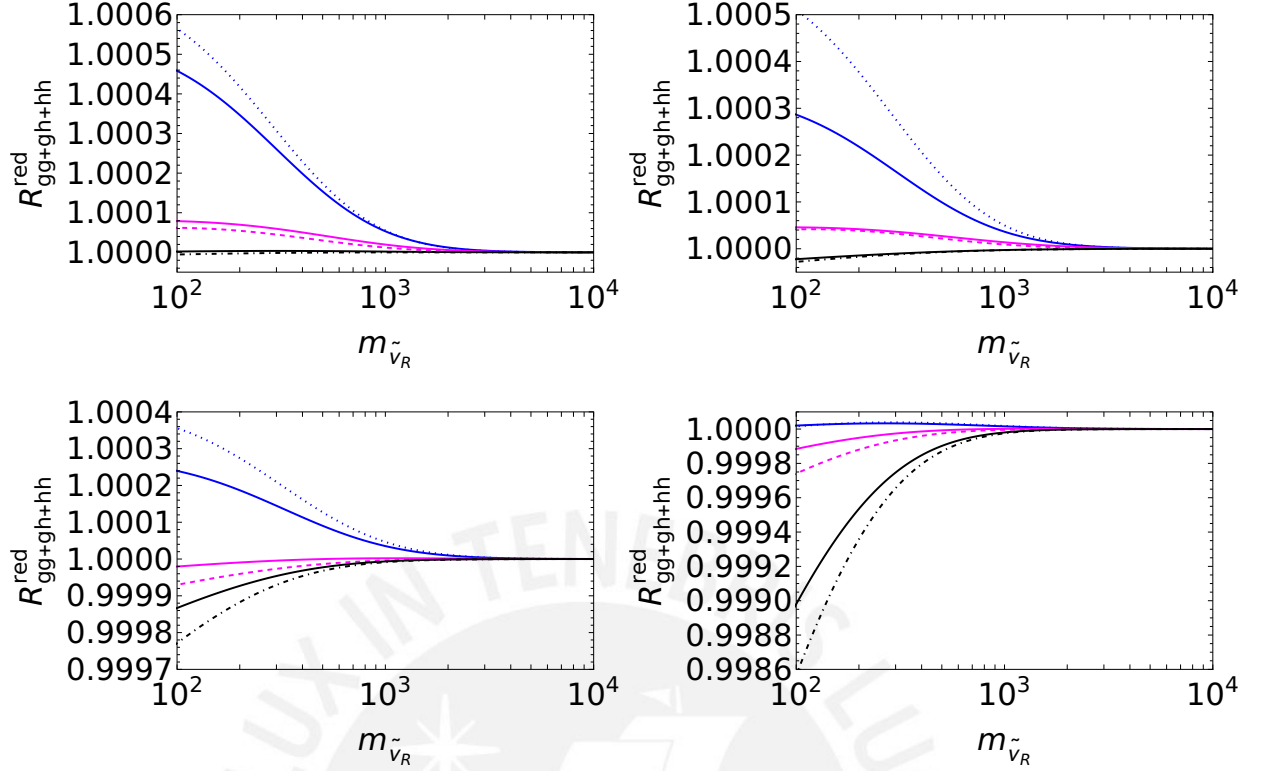


Figure 4.9: We have the same hierarchy in the parameters described in Fig. 4.4 for  $b_\nu < 0$  and  $\mu < 0$ .

have sufficient relevance in the analysis.

In Fig. 4.11, we show the behavior of  $b_\nu$  versus the maximum allowed  $\Delta M_{65}$  for  $\tan \beta = 2$  and  $\gamma_{56} = 8$ . For a wide  $b_\nu$  interval, the two curves by SPHeno and the MI match numerically. However, it is not possible to reach very large values with SPHeno. The peak found (dashed line) is only obtained with the expressions found for the mass insertions. This result is again contrary to the claims in [9], where a cancellation should be found for small values of  $b_\nu$  (This article additionally shows the case for  $\tan \beta = 20$ . However, we do not reproduce it, so we only display one scenario).

Thus, according to our results, it is impossible to reproduce this with the mass insertions calculated in Chapter 4. What we get is that the cancellation is achieved at very large values of  $b_\nu$ . As we did previously for  $\mu$  and  $a_\nu$ , we verified the results with SPHeno. We can see that it is not possible to reproduce what was obtained with the mass insertions for the entire range of  $b_\nu$ , due to the appearance of tachyons. However, we also confirm that no cancellation appears for small values of  $b_\nu$ , indicating that reducible contributions, similarly to the irreducible ones, do not solve the fine-tuning problem for light neutrino

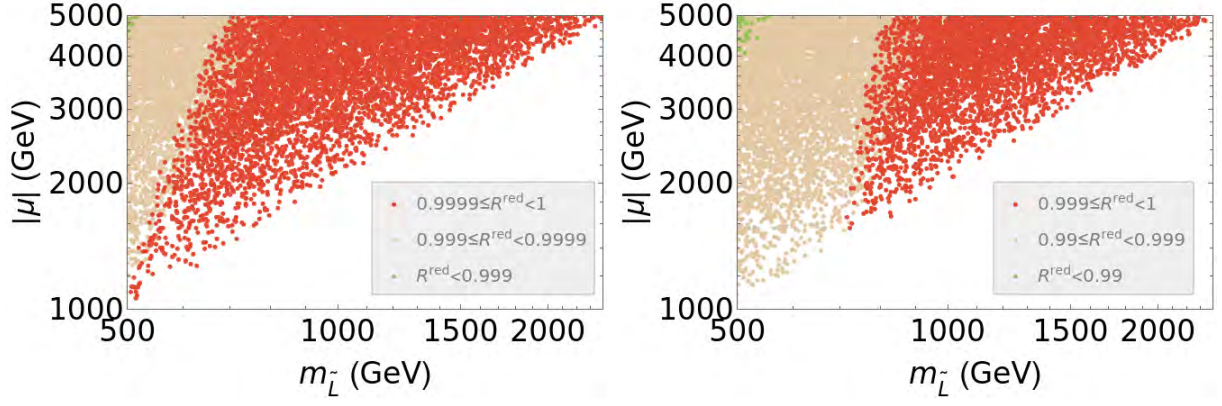


Figure 4.10: Values of  $R_{gg+gh+hh}^{\text{red}}$  parameter for different values of  $m_{\tilde{L}}$  and  $|\mu|$ , with  $M_5 = 200$  GeV (right) and  $M_5 = 40$  GeV (left).

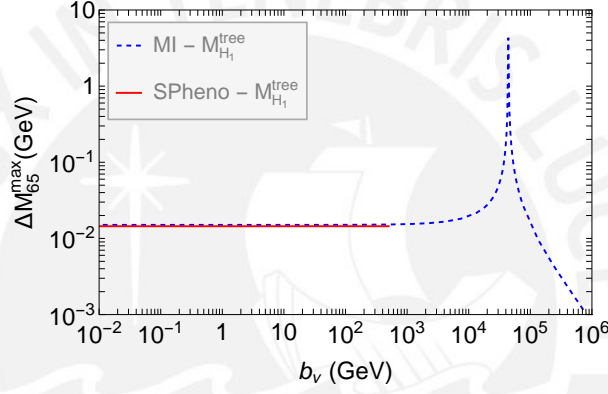


Figure 4.11: Maximum allowed  $\Delta M_{65}$  as a function of  $b_{\nu}$ , for the SUSY spectrum considered in Table 4.3 , with  $\tan \beta = 2$ . We set  $\gamma_{56} = 8$ , such that  $|U_{\mu 5}|^2 = 1.3 \times 10^{-7}$ .

masses.

## CONCLUSIONS

At the beginning of the work, a brief description of the contributions to loop corrections was made within the framework of the type-I seesaw model. In this description, large corrections to the light neutrino masses are obtained. By introducing the lepton number symmetry to the model, when it is slightly broken, it leads to states called pseudo-Dirac and avoids the aforementioned problem. However, this constrains the search for any kind of LNV signal in collider experiments.

We compare the results found with those described in a work shown a few years ago, which proposes an extension of the supersymmetric model where quantum corrections are kept under control. The fact that in unbroken SUSY the quantum corrections to terms in the superpotential cancel gave rise to the hope that in the broken situation, a soft SUSY screening effect would follow. As a result, it was anticipated that the neutrino sector would be allowed to have bigger LNV parameters, which would be reflected in larger heavy neutrino mass splittings. This would improve the motivation for collider studies for LNV occurrences linked to a single heavy neutrino.

The two irreducible and three reducible SUSY contributions to the loop-corrected masses were therefore thoroughly examined. By focusing on heavy neutrino mass ranges that are currently available to collider experiments, we identified the regions of parameter space that ensure cancellations between the latter and the non-SUSY loops. However, the efficiency of these cancellations is not very good, despite the fact that scenarios were sought to maximize and improve these results.

We found that the irreducible SUSY quantum corrections were the strongest. We

discovered no discernible screening effect in the case of degenerate sneutrinos with values below the TeV scale. For very large values of  $|\mu|$  and  $a_\nu$ , we did confirm that the pure gaugino loops could be tuned to cancel the non-SUSY contributions, but we argued that doing so could lead to issues in other areas of the model.

Additionally, we presented a situation with non-degenerate sneutrinos and discovered that the screening could be done more effectively without the need for a large  $|\mu|$  or  $a_\nu$ . Despite this, the LNV restrictions were only very slightly loosened.

It should be observed that none of the aforementioned scenarios in which cancellations could be effective result from non-renormalization theorems. The irreducible gaugino-higgsino loop, which, as we have shown, only dominates for tiny  $|\mu|$ , is the only SUSY screening contribution that does not depend on SUSY breaking and may therefore be assigned to the theorems. None of the instances where cancellations are effective rely on this modification. Instead, they all require extremely precise parameter values, indicating that what we are seeing is a transfer of fine-tuning from the neutrino model sector to its SUSY sector. Although SUSY screening does, in theory, appear interesting, in practice, it does not seem reasonable to use the entire supersymmetric framework to handle this problem, in our opinion.



## Casas-Ibarra Parametrization

This appendix is based on the article [31]. We start with the full neutrino mass matrix  $M_\nu$ , which is diagonalized via:

$$M_\nu = U^* \hat{M}_\nu U^\dagger \quad (\text{A.1})$$

where  $\hat{M}_\nu$  is a diagonal matrix and  $U$  is unitary. These can be written in terms of blocks:

$$M_\nu = \begin{pmatrix} 0 & M_D \\ M_D^T & M_R \end{pmatrix} \quad (\text{A.2})$$

$$= U^* \begin{pmatrix} \hat{m}_\ell & 0 \\ 0 & \hat{M}_h \end{pmatrix} U^\dagger \quad (\text{A.3})$$

Where  $\hat{m}_\ell$  and  $\hat{M}_h$  are diagonal matrices with the light and heavy neutrino eigenvalues. We consider a general expression for mixing matrix  $U$  as

$$U = \begin{pmatrix} X & Q \\ T & Z \end{pmatrix} \quad (\text{A.4})$$

We will assume that  $X, Q, T$  and  $Z$  are invertible matrices. For a unitary matrix  $UU^\dagger = U^\dagger U = \mathbb{1}$ . Using Eq. (A.31), we can rewrite  $M_\nu$  as

$$M_\nu = \begin{pmatrix} X^* \hat{m}_\ell X^\dagger + Q^* \hat{M}_h Q^\dagger & X^* \hat{m}_\ell T^\dagger + Q^* \hat{M}_h Z^\dagger \\ T^* \hat{m}_\ell X^\dagger + Z^* \hat{M}_h Q^\dagger & T^* \hat{m}_\ell T^\dagger + Z^* \hat{M}_h Z^\dagger \end{pmatrix} \quad (\text{A.5})$$

Comparing with the active-active sector in the neutrino mass matrix, we find:

$$0 = X^* \hat{m}_\ell X^\dagger + Q^* \hat{M}_h Q^\dagger \quad (\text{A.6})$$

$$\Rightarrow \mathbb{1} = -\hat{M}_h^{-1/2} Q^{*-1} X^* \hat{m}_\ell^{1/2} \hat{m}_\ell^{1/2} X^\dagger Q^{\dagger-1} \hat{M}_h^{-1/2} \quad (\text{A.7})$$

We define

$$R^T = -i \hat{m}_\ell^{1/2} X^\dagger Q^{\dagger-1} \hat{M}_h^{-1/2} \quad (\text{A.8})$$

where  $R$  is a orthogonal matrix ( $RR^T = \mathbb{1}$ ). Thus  $Q$  can be written:

$$Q = i X \hat{m}_\ell^{1/2} R^\dagger \hat{M}_h^{-1/2}. \quad (\text{A.9})$$

Using the definition of unitary matrix  $U$

$$UU^\dagger = \begin{pmatrix} XX^\dagger + QQ^\dagger & XT^\dagger + QZ^\dagger \\ TX^\dagger + ZQ^\dagger & TT^\dagger + ZZ^\dagger \end{pmatrix}. \quad (\text{A.10})$$

From Eq. (A.10) we have

$$XX^\dagger + QQ^\dagger = \mathbb{1} \quad (\text{A.11})$$

$$\Rightarrow XX^\dagger = \mathbb{1} - QQ^\dagger \quad (\text{A.12})$$

Using the definition of  $Q$  (Eq. (A.9))

$$XX^\dagger = \mathbb{1} - X \hat{m}_\ell^{1/2} R^\dagger \hat{M}_h^{-1/2} \hat{M}_h^{-1/2} R \hat{m}_\ell^{1/2} X^\dagger \quad (\text{A.13})$$

$$\Rightarrow \mathbb{1} = X^{-1} X^{\dagger-1} - \hat{m}_\ell^{1/2} R^\dagger \hat{M}_h^{-1} R \hat{m}_\ell^{1/2} \quad (\text{A.14})$$

$$\Rightarrow X^{-1} X^{\dagger-1} = \mathbb{1} + \hat{m}_\ell^{1/2} R^\dagger \hat{M}_h^{-1} R \hat{m}_\ell^{1/2}. \quad (\text{A.15})$$

For any matrix we can do the Polar decomposition

$$A = UP \begin{cases} U : \text{Unitary Matrix} \\ P : \text{Positive Hermitian Matrix} \end{cases}$$

Thus, we can decompose  $X$

$$X = WH \quad H = H^\dagger \quad WW^\dagger = \mathbb{1} \quad (\text{A.16})$$

$$X^{-1} X^{\dagger-1} = (WH)^{-1} (H^\dagger W^\dagger)^{-1} \quad (\text{A.17})$$

$$= H^{-2} \quad (\text{A.18})$$

Using A.15 and A.18

$$H^{-2} = \mathbb{1} + \hat{m}_\ell^{1/2} R^\dagger \hat{M}_h^{-1} R \hat{M}_\ell^{1/2} \quad (\text{A.19})$$

$$\Rightarrow H = \left( \mathbb{1} + \hat{m}_\ell^{1/2} R^\dagger \hat{M}_h^{-1} R \hat{m}_\ell^{1/2} \right)^{-1/2} \quad (\text{A.20})$$

From Eq. (A.10)

$$XT^\dagger + QZ^\dagger = 0 \quad (\text{A.21})$$

$$\Rightarrow T^\dagger = -X^{-1}QZ^\dagger \quad (\text{A.22})$$

$$\Rightarrow T = i Z \hat{M}_h^{-1/2} R \hat{m}_\ell^{1/2} \quad (\text{A.23})$$

We do the Polar decomposition for  $Z$

$$Z = \bar{W} \bar{H} \quad \bar{H} = \bar{H}^\dagger \quad \bar{W} \bar{W}^\dagger = \mathbb{1} \quad (\text{A.24})$$

Using unitarity of  $U$ , we also have:

$$TT^\dagger + ZZ^\dagger = \mathbb{1} \quad (\text{A.25})$$

$$\Rightarrow ZZ^\dagger = \mathbb{1} - TT^\dagger \quad (\text{A.26})$$

Using Eq. (A.23)

$$\bar{H}^{-2} = \mathbb{1} + \hat{M}_h^{-1/2} R \hat{m}_\ell R^\dagger \hat{M}_h^{-1/2} \quad (\text{A.27})$$

$$\Rightarrow \bar{H} = \left( \mathbb{1} + \hat{M}_h^{-1/2} R \hat{m}_\ell R^\dagger \hat{M}_h^{-1/2} \right)^{-1/2} \quad (\text{A.28})$$

Finally, we have the next definitions for  $H$  and  $\bar{H}$

$$H = \left( \mathbb{1} + \hat{m}_\ell^{1/2} R^\dagger \hat{M}_h^{-1} R \hat{m}_\ell^{1/2} \right)^{-1/2} \quad (\text{A.29})$$

$$\bar{H} = \left( \mathbb{1} + \hat{M}_h^{-1/2} R \hat{m}_\ell R^\dagger \hat{M}_h^{-1/2} \right)^{-1/2} \quad (\text{A.30})$$

Then the mixing matrix in this parametrization is:

$$U = \begin{pmatrix} WH & iWH\hat{m}_\ell^{1/2}R^\dagger\hat{M}_h^{-1/2} \\ i\bar{W}\bar{H}\hat{M}_h^{-1/2}R\hat{m}_\ell^{1/2} & \bar{W}\bar{H} \end{pmatrix} \quad (\text{A.31})$$

Where  $W$  is a unitary matrix, when  $H = I$  it can be identified with the PMNS matrix.

We are interested in the heavy neutrinos  $M_5$  and  $M_6$  ( $\rho_{56}, \gamma_{56} \neq 0$ ). The terms in the  $R$  matrix  $\tilde{s}_{kj}$  and  $\tilde{c}_{kj}$  can be written as (See the general definition of  $R$  in Eq. (1.27)):

$$\tilde{s}_{kj} = \sin(\rho_{kj}) \cos(i\gamma_{kj}) + \sin(i\gamma_{kj}) \cos(\rho_{kj}) \quad (\text{A.32})$$

$$= \sin(\rho_{kj}) ch(\gamma_{kj}) + i sh(\gamma_{kj}) \cos(\rho_{kj}) \quad (\text{A.33})$$

$$\tilde{c}_{kj} = \cos(\rho_{kj}) \cos(i\gamma_{kj}) - \sin(\rho_{kj}) \sin(i\gamma_{kj}) \quad (\text{A.34})$$

$$= \cos(\rho_{kj}) ch(\gamma_{kj}) - i \sin(\rho_{kj}) sh(\gamma_{kj}) \quad (\text{A.35})$$

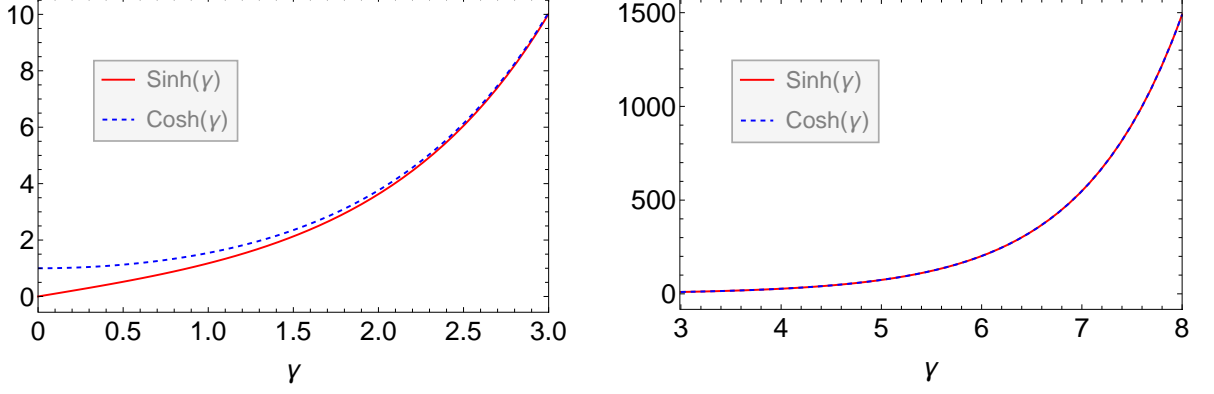


Figure A.1: Behavior of  $\sinh \gamma$  and  $\cosh \gamma$  for small values of gamma. For values greater than 3, both hyperbolic functions are equal.

where  $sh$  and  $ch$  are the hyperbolic functions  $\sinh$  and  $\cosh$ . We can see in Fig. A.1 that  $\cosh \gamma \approx \sinh \gamma$  for  $\gamma \geq 3$ . Therefore, we can approximate our trigonometric functions as:

$$\tilde{s}_{kj} = ie^{-i\rho_{kj}} ch(\gamma_{kj}) \quad (\text{A.36})$$

$$\tilde{c}_{kj} = e^{-i\rho_{kj}} ch(\gamma_{kj}) \quad (\text{A.37})$$

and for the  $R$  matrix with  $\rho_{45,46} = \gamma_{45,46} = 0$  :

$$R \approx \begin{pmatrix} e^{i\rho_{56}} & 0 & 0 \\ 0 & ch(\gamma_{56}) & i ch(\gamma_{56}) \\ 0 & -i ch(\gamma_{56}) & ch(\gamma_{56}) \end{pmatrix} e^{-i\rho_{56}} . \quad (\text{A.38})$$

With this approximation we can find the mixings  $U_{a4}$ ,  $U_{a5}$  and  $U_{a6}$  shown in the Equations (2.58), (2.59) and (2.60). From Eq. (A.3), we can rebuild the Dirac and Majorana masses:

$$M_D = X^* \hat{m}_\ell T^\dagger + Q^* \hat{M}_h Z^\dagger \quad (\text{A.39})$$

$$= -i W^* H^* \hat{m}_\ell^{1/2} (\hat{m}_\ell R^\dagger + R^T \hat{M}_h) \hat{M}_h^{-1/2} \bar{H}^\dagger \bar{W}^\dagger \quad (\text{A.40})$$

$$M_R = T^* \hat{m}_\ell T^\dagger + Z^* \hat{M}_h Z^\dagger \quad (\text{A.41})$$

$$= W^* H^* (\hat{M}_h - \hat{M}_h^{-1/2} R^* \hat{m}_\ell^2 R^\dagger \hat{M}_h^{-1/2}) \bar{H}^\dagger \bar{W}^\dagger \quad (\text{A.42})$$

# Appendix **B**

## Generalities

### B.1 Propagators

Z boson propagator

$$S_{\mu\nu} = \frac{-i}{q^2 - m_Z^2 + i\epsilon} \left( g_{\mu\nu} - \frac{(1 - \xi)q_\mu q_\nu}{q^2 - \xi m_Z^2} \right) \quad (\text{B.1})$$

Fermion propagator

$$S_F = \frac{i(\not{q} + m_F)}{q^2 - m_F^2 + i\epsilon} \quad (\text{B.2})$$

Scalar propagator

$$S_{S^0} = \frac{i}{q^2 - m_{S^0}^2} \quad (\text{B.3})$$

Goldstone Boson propagator

$$S_{G^0} = \frac{i}{q^2 - \xi m_Z^2} \quad (\text{B.4})$$

### B.2 Loop Integral Approximation

We want to evaluate the integral

$$I(m_0^2, m^2) = \int \frac{d^d k}{(2\pi)^d} \frac{Q^\epsilon}{(k^2 - m^2 - i\epsilon)(q^2 - m_0^2 + i\epsilon)} \quad (\text{B.5})$$

We use the Feynman parameters:

$$\frac{1}{AB} = \int_0^1 \frac{dx dy \delta(x + y - 1)}{(xA + yB)^2} \quad (\text{B.6})$$

Then it is possible to separate the denominator  $AB$  of the propagators into a single polynomial  $D = xA + yB$ . For the case that is being analyzed, we have

$$D = xA + yB \quad (\text{B.7})$$

$$= x(q^2 - m_0^2 + i\epsilon) + (1-x)(k^2 - m^2 + i\epsilon) \quad (\text{B.8})$$

We define :  $\ell = k - x p$  . In this case  $D$  can be written as:

$$D = (k - x p)^2 - \Delta + i\epsilon \quad (\text{B.9})$$

where:

$$\Delta = x^2 p^2 - x(p^2 + m^2 - m_0^2) + m^2 \quad (\text{B.10})$$

If  $p^2 \approx 0$ , we obtain

$$\Delta_{p^2 \approx 0} = x(m^2 - m_0^2) + m^2 \quad (\text{B.11})$$

We can write the integral in Eq. (B.6) as

$$\int \frac{d^d k}{(2\pi)^d} \frac{1}{(q^2 - m_0^2 + i\epsilon)(k^2 - m^2 + i\epsilon)} = \int \frac{d^d \ell}{(2\pi)^d} \int_0^1 dx \frac{Q^\epsilon}{(\ell^2 - \Delta + i\epsilon)^2} \quad (\text{B.12})$$

Applying the Wick rotation with  $\ell_0 = i\ell_s$  and  $\vec{\ell} = \vec{\ell}_s$

$$\int \frac{d^d k}{(2\pi)^d} \frac{1}{(q^2 - m_0^2 + i\epsilon)(k^2 - m^2 + i\epsilon)} = i \int \frac{d^d \ell_s}{(2\pi)^d} \int_0^1 dx \frac{Q^\epsilon}{(\ell_s^2 + \Delta)^2} \quad (\text{B.13})$$

$$\int \frac{d^d \ell_s}{(2\pi)^d} \frac{1}{(\ell_s^2 + \Delta)^2} = \int \frac{d\Omega_d}{(2\pi)^d} \int_0^\infty d\ell_s \frac{\ell_s^{d-1}}{(\ell_s^2 + \Delta)^2} \quad (\text{B.14})$$

where the area of the  $d$  dimensional sphere

$$\int d\Omega_d = \frac{2\pi^{d/2}}{\Gamma(d/2)} \quad (\text{B.15})$$

In the dimensional regularization  $\epsilon = 4 - d$ . The last integral in eq. (B.13) has a well known solution

$$\int \frac{d^d \ell_s}{(2\pi)^d} \frac{1}{(\ell_s^2 + \Delta)^2} = \frac{1}{2} \left( \frac{1}{\Delta} \right)^{2-\frac{d}{2}} \int dy y^{1-\frac{d}{2}} (1-y)^{\frac{d}{2}-1} \quad (\text{B.16})$$

This represent the Beta function.

$$\int_0^1 dy y^{\alpha-1} (1-y)^{\beta-1} = \frac{\Gamma(\alpha)\Gamma(\beta)}{\Gamma(\alpha+\beta)} \quad (\text{B.17})$$

$$\Rightarrow \int \frac{d^d \ell_s}{(2\pi)^d} \frac{1}{(\ell_s^2 + \Delta)^2} = \frac{\Gamma(\frac{\varepsilon}{2})}{(4\pi)^2} \left(\frac{4\pi}{\Delta}\right)^{\frac{\varepsilon}{2}} \quad (\text{B.18})$$

We have this important approximations

$$\Gamma(\varepsilon/2) = \frac{2}{\varepsilon} - \gamma + \mathcal{O}(\varepsilon) \quad (\text{B.19})$$

$$\left(\frac{\Delta}{4\pi Q^2}\right)^{-\varepsilon/2} = 1 - \frac{\varepsilon}{2} \ln\left(\frac{\Delta}{4\pi Q^2}\right) + \mathcal{O}\left(\frac{\varepsilon^2}{4}\right) \quad (\text{B.20})$$

We will call these approximations *A* and *B*. The first includes the product of Equations (B.19), (B.20) and  $d = 4 - \varepsilon$  and the second without  $d$ .

- Approximation *A*:

$$\begin{aligned} (4 - \varepsilon)\Gamma(\varepsilon/2) \left(\frac{\Delta}{4\pi Q^2}\right)^{-\varepsilon/2} &= 4 \left(\frac{2}{\varepsilon} + \ln(4\pi) - \frac{1}{2} - \gamma\right) - 4 \ln\left(\frac{\Delta}{Q^2}\right) \\ &= -4 \left(-\frac{2}{\varepsilon} - \ln(4\pi) + \frac{1}{2} + \gamma + \ln\left(\frac{\Delta}{Q^2}\right)\right) \end{aligned} \quad (\text{B.21})$$

- Approximation *B*:

$$\Gamma(\varepsilon/2) \left(\frac{4\pi Q^2}{\Delta}\right)^{\varepsilon/2} = \frac{2}{\varepsilon} - \gamma + \ln\left(\frac{4\pi Q^2}{\Delta}\right) \quad (\text{B.22})$$

These approximations are important for the solution of loop integrals. Using the approximation B, we have

$$I(m_0^2, m^2) = \int \frac{d^d k}{(2\pi)^d} \frac{Q^\varepsilon}{(k^2 - m^2 - i\epsilon)(q^2 - m_0^2 + i\epsilon)} \quad (\text{B.23})$$

$$= \frac{i}{16\pi^2} \left(\frac{2}{\varepsilon} - \gamma + \ln(4\pi) - \int_0^1 dx \ln\left(\frac{\Delta}{Q^2}\right)\right) \quad (\text{B.24})$$

The last term in Eq. (B.24) has the next general solution:

$$\int_0^1 dx \ln(v + ux) = -1 - \frac{v}{u} \ln v + \frac{v+u}{u} \ln(v+u) \quad (\text{B.25})$$

$$\int_0^1 dx \ln\left(\frac{\Delta_{p^2 \approx 0}}{Q^2}\right) = -1 + \ln\frac{m^2}{Q^2} - \left(\frac{m^2}{m_0^2} - 1\right)^{-1} \ln\frac{m_0^2}{m^2} \quad (\text{B.26})$$

$$I_2(m_0^2, m^2) = -\frac{i}{16\pi^2} \left(\tilde{k} - 1 + \ln\frac{m^2}{Q^2} + \left(\frac{m^2}{m_0^2} - 1\right)^{-1} \ln\frac{m^2}{m_0^2}\right) \quad (\text{B.27})$$

Using the approximation A

$$\begin{aligned}
 d I(m_0^2, m^2) &= \int \frac{d^d k}{(2\pi)^d} \frac{d Q^\varepsilon}{(k^2 - m^2 - i\varepsilon)(q^2 - m_0^2 + i\varepsilon)} \\
 &= -\frac{i}{4\pi^2} \left( \tilde{k} - \frac{1}{2} + \ln \frac{m^2}{Q^2} + \left( \frac{m^2}{m_0^2} - 1 \right)^{-1} \ln \frac{m^2}{m_0^2} \right)
 \end{aligned} \tag{B.28}$$

The divergence factor is defined as  $\tilde{k} = -\frac{2}{\varepsilon} - \ln 4\pi + \gamma$ .





# Bibliography

- [1] P. Hernández, J. Jones-Pérez, and O. Suarez-Navarro, “Majorana vs pseudo-dirac neutrinos at the ilc,” *The European Physical Journal C*, vol. 79, no. 3, Mar. 2019, ISSN: 1434-6052. DOI: 10.1140/epjc/s10052-019-6728-1. [Online]. Available: <http://dx.doi.org/10.1140/epjc/s10052-019-6728-1>.
- [2] S. T. Petcov, *The nature of massive neutrinos*, 2013. arXiv: 1303.5819 [hep-ph].
- [3] S. T. Petcov, “Neutrino Mixing and the Nature of Massive Neutrinos,” *AIP Conference Proceedings*, vol. 805, no. 1, pp. 135–141, Dec. 2005, ISSN: 0094-243X. DOI: 10.1063/1.2149689. eprint: [https://pubs.aip.org/aip/acp/article-pdf/805/1/135/12092590/135\\_1\\_1\\_online.pdf](https://pubs.aip.org/aip/acp/article-pdf/805/1/135/12092590/135_1_1_online.pdf). [Online]. Available: <https://doi.org/10.1063/1.2149689>.
- [4] S. Bilenky, “Neutrino oscillations: From a historical perspective to the present status,” *Nuclear Physics B*, vol. 908, pp. 2–13, 2016, Neutrino Oscillations: Celebrating the Nobel Prize in Physics 2015, ISSN: 0550-3213. DOI: <https://doi.org/10.1016/j.nuclphysb.2016.01.025>. [Online]. Available: <https://www.sciencedirect.com/science/article/pii/S0550321316000353>.
- [5] P. Minkowski, “ $\mu \rightarrow e$  at a rate of one out of 10<sup>9</sup> muon decays?” *Physics Letters B*, vol. 67, no. 4, pp. 421–428, 1977, ISSN: 0370-2693. DOI: [https://doi.org/10.1016/0370-2693\(77\)90435-X](https://doi.org/10.1016/0370-2693(77)90435-X). [Online]. Available: <https://www.sciencedirect.com/science/article/pii/037026937790435X>.
- [6] O. Sawada and A. Sugamoto, Eds., *Proceedings: Workshop on the Unified Theories and the Baryon Number in the Universe: Tsukuba, Japan, February 13-14, 1979*, Tsukuba, Japan: Natl.Lab.High Energy Phys., 1979.

- [7] M. Gell-Mann, P. Ramond, and R. Slansky, *Complex spinors and unified theories*, 2013. arXiv: 1306.4669 [hep-th].
- [8] R. N. Mohapatra and G. Senjanovi ć, “Neutrino mass and spontaneous parity non-conservation,” *Phys. Rev. Lett.*, vol. 44, pp. 912–915, 14 Apr. 1980. DOI: 10.1103/PhysRevLett.44.912. [Online]. Available: <https://link.aps.org/doi/10.1103/PhysRevLett.44.912>.
- [9] P. Candia da Silva and A. Pilaftsis, “Radiative neutrino masses in the  $\nu_R$ MSSM,” *Phys. Rev. D*, vol. 102, no. 9, p. 095013, 2020. DOI: 10.1103/PhysRevD.102.095013. arXiv: 2008.05450 [hep-ph].
- [10] S. Fukuda *et al.*, “Solar B-8 and hep neutrino measurements from 1258 days of Super-Kamiokande data,” *Phys. Rev. Lett.*, vol. 86, pp. 5651–5655, 2001. DOI: 10.1103/PhysRevLett.86.5651. arXiv: hep-ex/0103032.
- [11] Y. Fukuda *et al.*, “Evidence for oscillation of atmospheric neutrinos,” *Phys. Rev. Lett.*, vol. 81, pp. 1562–1567, 1998. DOI: 10.1103/PhysRevLett.81.1562. arXiv: hep-ex/9807003.
- [12] T. Kajita, “Discovery of neutrino oscillations,” *Reports on Progress in Physics*, vol. 69, no. 6, p. 1607, May 2006. DOI: 10.1088/0034-4885/69/6/R01. [Online]. Available: <https://dx.doi.org/10.1088/0034-4885/69/6/R01>.
- [13] T. Kajita, “ATMOSPHERIC NEUTRINOS AND DISCOVERY OF NEUTRINO OSCILLATIONS,” *Proc. Japan Acad. B*, vol. 86, pp. 303–321, 2010. DOI: 10.2183/pjab.86.303.
- [14] B. Pontecorvo, “Inverse beta processes and nonconservation of lepton charge,” *Zh. Eksp. Teor. Fiz.*, vol. 34, p. 247, 1957.
- [15] C. Giunti and C. W. Kim, *Fundamentals of Neutrino Physics and Astrophysics*. 2007, ISBN: 978-0-19-850871-7.
- [16] N. Haba and T. Yamada, “Prediction on neutrino dirac and majorana phases and absolute mass scale from the CKM matrix,” *Physical Review D*, vol. 97, no. 5, Mar. 2018. DOI: 10.1103/physrevd.97.055018. [Online]. Available: <https://doi.org/10.1103/physrevd.97.055018>.

- [17] B. Soni, S. Shafaq, and P. Mehta, *Distinguishing between dirac and majorana neutrinos using temporal correlations*, 2023. arXiv: 2307.04496 [hep-ph].
- [18] K. S. Hirata *et al.*, “Experimental Study of the Atmospheric Neutrino Flux,” *Phys. Lett. B*, vol. 205, J. Tran Thanh Van, Ed., p. 416, 1988. DOI: 10.1016/0370-2693(88)91690-5.
- [19] D. Casper, R. Becker-Szendy, C. B. Bratton, *et al.*, “Measurement of atmospheric neutrino composition with the imb-3 detector,” *Phys. Rev. Lett.*, vol. 66, pp. 2561–2564, 20 May 1991. DOI: 10.1103/PhysRevLett.66.2561. [Online]. Available: <https://link.aps.org/doi/10.1103/PhysRevLett.66.2561>.
- [20] I. Cordero-Carrión, M. Hirsch, and A. Vicente, “General parametrization of Majorana neutrino mass models,” *Phys. Rev. D*, vol. 101, no. 7, p. 075032, 2020. DOI: 10.1103/PhysRevD.101.075032. arXiv: 1912.08858 [hep-ph].
- [21] R. N. Mohapatra, “Seesaw mechanism and its implications,” in *SEESAW 25*, World Scientific, 2005, pp. 29–44.
- [22] S. Antusch, J. Kersten, M. Lindner, and M. Ratz, “Running neutrino masses, mixings and CP phases: Analytical results and phenomenological consequences,” *Nucl. Phys. B*, vol. 674, pp. 401–433, 2003. DOI: 10.1016/j.nuclphysb.2003.09.050. arXiv: hep-ph/0305273.
- [23] A. B. Balantekin and B. Kayser, *On the properties of neutrinos*, 2018. DOI: 10.48550/ARXIV.1805.00922. [Online]. Available: <https://arxiv.org/abs/1805.00922>.
- [24] F. Halzen and A. D. Martin, *QUARKS AND LEPTONS: AN INTRODUCTORY COURSE IN MODERN PARTICLE PHYSICS*. 1984, ISBN: 978-0-471-88741-6.
- [25] D. Griffiths, *Introduction to elementary particles*. 2008, ISBN: 978-3-527-40601-2.
- [26] J. Jones-Pérez, J. Masias, and J. D. Ruiz-Álvarez, “Search for Long-Lived Heavy Neutrinos at the LHC with a VBF Trigger,” *Eur. Phys. J. C*, vol. 80, no. 7, p. 642, 2020. DOI: 10.1140/epjc/s10052-020-8188-z. arXiv: 1912.08206 [hep-ph].
- [27] A. Donini, P. Hernandez, J. Lopez-Pavon, M. Maltoni, and T. Schwetz, “The minimal 3+2 neutrino model versus oscillation anomalies,” *JHEP*, vol. 07, p. 161, 2012. DOI: 10.1007/JHEP07(2012)161. arXiv: 1205.5230 [hep-ph].

- [28] S. Antusch and O. Fischer, “Testing sterile neutrino extensions of the standard model at future lepton colliders,” *Journal of High Energy Physics*, vol. 2015, no. 5, May 2015. DOI: 10.1007/jhep05(2015)053. [Online]. Available: <https://doi.org/10.1007%2Fjhep05%282015%29053>.
- [29] S. Antusch, J. Hajer, and B. M. S. Oliveira, *Heavy neutrino-antineutrino oscillations at the fcc-ee*, 2023. arXiv: 2308.07297 [hep-ph].
- [30] W. Grimus and L. Lavoura, “One-loop corrections to the seesaw mechanism in the multi-higgs-doublet standard model,” *Physics Letters B*, vol. 546, no. 1, pp. 86–95, 2002, ISSN: 0370-2693. DOI: [https://doi.org/10.1016/S0370-2693\(02\)02672-2](https://doi.org/10.1016/S0370-2693(02)02672-2). [Online]. Available: <https://www.sciencedirect.com/science/article/pii/S0370269302026722>.
- [31] J. A. Casas and A. Ibarra, “Oscillating neutrinos and  $\mu \rightarrow e, \gamma$ ,” *Nucl. Phys. B*, vol. 618, pp. 171–204, 2001. DOI: 10.1016/S0550-3213(01)00475-8. arXiv: hep-ph/0103065.
- [32] M. E. Peskin and D. V. Schroeder, *An Introduction to quantum field theory*. Reading, USA: Addison-Wesley, 1995, ISBN: 978-0-201-50397-5.
- [33] W. Grimus and M. Lössner, “Revisiting on-shell renormalization conditions in theories with flavor mixing,” *International Journal of Modern Physics A*, vol. 31, no. 24, p. 1630038, Aug. 2016. DOI: 10.1142/s0217751x16300386. [Online]. Available: <https://doi.org/10.1142%2Fs0217751x16300386>.
- [34] B. A. Kniehl and A. Pilaftsis, “Mixing renormalization in majorana neutrino theories,” *Nuclear Physics B*, vol. 474, no. 2, pp. 286–308, Aug. 1996. DOI: 10.1016/0550-3213(96)00280-5. [Online]. Available: <https://doi.org/10.1016%2F0550-3213%2896%2900280-5>.
- [35] D. A. Sierra, “Implications of finite one-loop corrections for see-saw neutrino masses,” *Journal of Physics: Conference Series*, vol. 375, no. 4, p. 042003, Jul. 2012. DOI: 10.1088/1742-6596/375/1/042003. [Online]. Available: <https://doi.org/10.1088%2F1742-6596%2F375%2F1%2F042003>.
- [36] D. A. Sierra and C. E. Yaguna, “On the importance of the 1-loop finite corrections to seesaw neutrino masses,” *Journal of High Energy Physics*, vol. 2011, no. 8, Aug.

2011. DOI: 10.1007/jhep08(2011)013. [Online]. Available: <https://doi.org/10.1007%2Fjhep08%282011%29013>.

- [37] W. Grimus and L. Lavoura, “One-loop corrections to the seesaw mechanism in the multi-Higgs-doublet standard model,” *Phys. Lett. B*, vol. 546, pp. 86–95, 2002. DOI: 10.1016/S0370-2693(02)02672-2. arXiv: hep-ph/0207229.
- [38] W. Grimus and H. Neufeld, “Radiative Neutrino Masses in an SU(2) X U(1) Model,” *Nucl. Phys. B*, vol. 325, pp. 18–32, 1989. DOI: 10.1016/0550-3213(89)90370-2.
- [39] A. M. Gago, P. Hernández, J. Jones-Pérez, M. Losada, and A. Moreno Briceño, “Probing the Type I Seesaw Mechanism with Displaced Vertices at the LHC,” *Eur. Phys. J. C*, vol. 75, no. 10, p. 470, 2015. DOI: 10.1140/epjc/s10052-015-3693-1. arXiv: 1505.05880 [hep-ph].
- [40] D. Wyler and L. Wolfenstein, “Massless Neutrinos in Left-Right Symmetric Models,” *Nucl. Phys. B*, vol. 218, pp. 205–214, 1983. DOI: 10.1016/0550-3213(83)90482-0.
- [41] R. N. Mohapatra and J. W. F. Valle, “Neutrino Mass and Baryon Number Non-conservation in Superstring Models,” *Phys. Rev. D*, vol. 34, p. 1642, 1986. DOI: 10.1103/PhysRevD.34.1642.
- [42] M. B. Gavela, T. Hambye, D. Hernandez, and P. Hernandez, “Minimal Flavour Seesaw Models,” *JHEP*, vol. 09, p. 038, 2009. DOI: 10.1088/1126-6708/2009/09/038. arXiv: 0906.1461 [hep-ph].
- [43] G. C. Branco, W. Grimus, and L. Lavoura, “The Seesaw Mechanism in the Presence of a Conserved Lepton Number,” *Nucl. Phys. B*, vol. 312, pp. 492–508, 1989. DOI: 10.1016/0550-3213(89)90304-0.
- [44] M. Shaposhnikov, “A Possible symmetry of the nuMSM,” *Nucl. Phys. B*, vol. 763, pp. 49–59, 2007. DOI: 10.1016/j.nuclphysb.2006.11.003. arXiv: hep-ph/0605047.
- [45] J. Kersten and A. Y. Smirnov, “Right-Handed Neutrinos at CERN LHC and the Mechanism of Neutrino Mass Generation,” *Phys. Rev. D*, vol. 76, p. 073005, 2007. DOI: 10.1103/PhysRevD.76.073005. arXiv: 0705.3221 [hep-ph].
- [46] M. Malinsky, J. C. Romao, and J. W. F. Valle, “Novel supersymmetric SO(10) seesaw mechanism,” *Phys. Rev. Lett.*, vol. 95, p. 161801, 2005. DOI: 10.1103/PhysRevLett.95.161801. arXiv: hep-ph/0506296.

- [47] S. Antusch, E. Cazzato, and O. Fischer, *Resolvable heavy neutrino-antineutrino oscillations at colliders*, 2017. DOI: 10.48550/ARXIV.1709.03797. [Online]. Available: <https://arxiv.org/abs/1709.03797>.
- [48] I. Cordero-Carrión, M. Hirsch, and A. Vicente, “General parametrization of majorana neutrino mass models,” *Physical Review D*, vol. 101, no. 7, Apr. 2020. DOI: 10.1103/physrevd.101.075032. [Online]. Available: <https://doi.org/10.1103/PhysRevD.101.075032>.
- [49] J. Lopez-Pavon, S. Pascoli, and C.-f. Wong, “Can heavy neutrinos dominate neutrinoless double beta decay?” *Phys. Rev. D*, vol. 87, no. 9, p. 093007, 2013. DOI: 10.1103/PhysRevD.87.093007. arXiv: 1209.5342 [hep-ph].
- [50] J. Lopez-Pavon, E. Molinaro, and S. T. Petcov, “Radiative Corrections to Light Neutrino Masses in Low Scale Type I Seesaw Scenarios and Neutrinoless Double Beta Decay,” *JHEP*, vol. 11, p. 030, 2015. DOI: 10.1007/JHEP11(2015)030. arXiv: 1506.05296 [hep-ph].
- [51] S. P. MARTIN, “A SUPERSYMMETRY PRIMER,” in *Perspectives on Supersymmetry*, WORLD SCIENTIFIC, Jul. 1998, pp. 1–98. DOI: 10.1142/9789812839657\_0001. [Online]. Available: [https://doi.org/10.1142/9789812839657\\_0001](https://doi.org/10.1142/9789812839657_0001).
- [52] S. Moretti and S. Khalil, *Supersymmetry beyond minimality: from theory to experiment*. CRC Press, 2017. [Online]. Available: <https://eprints.soton.ac.uk/411745/>.
- [53] N. Cerna-Velazco, T. Faber, J. Jones-Perez, and W. Porod, “Constraining sleptons at the LHC in a supersymmetric low-scale seesaw scenario,” *Eur. Phys. J. C*, vol. 77, no. 10, p. 661, 2017. DOI: 10.1140/epjc/s10052-017-5231-9. arXiv: 1705.06583 [hep-ph].
- [54] T. Faber, Y. Liu, W. Porod, and J. Jones-Pérez, “Revisiting neutrino and sneutrino dark matter in natural SUSY scenarios,” *Phys. Rev. D*, vol. 101, no. 5, p. 055029, 2020. DOI: 10.1103/PhysRevD.101.055029. arXiv: 1909.11686 [hep-ph].
- [55] J. Masias, N. Cerna-Velazco, J. Jones-Perez, and W. Porod, “Resolving a challenging supersymmetric low-scale seesaw scenario at the ILC,” *Phys. Rev. D*, vol. 103, no. 11, p. 115028, 2021. DOI: 10.1103/PhysRevD.103.115028. arXiv: 2102.06236 [hep-ph].

- [56] G. Raz, “Mass insertion approximation without squark degeneracy,” *Physical Review D*, vol. 66, no. 3, Aug. 2002. DOI: 10.1103/physrevd.66.037701. [Online]. Available: <https://doi.org/10.1103%2Fphysrevd.66.037701>.
- [57] F. Gabbiani, E. Gabrielli, A. Masiero, and L. Silvestrini, “A complete analysis of FCNC and CP constraints in general SUSY extensions of the standard model,” *Nuclear Physics B*, vol. 477, no. 2, pp. 321–352, Oct. 1996. DOI: 10.1016/0550-3213(96)00390-2. [Online]. Available: <https://doi.org/10.1016%2F0550-3213%2896%2900390-2>.
- [58] J. Hisano and D. Nomura, “Solar and atmospheric neutrino oscillations and lepton flavor violation in supersymmetric models with right-handed neutrinos,” *Physical Review D*, vol. 59, no. 11, Apr. 1999. DOI: 10.1103/physrevd.59.116005. [Online]. Available: <https://doi.org/10.1103%2Fphysrevd.59.116005>.
- [59] A. Collaboration, *Search for heavy higgs bosons decaying into two tau leptons with the atlas detector using pp collisions at  $\sqrt{s} = 13$  tev*, 2020. arXiv: 2002.12223 [hep-ex].
- [60] G. Aad *et al.*, “Search for charged Higgs bosons decaying into a top quark and a bottom quark at  $\sqrt{s} = 13$  TeV with the ATLAS detector,” *JHEP*, vol. 06, p. 145, 2021. DOI: 10.1007/JHEP06(2021)145. arXiv: 2102.10076 [hep-ex].
- [61] G. Aad *et al.*, “Combined measurements of Higgs boson production and decay using up to 80 fb<sup>-1</sup> of proton-proton collision data at  $\sqrt{s} = 13$  TeV collected with the ATLAS experiment,” *Phys. Rev. D*, vol. 101, no. 1, p. 012002, 2020. DOI: 10.1103/PhysRevD.101.012002. arXiv: 1909.02845 [hep-ex].
- [62] M. Drees, R. Godbole, and P. Roy, *Theory and Phenomenology of Sparticles*. WORLD SCIENTIFIC, 2005. DOI: 10.1142/4001. eprint: <https://www.worldscientific.com/doi/pdf/10.1142/4001>. [Online]. Available: <https://www.worldscientific.com/doi/abs/10.1142/4001>.
- [63] W. Porod and F. Staub, “SPHeno 3.1: Extensions including flavour, CP-phases and models beyond the MSSM,” *Comput. Phys. Commun.*, vol. 183, pp. 2458–2469, 2012. DOI: 10.1016/j.cpc.2012.05.021. arXiv: 1104.1573 [hep-ph].
- [64] W. Porod, “SPHeno, a program for calculating supersymmetric spectra, SUSY particle decays and SUSY particle production at e+ e- colliders,” *Comput. Phys. Com-*

*mun.*, vol. 153, pp. 275–315, 2003. DOI: 10.1016/S0010-4655(03)00222-4. arXiv:  
hep-ph/0301101 [hep-ph].

